Crop Separation Using Spatial, Spectral, and Temporal Remote Sensing Data

Dissertation
zur
Erlangung der naturwissenschaftlichen Doktorwürde
(Dr. sc. nat.)
vorgelegt der
Mathematisch-naturwissenschaftlichen Fakultät
der
Universität Zürich

von
Jonas E. Böhler
von
Winterthur ZH und Lampenberg BL

Promotionskommission
Prof. Dr. Michael E. Schaepman
(Vorsitz der Dissertation)
Dr. Mathias Kneubühler (Leitung der Dissertation)
Prof. Dr. Alexander Damm-Reiser

Zürich, 2020

Summary

Crop species separation is essential for many agricultural applications, as well as decision making, monitoring and management issues. There is a need for such information within the season, which can be provided for a wide range of agricultural areas (spatial and thematic) in time by remote sensing. In the case of small-structured agricultural landscapes, however, the well-known satellite based approaches often fail and very high resolution (VHR) datasets are needed. To achieve optimal results, the spatial, spectral and temporal resolution needs to be thoroughly selected. In order to analyze the influence of these three dimensions, a multitemporal near-infrared, red, green and blue (NIR-RGB) dataset was acquired with a consumer-grade camera mounted on an unmanned aerial vehicle (UAV), along with a monotemporal imaging spectroscopy (IS) dataset acquired by airborne means.

In this thesis, a methodology was developed that allows analyzing these three aspects of resolution. On the one hand, it allows the separation of crops with datasets of different spatial and spectral resolution. These datasets were collected multiple times at different phenological stages using uncalibrated, consumer-grade cameras mounted on an UAV, as well as once an imaging spectrometer. Based on these datasets, various settings with different spatial and spectral resolution could be assembled. On the other hand, the methodology enables the comparison between different settings and a statistical comparison of the respective accuracies.

In a first study, the influence of spatial resolution on crop separation was evaluated. For this purpose, the NIR-RGB dataset was resampled to different spatial and spectral resolution settings, and textural features (statistical and morphological) of different kernel sizes were implemented to account for an additional structuring element. The best performance is achieved with a spatial resolution of 0.5 m, three spectral bands (RGB) and five different sizes of the structuring element The overall accuracy (OA) is 66.7% for all existing crop types, and 74.0% for a merged set of crop types. In case of additional spatial support by field boundaries, OA is increased by approximately 20% (OA of 86.3% for the complete set of crop types, and 94.6% for the merged set). In a heterogeneous agricultural landscape, a spatial resolution of 0.5 m proved to be most promising.

A second study examined the temporal dimension of crop separation. For this purpose, 11 NIR-RGB VHR datasets from remotely sensed observations made between May 5 and September 29, 2015 were investigated. Three distinct temporal windows of observations based on accumulated growing degree days (AGDD) could be identified: an early temporal window (515-1232 AGDD, May 5- June 17, 2015) with an average accuracy (AA) of crop separation of 70-75%; a mid-season window (1362-2016 AGDD, June 25- July 22, 2015) with an AA of about 80%; and a late window (2626-3238 AGDD, August 21-September 29, 2015) with an AA of $<$65%. Consequently, the separation of crops is most promising in the middle of the growing

season. However, the differentiation of winter crops compared to other crops proved to be most effective in the early temporal window, which gives additional importance to this temporal window.

In a third study, the influence of spectral resolution on crop separation was evaluated in detail. In addition to the NIR-RGB dataset acquired on June 25, 2015, an IS dataset of 2 m spatial resolution, acquired one day before, was used. Both single use and combination of these datasets were analyzed, as well as different degrees of band reduction based on the feature factor loading. In the combined setting, spectral and textural features from the NIR-RGB dataset and the spectral features from the IS dataset were used. The most precise separation of crops is possible using the two combined datasets (AA >92%), closely followed by the sole use of the IS dataset. Furthermore, we conclude that in case of a reduced number of bands from the IS dataset (down to 10 bands), the loss of accuracy can be compensated by using additional textural features from the NIR-RGB dataset (AA >90%).

This thesis highlights the potential of uncalibrated multispectral VHR datasets for crop separation in small-structured agricultural landscapes, partially combined with IS data. Furthermore the influence of very high spatial resolution and different observation times over the phenological cycle was investigated. As such, it contributes to closing gaps in accurate crop separation needs in small structured agricultural areas using remotely sensed datasets.

Zusammenfassung

Die Trennung von Nutzpflanzenarten ist für viele landwirtschaftliche Anwendungen sowie für die Entscheidungsfindung, Überwachung und Verwaltung von entscheidender Bedeutung. Es besteht ein Bedarf an solchen Informationen innerhalb der Saison, die durch Fernerkundung für ein breites Spektrum landwirtschaftlicher Gebiete (räumlich und thematisch) zeitnah zur Verfügung gestellt werden können. Im Falle kleinstrukturierter Agrarlandschaften scheitern jedoch oft die bekannten satellitengestützten Ansätze und es werden sehr hochauflösende Datensätze benötigt. Um optimale Ergebnisse zu erzielen, muss dabei die räumliche, spektrale und zeitliche Auflösung sorgfältig ausgewählt werden. Um den Einfluss dieser drei Dimensionen zu analysieren, wurde ein multitemporaler Nahinfrarot-, Rot-, Grün- und Blau- (NIR-RGB) Datensatz mit auf einer Drohne (UAV) montierten standardmässigen Kleinkameras, sowie ein monotemporaler flugzeuggetragener abbildender Spektroskopiedatensatz (IS-Datensatz) aufgenommen.

In dieser Arbeit wurde eine Methodik entwickelt, die es erlaubt, diese drei Aspekte der Auflösung zu analysieren. Einerseits erlaubt sie die Trennung von Feldfrüchten mit Datensätzen unterschiedlicher räumlicher und spektraler Auflösung. Diese Datensätze wurden mehrfach in verschiedenen phänologischen Stadien mit Hilfe drohnenbasierter unkalibrierter Kleinkameras, sowie einmal mit einem abbildenden Spektrometer erfasst. Auf der Grundlage dieser Datensätze konnten verschiedene Settings mit unterschiedlicher räumlicher und spektraler Auflösung zusammengestellt werden. Zum anderen ermöglicht die Methodik den Vergleich zwischen verschiedenen Settings und einen statistischen Vergleich der jeweiligen Genauigkeiten.

In einer ersten Studie wurde der Einfluss der räumlichen Auflösung auf die Trennbarkeit von Feldfrüchten evaluiert. Zu diesem Zweck wurden verschiedene Settings des NIR-RGB-Datensatzes mit unterschiedlichen räumlichen und spektralen Auflösungen erstellt, und texturale Merkmale (statistisch und morphologisch) unterschiedlicher Kernelgrössen implementiert (strukturierendes Element). Die beste Trennbarkeit wird mit einer räumlichen Auflösung von 0.5 m, drei Spektralbändern (RGB) und fünf verschiedenen Grössen des strukturierenden Elements erzielt. Die Gesamtgenauigkeit (OA) beträgt 66.7 % für alle vorhandenen Kulturarten und 74.0 % für einen reduzierten Satz von Kulturarten. Im Falle einer zusätzlichen räumlichen Unterstützung durch Feldgrenzen wird die OA um etwa 20% erhöht (OA von 86.3% für den vollständigen Satz von Kulturpflanzenarten und 94.6% für den reduzierten Satz). In einer heterogenen Agrarlandschaft erwies sich eine räumliche Auflösung von 0.5 m als am vielversprechendsten.

Eine zweite Studie untersuchte die zeitliche Dimension der Trennbarkeit von Feldfrüchten. Zu diesem Zweck wurden 11 NIR-RGB VHR-Datensätze aus drohnenbasierten Erhebungen, die zwischen dem 5. Mai und dem 29. September 2015 gemacht wurden, untersucht. Es konnten drei verschiedene zeitliche Beobachtungsperioden

auf der Grundlage der akkumulierten Wachstumsgradtage (AGDD) identifiziert werden: ein frühes zeitliches Fenster (515-1232 AGDD, 5. Mai bis 17. Juni 2015) mit einer durchschnittlichen Genauigkeit (AA) der Trennbarkeit der Feldfrüchte von 70-75%, ein Fenster in der Mitte der Saison (1362-2016 AGDD, 25. Juni bis 22. Juli 2015) mit einer AA von etwa 80%, sowie ein spätes Fenster (2626-3238 AGDD, 21. August bis 29. September 2015) mit einer AA von $<$65%. Folglich ist die Trennung der Feldfrüchte in der Mitte der Vegetationsperiode am vielversprechendsten. Die Differenzierung von Winterkulturen im Vergleich zu anderen Kulturen erwies sich jedoch im frühen Zeitfenster als am wirksamsten, was diesem Zeitfenster zusätzliche Bedeutung verleiht.

In einer dritten Studie wurde der Einfluss der spektralen Auflösung auf die Trennbarkeit der Feldfrüchte im Detail evaluiert. Zusätzlich zu dem am 25. Juni 2015 erfassten NIR-RGB-Datensatz wurde ein IS-Datensatz mit 2 m räumlicher Auflösung verwendet, der einen Tag zuvor erhoben worden war. Sowohl die einzelne Verwendung als auch die Kombination dieser Datensätze wurden analysiert, ebenso wie verschiedene Grade der Bandreduktion basierend auf einem *Feature-Faktor-Loading* Ansatz. Im kombinierten Setting wurden spektrale und texturale Merkmale aus dem NIR-RGB-Datensatz, sowie die spektralen Merkmale aus dem IS-Datensatz verwendet. Die genaueste Trennung der Feldfrüchte ist mit den kombinierten Datensätzen möglich (AA $>$92%), knapp gefolgt von der alleinigen Verwendung des IS-Datensatzes. Darüber hinaus kommt die Analyse zum Schluss, dass im Falle einer reduzierten Anzahl von Bändern aus dem IS-Datensatz (Reduktion bis auf 10 Bänder) der Genauigkeitsverlust durch die Verwendung zusätzlicher Texturmerkmale aus dem NIR-RGB-Datensatz (AA $>$90%) kompensiert werden kann.

Diese Dissertation unterstreicht das Potenzial unkalibrierter multispektraler VHR-Datensätze für die Trennbarkeit von Feldfrüchten in kleinstrukturierten Agrarlandschaften, teilweise kombiniert mit IS-Daten. Überdies wurde der Einfluss einer sehr hohen räumlichen Auflösung und unterschiedlicher Beobachtungszeitpunkte im phänologischen Zyklus untersucht. Damit trägt die Arbeit dazu bei, Lücken in der genauen Trennung von Nutzpflanzen in klein strukturierten landwirtschaftlichen Gebieten mit Hilfe von Datensätzen der Fernerkundung zu schliessen.

Table of Contents

List of Abbreviations

a.s.l. ..... Above Sea Level
AA ..... Average Accuracy
AGDD ..... Accumulated Growing Degree Days
APEX ..... Airborne Prism Experiment
AR ..... Average Reliability
ASAP ..... Anomaly Hot Spots of Agricultural Production
B ..... Blue
BBCH ..... Biologische Bundesanstalt, Bundessortenamt und CHemische Industrie
CAS ..... Chinese Academy of Sciences
CNN ..... Convolutional Neural Networks
CRF ..... Conditional Random Field
dGPS ..... differential GPS
EFA ..... Ecological Focus Areas
EU ..... European Union
FAO ..... Food and Agriculture Organization of the United Nations
FAS ..... Foreign Agricultural Service
FEWS NET .... Famine Early Warning Systems Network
FWHM ..... Full Width at Half Maximum
G ..... Green
GCP ..... Ground Control Points
GDVI ..... Generalized Difference Vegetation Index
GIEWS ..... Global Information and Early Warning System
GIS ..... Geographical Information System
GLAM ..... Global Agricultural Monitoring
GLCM ..... Gray Level Co-occurrence Matrix
GPS ..... Global Positioning System
IACS ..... Integrated Administration and Control System
IRSA ..... Institute of Remote Sensing Applications
IS ..... Imaging Spectrometer
JRC ..... Joint Research Centre
MARS ..... Monitoring Agricultural ResourceS
ML ..... Machine Learning
MLC ..... Maximum Likelihood Classification
MODIS ..... Moderate Resolution Imaging Spectrometer
NDVI ..... Normalized Difference Vegetation Index
NIR ..... Near-Infrared
NIR-RGB ..... Near-Infrared, Red, Green and Blue
NirGB ..... Near-infrared, Green, and Blue
NN ..... Neural Networks
OA ..... overall accuracy
PA ..... Producer Accuracy
R ..... Red
RF ..... Random Forest

RGB ..... Red, Green and Blue
SAR ..... Synthetic Aperture Radar
SAVI ..... Soil-Adjusted Vegetation Index
SE ..... Structuring Element
Sen4CAP ..... Sentinels for Common Agricultural Policy
SfM ..... Structure from Motion
SVM ..... Support Vector Machine
UA ..... User Accuracy
UAV ..... Unmanned Aerial Vehicle
USDA ..... United States Department of Agriculture
VHR ..... Very High Resolution
VI ..... Vegetation Index
VIS ..... Visible
VNIR ..... visible and Near-Infrared
WFP ..... World Food Program

Chapter

1

Introduction

The world population is expected to grow to 9.6 billion people by 2050 [1]. As a result, the global demand for food is expected to increase [2] by up to 50 percent with modest economic growth[3]. Therefore, the availability of accurate and timely information on agriculture at both global [4] and local levels is becoming essential to ensure food security for a growing world population [5], especially, since agriculture is very sensitive to climate change [6], and also in order to achieve all the goals of the United Nations 2030 Agenda for Sustainable Development, in particular zero hunger [7,8]. Real-time or near real-time monitoring of crop status is required to respond to extreme weather events under changing climatic conditions [9] and to optimize management practices [10]. Short-term yield forecasts on a global, regional and farm level scale are essential for securing economic returns [11].

Accurate land cover assessments form the basis for numerous analyses in agricultural areas [12]. There is a wide range of demands for precise land cover information and therefore automated crop separation capabilities. Such knowledge is particularly important for climate change modeling [13], sustainable land management [14], crop growth modeling before the end of season [15], water resource planning [16], automated short-term monitoring for yield estimation [17], or plot extraction for high-throughput phenotyping [18–20].

The main stakeholders in agricultural land cover assessments are regional, national or international actors, such as policy makers or insurance companies [21]. Individual farmers usually know very well which crop they have planted where, and which soil is suitable. As a general rule, however, farmers do not report which crops they have grown until after the season. In addition, information on arable land cover is only available for administrative units and detailed information on spatial distribution is often missing [22] or is not publicly available due to data protection reasons [23]. Even if the reporting for subsidies takes place in a geographical information system (GIS), as is the practice in Switzerland, the data are only entered after the season or even in the following year [24]. Moreover, the data are not accessible to everyone. For a more up-to-date assessment of the state of crops, therefore, a different data collection source is necessary.

1.1 Agriculture in Switzerland

In 2013, agricultural land covered 23.4% of Switzerland and was managed by 55'200 farms in [25], whereby the agricultural landscape is largely characterized by small-scale farming [26]. The average area per farm has risen in the last two decades to 19 ha [25]. The size of individual field plots is therefore much smaller. For example, around Mönchaltorf (ZH), a typical region in the Swiss Plateau, the individual field plots have an average size of 1.3 ha. However, sizes vary widely between 0.03 ha and 7.4 ha.

Supporting farmers through direct payments plays a key role in Swiss agricultural policy. In 1996, Switzerland's agricultural policy underwent a fundamental change when it switched from the provision of guaranteed purchase for most agricultural products to compensation for services rendered [27]. Today, the focus of subsidies is on securing food supplies, sustainable production, preserving the cultural landscape, contributing to the quality of the landscape and enriching biodiversity. An attractive landscape is guaranteed by the small-scale subdivision of arable land into portions of different crops, which also promotes biodiversity [27,28]. Finally, the remaining direct payments are based on the total area of a farm, the compensation for hilly terrain, as well as the various crops and their combinations [24]. In addition, contributions are paid for certain crops, such as oilseeds or sugar beet [24].

Up to now, the respective reporting has been based on self-declaration and controlling by field visits. The close monitoring of crop species is important for subsidy control, for the monitoring of biodiversity-relevant farming practices such as crop rotation, soil protection and sustainable fertilization, and for the linking of protected areas and ecological compensation areas [27].

The exchange of information from reporting and controlling is often time- consuming and complicated. This is crucial when it comes to the need for early warning [29], for instance in the case of water scarcity, when sustainable planning is required [16]. Future projections of climate models indicate that water will become an increasingly limited resource in Switzerland [13,30]. Since water requirements for irrigation depend on the crop type, accurate and timely information on crop allocation and areas under cultivation is necessary for planning purposes. To obtain this kind of timely information about crop growth will become more important, also in Switzerland. However, as already mentioned, such information is only collected after the season, e.g., by farmers in the context of subsidies. Consequently, it is essential to consult an alternative source of information. Remote sensing methods offer a valuable alternative.

1.2 Remote sensing for agriculture

1.2.1 Challenges and needs

To address the many challenges in agriculture and agronomy, remote sensing technologies offer a wide range of possibilities to assess these issues [4,31]. They include yield [32] and biomass estimation [33], phenology and vitality monitoring [29], seasonal plant development and stress monitoring [34,35], crop succession [36] as well as land cover or land use change assessments [37,38].

Common to all these applications is the fact that their results are directly dependent on the crop type. It is therefore important that the crop type is known in

a single field plot. There are different approaches for global mapping of general land cover types such as forests and grasslands based on remote sensing (see e.g., [39]). However, if applied to agricultural areas, such classifications do not distinguish between different types of crops, but usually group them into a class called ”cropland” [11], as is the case with ESA-CCI Land Cover [40] or GlobeLand30 [41].

Monitoring agricultural land use is becoming increasingly important as agricultural systems are fundamentally under pressure from climate change or political influence, such as reducing pollutants or mitigating biodiversity loss [28]. Remote sensing offers excellent opportunities for monitoring changing spatial configurations [31]. Policy makers, in particular, need up-to-date information on the crop species cultivated to support their decisions.

There is a wide range of existing systems to monitor agriculture by remote sensing at global or regional level. In the early 1970's, the Global Information and Early Warning System (GIEWS) was established with the goal to provide information on global food production and food security within the Food and Agriculture Organization of the United Nations (FAO). Famine early warning systems network (FEWS NET) was initiated by USAID in 1985 to support food assistance programs and aid organizations. In 1992, the Joint Research Centre (JRC) Monitoring Agricultural ResourceS (MARS) started to estimate the agricultural production and to produce food security assessments for European Union (EU) member states. CropWatch4, which was launched in 1998 and is managed by the Institute of Remote Sensing Applications (IRSA) of the Chinese Academy of Sciences (CAS), evaluates national and global crop production. In 2001 the United States Department of Agriculture (USDA) started the Foreign Agricultural Service (FAS) to predict global crop production for agricultural economists and researchers. Global Agricultural Monitoring (GLAM), operational since 2013, produces a report on global production of wheat, maize, rice and soy. The Seasonal Monitor system of the World Food Program (WFP) has been operational since 2014. Main goals are early warnings for crop systems and pasture production in regions of interest defined by WFP. In 2017, JRC established the Anomaly Hot Spots of Agricultural Production (ASAP) as a source of information for several agencies and systems, including GEOGLAM. Further details and references can be found in reviews, e.g., [31,42].

Besides remote sensing products, which e.g., originate from Landsat or the EU Copernicus program [42], additional information like cropland maps, crop type, crop calendar, soil information, statistics, parcel borders and other datasets are needed. In particular, maps of crop types are considered to be critical information for six of the eight major monitoring programs listed in the previous paragraph [42].

Another example for the need to separate crops is the EU Common Agricultural Policy (CAP) and its Integrated Administration and Control System (IACS). The main objective of the CAP is to improve the competitiveness and sustainability of the agricultural sector in the EU Member States. This program manages a budget of

59 billion for direct payments, market measures and rural development. In order to distribute funds fairly and to improve the system of farmers' declarations of support, the CAP is periodically reviewed. The current 2020 reform provides for more satellite data to be implemented to improve cost efficiency and simplify the system. Part of this is the Sentinels for Common Agricultural Policy (Sen4CAP) project, which validates algorithms, products, workflows and best practices to improve agricultural management and monitoring. The products include a map of crop types, a grassland mowing product, a vegetation status indicator, a product for monitoring agricultural practices, together with interactive visualization services for satellite images, and use case products with Sentinel-1 and Sentinel-2 data. Several CAP subsidy programs are supported, e.g., crop diversification or catch crops in ecological focus areas (EFA). The total area per crop, as well as different crop types are of crucial importance[1].

Even though land use and land cover have been a topic in remote sensing for many years, its potential has not yet been fully researched to date [43]. Given that an agricultural landscape is structured into rather small plots, as it is the case in Switzerland, data with very high spatial resolution (VHR) are required to derive the type of crops and the extent of the individual fields [4,31,44]. The availability of datasets with a spatial resolution of a few centimeters captured by Unmanned Aerial Vehicles (UAV) has opened up new areas, e.g., in the mapping of weeds [45,46] or diseases [47]. This leads to new issues, as small objects can make accurate classification tricky.

1.2.2 Technology

Remote sensing has proven to be a viable alternative to human observation in the field and has shown the potential to provide such information even before the end of the season [31,48]. Land cover maps for crops are often based on satellite data, as these platforms provide datasets several times a month, and are suitable for both single-date and multi-temporal classification tasks [49,50]. In addition, several studies have demonstrated the ability to perform early-stage crop mapping using remote sensing data [16,17,51,52].

In particular, land cover assessment in agricultural areas has been carried out on a large scale with the support of multi-spectral satellite data, e.g., from WorldView-2 [53], WorldView-3 [12], SPOT 5 [54], RapidEye [55], QuickBird MS [17], or IKONOS [17,56]. These datasets have spatial resolutions between 0.5m - 6.5m and different spectral bands (in terms of number, central wavelength and bandwidth) mainly in the visible (VIS) and near infrared (NIR) spectral range.

However, these satellite data are not freely accessible and often associated with high costs. Openly available data from Landsat or Sentinel satellites are of coarser spatial resolution and therefore capture a high amount of mixed pixel information, especially in small structured agricultural areas like in Switzerland. Furthermore,

[1] Further details can be found at http://esa-sen4cap.org/

due to fixed orbits and thus fixed observation dates, the exact observation cannot be selected freely and clouds may further limit the quality of the data. Thus, a suitable acquisition date can be missed. Since spectrally pure pixels are required for algorithm training, datasets with higher spatial resolution are necessary [31,44,57]. To this day, datasets obtained by spaceborne sensors with adequate spatial resolution are still expensive and rare.

Alternatives comprise lower flying platforms, which are able to collect data at very high spatial resolution. Remote sensing has been used to conduct such crop separation studies with airborne imaging spectrometers (IS) [58,59] or UAVs [60–62]. Although IS sensors that can be used on UAVs exist, more sophisticated sensors with very high signal-to-noise ratios are mainly operated from airborne platforms [63]. IS datasets are used in a number of agricultural applications, e.g., for soil mapping [64], biophysical properties estimation [65,66], and especially for crop separation [58,67].

Today, an increasing number of UAVs offer the possibility to collect VHR data and 3D point-clouds at a spatial resolution of only a few centimeters [68]. This also opens up new opportunities in the agricultural sector [45,69,70], for instance related to erosion of soils [71], management techniques [72], detection of individual plants [73], assessment of plant health status [43], and water stress [74]. Such datasets have also been used to provide land cover maps of a few square kilometers in agricultural areas [75].

Compared to airborne or spaceborne systems, UAVs offer the possibility to collect data in a very flexible manner [68]. Various factors such as changing weather conditions, flight planning or an optimal spatial resolution can be taken into account [68,76]. Furthermore, UAVs are cost-effective to operate compared to other carrier systems [77,78], and they need less human interaction compared to destructive data sampling methods [76].

Although today a wide range of sensors from consumer-grade cameras over multi-spectral sensors to imaging spectrometers are available for operation on UAVs, less sophisticated sensors are usually deployed [68]. Spectral calibration for demanding higher level products requires additional effort [79,80]. On the one hand, the sensors must be calibrated during operation, e.g., by using a (white) standard reference in the field [81]. On the other hand, the exact spectral behavior of the sensor bands must be known in order to derive physical quantities [82]. Consumer-grade cameras are therefore often used, as the cost of the platform and the respective sensor should be in reasonable proportion. These cameras offer red, green and blue (RGB) wavelength bands, but can be modified to contain a band that is sensitive in the near infrared (NIR) [83]. Therefore, uncalibrated datasets have the potential to allow cost-effective, user-friendly and straightforward data collection, and to support subsequent processing methodologies for crop separation in agricultural areas.

Using approaches in which all available remotely sensed datasets are jointly processed for crop classification purposes, the accuracy of crop separation has been

found to increase [16,49,50,52]. Nevertheless, small field plots require data with a high spatial resolution. To date, a combined use of IS and VHR datasets has been used mainly for land cover studies in urban areas [84].

Since VHR datasets acquired by UAVs usually have a limited number of spectral bands, the performance of purely spectral-based classifications is limited. Consequently, the inclusion of texture information contained in the VHR data has large potential for data evaluation [76,85,86]. In general, additional textural features lead to the highest improvement of the classification compared to other additional information sources such as spectral indices, multitemporal datasets, or ancillary data [87].

In order to include spatial information in the classification chain, a multitude of texture characteristics exist [88,89], e.g., gray level co-occurrence matrix (GLCM) [90], (semi-) variogram [91], or Gabor filters [92]. However, mathematical-morphological features and first-order statistics offer a straightforward alternative [93–96].

The determination of both statistical and morphological feature types is commonly based on a moving window, the so-called structuring element (SE) [94]. The shape and size of an SE are crucial, which is why they are usually pre-selected on the basis of expert knowledge. The alignment of row-shaped, elongated surface structures, such as plant rows on fields, have a strong influence on the analyzed texture in an SE. The resulting characteristic SE values are thus dependent on the angle between plant rows and SE. This applies in particular to linear, but also to rectangular SE types. Consequently, textural features are generally calculated with a disc-shaped SE to be rotationally invariant.

The size of the SE, i.e., the diameter of the disc, should correspond to the distances between plant rows. It should be noted that at least two rows of plants are observed. Consequently, the diameter in pixels of the disc-shaped SE depends on the spatial resolution of the dataset and the distance between crop rows.

1.2.3 Product generation

In principle, higher-level products can be obtained either with empirical or physical models from remote sensing data, or from other data sources. However, physical models require sufficient theoretical knowledge of the processes and relationships between the measured data and the final product. This means that in an ideal world with complete theoretical knowledge, empirical models are not required. However, when theoretical knowledge is lacking, empirical approaches, including machine learning (ML), are a valuable alternative. Moreover, ML approaches are often efficient for adapting computationally intensive physical models.

Many ML algorithms can be used for both regression and supervised or unsupervised classification. They can map the relationships between a few or literally thousands of variables. Since the algorithms learn the relationships directly from the

data, parameter training requires datasets that represent the entire parameter space in the data. Therefore, these training datasets can or must be appropriately large. ML is ideal for tackling problems for which theoretical knowledge is insufficient, but for which sufficient training data are available.

There is a wide range of algorithms and methods available for empirical classifications that are applied in remote sensing, e.g., maximum likelihood classification (MLC), support vector machine (SVM), random forest (RF), or neural nets (NN) approaches, as well as many more [89]. It has been shown that an RF approach [97] can handle a large number of features and generally leads to high classification accuracy [98].

For classification purposes, the respective dataset may be split into several spatially separated data splits. These splits are then assigned to training, parameter validation, and testing tasks. This results in different assignment possibilities of the individual splits for the different tasks, so-called folds. This guarantees that only data that have not been used for training and validation are used for classification [99]. Furthermore, it is possible to statistically compare different classification results for different parameter settings, classification algorithms, or test sites [100].

The accuracy of a classification is commonly determined based on the confusion matrix of the test data and averaged over all folds. From this the known accuracy metrics of overall accuracy (OA) [101], kappa coefficient [102], as well as user accuracy (UA) and producer accuracy (PA) [101] were calculated. OA is used very frequently and is therefore suitable for comparability with other studies [87]. In addition, the mean accuracy (AA) may be calculated, which is based on the mean value of the UA of all classes, together with the average reliability (AR), which is based on the mean value of the PA.

1.3 Thesis aims and structure

The up-to-date monitoring of individual field plots is a key issue in agricultural management and policy. To date, remote sensing can be operationally used to determine the necessary information for large-scale field plots. However, there are almost no studies exploring its potential on small-scale field plots so far. Data from uncalibrated consumer-grade cameras carried by a UAV provide a sufficiently high spatial resolution. Furthermore, the combination of IS data and additional textural features promises an improved separation of crops.

The overall aim of this thesis is to evaluate the usefulness of uncalibrated NIR-RGB VHR datasets and the influence of the observation date on the separation of crops in small structured agricultural areas. In addition, the added value of IS data as a whole, or from individual bands thereof will be of interest. The required VHR datasets from a dedicated test site on the Swiss Plateau were acquired with consumer-grade

cameras mounted on a UAV. The airborne IS data were acquired with the Airborne Prism Experiment (APEX) sensor. The specific research goals are to:

- develop a methodology to separate crops based on uncalibrated multispectral VHR data and their textural features,
- determine optimal times of data acquisition over a phenological cycle for the separation of individual crops,
- elaborate the extent to which an IS dataset or individual bands thereof improve crop separation compared to UAV multispectral data as a baseline.

1.3.1 Research questions

In this thesis the following three research questions are addressed:

1) At which spatial resolution and which spectral bands from uncalibrated UAV data can agricultural crops best be separated?

Most analyses of crop separation by remote sensing are carried out in regions with large field plots, which may not be the case for many other agricultural systems, such as in Switzerland. Spatial high-resolution data can be acquired cost-effectively using a UAV. Most UAVs have a built in consumer-grade camera. Given the fact that these UAVs are inexpensive and easy to operate, as long as no spectral calibration is necessary, it is therefore important to scientifically study their performance for a range of purposes. The question of spectral and spatial resolution is of relevance in terms of performance. On the one hand, a lower spatial resolution allows higher flight altitudes for UAVs, so that larger areas can be flown at the same time. On the other hand, lower spectral and spatial resolution results in a leaner digital processing chain. This applies to both processing time and memory requirements.

The issue of differences in spatial support (pixel- or parcel-based classification) is also addressed. In particular, we quantify the value of the additional information content of plot information from an ancillary source (e.g., field boundaries) compared to a pixel-based model.

2) What is the optimal temporal window during the growing season to separate crop types in an uncalibrated NIR-RGB dataset including textural features?

The aim related to this research question is to find an optimal time period for a single remotely sensed data acquisition. For this purpose data spanning the entire phenological cycle were collected. In order to keep the amount of data within a manageable range, individual points in time were compared to each other. A temporal window that extends over a certain period of time allows for larger operational flexibility. It is also possible to analyze at which point in time which crop types can best be distinguished from each other.

3) What is the added value of simultaneously using the spectral/textural features of a multispectral VHR drone dataset and spectral high-resolution IS data?

This question tackles the potential of data acquired by uncalibrated consumer-grade cameras on a UAV, as it can be purchased by virtually anyone nowadays, with data obtained using a well calibrated and sophisticated IS sensor. In addition, this setting can be used to investigate whether individually calibrated and spectrally well defined wavelength bands lead to a significant improvement in addition to the existing broadband NIR-RGB bands. This question is of relevance because of the increasing amount of sensors for UAVs offering both true color imaging capability and individual spectrally well-defined bands.

1.3.2 Structure of the thesis

Chapter 1 gives the background to the thesis and presents its goals and research questions.

Chapter 2 describes the general crop separation approach and the statistical evaluation of the achieved accuracies. Determination of the optimal spatial resolution of multispectral VHR data is specifically analyzed in this chapter. The first research question is evaluated in this chapter using uncalibrated NIR-RGB UAV based data.

Chapter 3 determines the optimal timing with phenology to separate crops using multispectral UAV data. The second research question is examined in this chapter.

Chapter 4 explores the potential of IS data for crop separation in combination with UAV multispectral data. In this chapter the third research question is studied.

Finally, in chapter 5 the main results of the thesis are discussed and general conclusions are drawn. An outlook on possible future research directions is given.

1.4 References

1. Gerland, P.; Raftery, A. E.; evkov, H.; Li, N.; Gu, D.; Spoorenberg, T.; Alkema, L.; Fosdick, B. K.; Chunn, J.; Lalic, N.; Bay, G.; Buettner, T.; Heilig, G. K.; Wilmoth, J. World population stabilization unlikely this century. *Science (80-.)*. **2014**, *346*, 234 LP – 237, doi:10.1126/science.1257469.
2. Tilman, D.; Balzer, C.; Hill, J.; Befort, B. L. Global food demand and the sustainable intensification of agriculture. *Proc. Natl. Acad. Sci.* **2011**, *108*, 20260 LP – 20264, doi:10.1073/pnas.1116437108.
3. FAO, F. A. O. The future of food and agriculture–Trends and challenges. *Annu. Rep.* 2017.
4. Whitcraft, A. K.; Becker-Reshef, I.; Justice, C. O. A framework for defining spatially explicit earth observation requirements for a global agricultural monitoring initiative (GEOGLAM). *Remote Sens.* **2015**, *7*, 1461–1481, doi:10.3390/rs70201461.
5. Fuhrer, J.; Gregory, P. J. *Climate Change Impact and Adaptation in Agricultural Systems*; CABI: Wallingford, 2014; ISBN 9781780642895.
6. Rosenzweig, C.; Elliott, J.; Deryng, D.; Ruane, A. C.; Müller, C.; Arneth, A.; Boote, K. J.; Folberth, C.; Glotter, M.; Khabarov, N.; Neumann, K.; Piontek, F.; Pugh, T. A. M.; Schmid, E.; Stehfest, E.; Yang, H.; Jones, J. W. Assessing agricultural risks of climate change in the 21st century in a global gridded crop model intercomparison. *Proc. Natl. Acad. Sci. U. S. A.* **2014**, *111*, 3268–73, doi:10.1073/pnas.1222463110.
7. Anderson, K.; Ryan, B.; Sonntag, W.; Kavvada, A.; Friedl, L. Earth observation in service of the 2030 Agenda for Sustainable Development. *Geo-spatial Inf. Sci.* **2017**, *20*, 77–96, doi:10.1080/10095020.2017.1333230.
8. Holloway, J.; Mengersen, K. Statistical Machine Learning Methods and Remote Sensing for Sustainable Development Goals: A Review. *Remote Sens.* **2018**, *10*, 1365, doi:10.3390/rs10091365.
9. Wheeler, T.; von Braun, J. Climate Change Impacts on Global Food Security. *Science (80-.)*. **2013**, *341*, 508 LP – 513, doi:10.1126/science.1239402.
10. Areal, F. J.; Jones, P. J.; Mortimer, S. R.; Wilson, P. Measuring sustainable intensification: Combining composite indicators and efficiency analysis to account for positive externalities in cereal production. *Land use policy* **2018**, *75*, 314–326, doi:https://doi.org/10.1016/j.landusepol.2018.04.001.
11. Weiss, M.; Jacob, F.; Duveiller, G. Remote sensing for agricultural applications: A meta-review. *Remote Sens. Environ.* **2020**, *236*, 111402, doi:10.1016/j.rse.2019.111402.
12. Palchowdhuri, Y.; Valcarce-Dieiro, R.; King, P.; Sanabria-Soto, M. Classification of multi-temporal spectral indices for crop type mapping: a case study in Coalville, UK. *J. Agric. Sci.* **2018**, *156*, 24–36,

doi:10.1017/S0021859617000879.

13. Fuhrer, J.; Tendall, D.; Klein, T.; Lehmann, N.; Holzkämper, A. Water Demand in Swiss Agriculture – Sustainable Adaptive Options for Land and Water Management to Mitigate Impacts of Climate Change. *Art-schriftenr.* **2013**, *59*.
14. Inglada, J.; Arias, M.; Tardy, B.; Hagolle, O.; Valero, S.; Morin, D.; Dedieu, G.; Sepulcre, G.; Bontemps, S.; Defourny, P.; Koetz, B. Assessment of an operational system for crop type map production using high temporal and spatial resolution satellite optical imagery. *Remote Sens.* **2015**, *7*, 12356–12379, doi:10.3390/rs70912356.
15. Immitzer, M.; Vuolo, F.; Atzberger, C. First experience with Sentinel-2 data for crop and tree species classifications in central Europe. *Remote Sens.* **2016**, *8*, doi:10.3390/rs8030166.
16. Azar, R.; Villa, P.; Stroppiana, D.; Crema, A.; Boschetti, M.; Brivio, P. A. Assessing in-season crop classification performance using satellite data: a test case in Northern Italy. *Eur. J. Remote Sens.* **2016**, *49*, 361–380, doi:10.5721/EuJRS20164920.
17. Ozdarici-Ok, A.; Ok, A.; Schindler, K. Mapping of Agricultural Crops from Single High-Resolution Multispectral Images--Data-Driven Smoothing vs. Parcel-Based Smoothing. *Remote Sens.* **2015**, *7*, 5611–5638, doi:10.3390/rs70505611.
18. Shi, Y.; Thomasson, J. A.; Murray, S. C.; Pugh, N. A.; Rooney, W. L.; Shafian, S.; Rajan, N.; Rouze, G.; Morgan, C. L. S.; Neely, H. L.; Rana, A.; Bagavathiannan, M. V; Henrickson, J.; Bowden, E.; Valasek, J.; Olsenholler, J.; Bishop, M. P.; Sheridan, R.; Putman, E. B.; Popescu, S.; Burks, T.; Cope, D.; Ibrahim, A.; McCutchen, B. F.; Baltensperger, D. D.; Avant Jr, R. V; Vidrine, M.; Yang, C. Unmanned Aerial Vehicles for High-Throughput Phenotyping and Agronomic Research. *PLoS One* **2016**, *11*, 1–26, doi:10.1371/journal.pone.0159781.
19. Tattaris, M.; Reynolds, M. P.; Chapman, S. C. A Direct Comparison of Remote Sensing Approaches for High-Throughput Phenotyping in Plant Breeding. *Front. Plant Sci.* **2016**, *7*, 1131, doi:10.3389/fpls.2016.01131.
20. Holman, F. H.; Riche, A. B.; Michalski, A.; Castle, M.; Wooster, M. J.; Hawkesford, M. J. High Throughput Field Phenotyping of Wheat Plant Height and Growth Rate in Field Plot Trials Using UAV Based Remote Sensing. *Remote Sens.* **2016**, *8*, doi:10.3390/rs8121031.
21. de Leeuw, J.; Vrieling, A.; Shee, A.; Atzberger, C.; Hadgu, K. M.; Biradar, C. M.; Keah, H.; Turvey, C. The potential and uptake of remote sensing in insurance: A review. *Remote Sens.* 2014, *6*, 10888–10912.
22. De Wit, a. J. W.; Clevers, J. G. P. W. Efficiency and accuracy of per-field classification for operational crop mapping. *Int. J. Remote Sens.* **2004**, *25*, 4091–4112, doi:10.1080/01431160310001619580.
23. Waldhoff, G.; Lussem, U.; Bareth, G. Multi-Data Approach for remote sensing-based regional crop rotation mapping: A case study for the Rur catchment, Germany. *Int. J. Appl. Earth Obs. Geoinf.* **2017**, *61*, 55–69,

doi:10.1016/j.jag.2017.04.009.
24. Bundesrat, D. S. Verordnung über die Direktzahlungen an die Landwirtschaft 2017, *2013*, 1–152.
25. Bundesamt ür Statistik *Schweizer Landwirtschaft, Taschenstatistik 2015*; Neuchâtel, 2015;
26. Long, T. B.; Blok, V.; Coninx, I. Barriers to the adoption and diffusion of technological innovations for climate-smart agriculture in Europe: Evidence from the Netherlands, France, Switzerland and Italy. *J. Clean. Prod.* **2016**, *112*, 9–21, doi:10.1016/j.jclepro.2015.06.044.
27. Swiss Federal Office for Agriculture (FOAG) *Swiss Agricultural Policy*; Berne, Switzerland, 2004;
28. Benton, T. G.; Vickery, J. A.; Wilson, J. D. Farmland biodiversity: Is habitat heterogeneity the key? *Trends Ecol. Evol.* 2003, *18*, 182–188.
29. Rembold, F.; Atzberger, C.; Savin, I.; Rojas, O. Using low resolution satellite imagery for yield prediction and yield anomaly detection. *Remote Sens.* 2013, *5*, 1704–1733.
30. Akademien der Wissenschaften Schweiz Brennpunkt Klima Schweiz. Grundlagen, Folgen, Perspektiven. *Swiss Acad. Reports* **2016**, *11*, 1–128.
31. Atzberger, C. Advances in Remote Sensing of Agriculture: Context Description, Existing Operational Monitoring Systems and Major Information Needs. *Remote Sens.* **2013**, *5*, 949–981, doi:10.3390/rs5020949.
32. Kastens, J. H.; Kastens, T. L. A.; Kastens, D. L. A.; Price, K. P.; Martinko, E. A.; Lee, R. Y. Image masking for crop yield forecasting using AVHRR NDVI time series imagery. *Remote Sens. Environ.* **2005**, *99*, 341–356, doi:10.1016/j.rse.2005.09.010.
33. Zhang, P.; Anderson, B.; Tan, B.; Huang, D.; Myneni, R. Potential monitoring of crop production using a satellite-based Climate-Variability Impact Index. *Agric. For. Meteorol.* **2005**, *132*, 344–358, doi:10.1016/j.agrformet.2005.09.004.
34. Mueller, N. D.; Gerber, J. S.; Johnston, M.; Ray, D. K.; Ramankutty, N.; Foley, J. A. Closing yield gaps through nutrient and water management. *Nature* **2012**, *490*, 254–257, doi:10.1038/nature11420.
35. Verbesselt, J.; Hyndman, R.; Newnham, G.; Culvenor, D. Detecting trend and seasonal changes in satellite image time series. *Remote Sens. Environ.* **2010**, *114*, 106–115, doi:10.1016/j.rse.2009.08.014.
36. Bgu, A.; Arvor, D.; Bellon, B.; Betbeder, J.; de Abelleyra, D.; P. D. Ferraz, R.; Lebourgeois, V.; Lelong, C.; Simes, M.; R. Vern, S.; Ferraz, R. P. D.; Lebourgeois, V.; Lelong, C.; Simes, M.; Vern, S. R. Remote sensing and cropping practices: A review. *Remote Sens.* **2018**, *10*, 1–32, doi:10.3390/rs10010099.
37. Galford, G. L.; Mustard, J. F.; Melillo, J.; Gendrin, A.; Cerri, C. C.; Cerri, C. E. P. Wavelet analysis of MODIS time series to detect expansion and intensification of row-crop agriculture in Brazil. *Remote Sens. Environ.* **2008**, *112*, 576–587, doi:10.1016/j.rse.2007.05.017.

38. Wardlow, B. D.; Egbert, S. L.; Kastens, J. H. Analysis of time-series MODIS 250 m vegetation index data for crop classification in the U.S. Central Great Plains. *Remote Sens. Environ.* **2007**, *108*, 290–310, doi:10.1016/j.rse.2006.11.021.
39. Gmez, C.; White, J. C.; Wulder, M. A. Optical remotely sensed time series data for land cover classification: A review. *ISPRS J. Photogramm. Remote Sens.* **2016**, *116*, 55–72, doi:10.1016/j.isprsjprs.2016.03.008.
40. Bontemps, S.; Defourny, P.; Radoux, J.; Van Bogaert, E.; Lamarche, C.; Achard, F.; Mayaux, P.; Boettcher, M.; Brockmann, C.; Kirches, G.; Zülkhe, M.; Kalogirou, V.; Arino, O. Consistent Global Land Cover Maps for Climate Modeling Communities: Current Achievements of the ESA's Land Cover CCI. *ESA Living Planet Symp.* **2013**, *2013*, 9–13.
41. Chen, J.; Cao, X.; Peng, S.; Ren, H. Analysis and applications of GlobeLand30: A review. *ISPRS Int. J. Geo-Information* **2017**, *6*, 230, doi:10.3390/ijgi6080230.
42. Fritz, S.; See, L.; Bayas, J. C. L.; Waldner, F.; Jacques, D.; Becker-Reshef, I.; Whitcraft, A.; Baruth, B.; Bonifacio, R.; Crutchfield, J.; Rembold, F.; Rojas, O.; Schucknecht, A.; Van der Velde, M.; Verdin, J.; Wu, B.; Yan, N.; You, L.; Gilliams, S.; Mücher, S.; Tetrault, R.; Moorthy, I.; McCallum, I. A comparison of global agricultural monitoring systems and current gaps. *Agric. Syst.* **2019**, *168*, 258–272, doi:10.1016/j.agsy.2018.05.010.
43. Yao, H.; Qin, R.; Chen, X. Unmanned Aerial Vehicle for Remote Sensing Applications—A Review. *Remote Sens.* **2019**, *11*, 1443, doi:10.3390/rs11121443.
44. Vuolo, F.; Neugebauer, N.; Bolognesi, S.; Atzberger, C.; D'Urso, G. Estimation of Leaf Area Index Using DEIMOS-1 Data: Application and Transferability of a Semi-Empirical Relationship between two Agricultural Areas. *Remote Sens.* **2013**, *5*, 1274–1291, doi:10.3390/rs5031274.
45. Maes, W. H.; Steppe, K. Perspectives for Remote Sensing with Unmanned Aerial Vehicles in Precision Agriculture. *Trends Plant Sci.* **2019**, *24*, 152–164, doi:10.1016/j.tplants.2018.11.007.
46. Pea, J. M.; Torres-Snchez, J.; de Castro, A. I.; Kelly, M.; Lpez-Granados, F. Weed Mapping in Early-Season Maize Fields Using Object-Based Analysis of Unmanned Aerial Vehicle (UAV) Images. *PLoS One* **2013**, *8*, 1–11, doi:10.1371/journal.pone.0077151.
47. Sankaran, S.; Khot, L. R.; Espinoza, C. Z.; Jarolmasjed, S.; Sathuvalli, V. R.; Vandemark, G. J.; Miklas, P. N.; Carter, A. H.; Pumphrey, M. O.; Knowles, R. R. N.; Pavek, M. J. Low-altitude, high-resolution aerial imaging systems for row and field crop phenotyping: A review. *Eur. J. Agron.* **2015**, *70*, 112–123, doi:10.1016/j.eja.2015.07.004.
48. Burke, M.; Lobell, D. B. Satellite-based assessment of yield variation and its determinants in smallholder African systems. *Proc. Natl. Acad. Sci.* **2017**, *114*, 2189–2194, doi:10.1073/pnas.1616919114.
49. Zhong, L.; Hu, L.; Zhou, H. Deep learning based multi-temporal crop classification. *Remote Sens. Environ.* **2019**, *221*, 430–443, doi:10.1016/j.rse.2018.11.032.

50. Ouzemou, J.-E.; El Harti, A.; Lhissou, R.; El Moujahid, A.; Bouch, N.; El Ouazzani, R.; Bachaoui, E. M.; El Ghmari, A. Crop type mapping from pan-sharpened Landsat 8 NDVI data: A case of a highly fragmented and intensive agricultural system. *Remote Sens. Appl. Soc. Environ.* **2018**, *11*, 94–103, doi:10.1016/J.RSASE.2018.05.002.
51. Löw, F.; Duveiller, G. Defining the spatial resolution requirements for crop identification using optical remote sensing. *Remote Sens.* **2014**, *6*, 9034–9063, doi:10.3390/rs6099034.
52. Conrad, C.; Dech, S.; Dubovyk, O.; Fritsch, S.; Klein, D.; Löw, F.; Schorcht, G.; Zeidler, J. Derivation of temporal windows for accurate crop discrimination in heterogeneous croplands of Uzbekistan using multitemporal RapidEye images. *Comput. Electron. Agric.* **2014**, *103*, 63–74, doi:10.1016/j.compag.2014.02.003.
53. Debats, S. R.; Luo, D.; Estes, L. D.; Fuchs, T. J.; Caylor, K. K. A generalized computer vision approach to mapping crop fields in heterogeneous agricultural landscapes. *Remote Sens. Environ.* **2016**, *179*, 210–221, doi:10.1016/j.rse.2016.03.010.
54. Topaloglou, C. A.; Mylonas, S. K.; Stavrakoudis, D. G.; Mastorocostas, P. A.; Theocharis, J. B. Accurate crop classification using hierarchical genetic fuzzy rule-based systems. In *Proceedings of SPIE - The International Society for Optical Engineering*; 2014; Vol. 9239.
55. Zhang, H.; Li, Q.; Liu, J.; Shang, J.; Du, X.; McNairn, H.; Champagne, C.; Dong, T.; Liu, M. Image Classification Using RapidEye Data: Integration of Spectral and Textual Features in a Random Forest Classifier. *IEEE J. Sel. Top. Appl. Earth Obs. Remote Sens.* **2017**, *10*, 5334–5349, doi:10.1109/JSTARS.2017.2774807.
56. Helmholz, P.; Rottensteiner, F.; Heipke, C. Semi-automatic verification of cropland and grassland using very high resolution mono-temporal satellite images. *ISPRS J. Photogramm. Remote Sens.* **2014**, *97*, 204–218, doi:10.1016/j.isprsjprs.2014.09.008.
57. Whitcraft, A. K.; Becker-Reshef, I.; Killough, B. D.; Justice, C. O. Meeting earth observation requirements for global agricultural monitoring: An evaluation of the revisit capabilities of current and planned moderate resolution optical earth observing missions. *Remote Sens.* **2015**, *7*, 1482–1503, doi:10.3390/rs70201482.
58. Aneece, I.; Thenkabail, P. Accuracies Achieved in Classifying Five Leading World Crop Types and their Growth Stages Using Optimal Earth Observing-1 Hyperion Hyperspectral Narrowbands on Google Earth Engine. *Remote Sens.* **2018**, *10*, 2027, doi:10.3390/rs10122027.
59. Thenkabail, P. S.; Gumma, M. K.; Teluguntla, P.; Mohammed, I. A. Hyperspectral remote sensing of vegetation and agricultural crops. *Photogramm. Eng. Remote Sensing* **2014**, *80*, 697–709, doi:10.1201/b11222-41.
60. Zhang, J.; Zhao, Y.; Abbott, A. L.; Wynne, R. H.; Hu, Z.; Zou, Y.; Tian, S. Automated mapping of typical cropland strips in the North China Plain using

small Unmanned Aircraft Systems (sUAS) photogrammetry. *Remote Sens.* **2019**, *11*, doi:10.3390/rs11202343.

61. Zhao, L.; Shi, Y.; Liu, B.; Hovis, C.; Duan, Y.; Shi, Z. Finer Classification of Crops by Fusing UAV Images and Sentinel-2A Data. *Remote Sens.* **2019**, *11*, 3012, doi:10.3390/rs11243012.
62. Yan, Y.; Deng, D.; Liu, L.; Zhu, Z. Application of UAV-Based Multi-Angle Hyperspectral Remote Sensing in Fine Vegetation Classification. *Remote Sens.* **2019**, *11*, 2753, doi:10.3390/rs11232753.
63. Aasen, H.; Honkavaara, E.; Lucieer, A.; Zarco-Tejada, P. Quantitative Remote Sensing at Ultra-High Resolution with UAV Spectroscopy: A Review of Sensor Technology, Measurement Procedures, and Data Correction Workflows. *Remote Sens.* **2018**, *10*, 1091, doi:10.3390/rs10071091.
64. Diek, S.; Chabrillat, S.; Nocita, M.; Schaepman, M. E.; de Jong, R. Minimizing soil moisture variations in multi-temporal airborne imaging spectrometer data for digital soil mapping. *Geoderma* **2019**, *337*, 607–621, doi:10.1016/j.geoderma.2018.09.052.
65. Thenkabail, P. S.; Mariotto, I.; Gumma, M. K.; Middleton, E. M.; Landis, D. R.; Huemmrich, K. F. Selection of hyperspectral narrowbands (hnbs) and composition of hyperspectral twoband vegetation indices (HVIS) for biophysical characterization and discrimination of crop types using field reflectance and hyperion/EO-1 data. *IEEE J. Sel. Top. Appl. Earth Obs. Remote Sens.* **2013**, *6*, 427–439, doi:10.1109/JSTARS.2013.2252601.
66. Hank, T. B.; Berger, K.; Bach, H.; Clevers, J. G. P. W.; Gitelson, A.; Zarco-Tejada, P.; Mauser, W. Spaceborne Imaging Spectroscopy for Sustainable Agriculture: Contributions and Challenges. *Surv. Geophys.* **2019**, *40*, 515–551, doi:10.1007/s10712-018-9492-0.
67. Marshall, M.; Thenkabail, P. Advantage of hyperspectral EO-1 Hyperion over multispectral IKONOS, GeoEye-1, WorldView-2, Landsat ETM+, and MODIS vegetation indices in crop biomass estimation. *ISPRS J. Photogramm. Remote Sens.* **2015**, *108*, 205–218, doi:10.1016/j.isprsjprs.2015.08.001.
68. Pajares, G. Overview and Current Status of Remote Sensing Applications Based on Unmanned Aerial Vehicles (UAVs). *Photogramm. Eng. Remote Sens.* **2015**, *81*, 281–330, doi:10.14358/PERS.81.4.281.
69. Manfreda, S.; Matthew F Mccabe; Pauline E Miller; Lucas, R.; Pajuelo, V. M.; Mallinis, G.; Dor, E. Ben; David Helman; Estes, L.; Ciraolo, G.; Müllerov, J.; Tauro, F.; de Lima, M. I.; de Lima, J. L. M. P.; Maltese, A.; Frances, F.; Caylor, K.; Kohv, M.; Perks, M.; Ruiz-Prez, G.; Su, Z.; Vico, G.; Toth, B. On the Use of Unmanned Aerial Systems for Environmental Monitoring. *Remote Sens.* **2018**, *10(4)*, 641, doi:10.3390/rs10040641.
70. Ado, T.; Hruka, J.; Pdua, L.; Bessa, J.; Peres, E.; Morais, R.; Sousa, J. J. Hyperspectral imaging: A review on UAV-based sensors, data processing

and applications for agriculture and forestry. *Remote Sens.* **2017**, *9*, 1110, doi:10.3390/rs9111110.

71. Glendell, M.; McShane, G.; Farrow, L.; James, M. R.; Quinton, J.; Anderson, K.; Evans, M.; Benaud, P.; Rawlins, B.; Morgan, D.; Jones, L.; Kirkham, M.; DeBell, L.; Quine, T. A.; Lark, M.; Rickson, J.; Brazier, R. E. Testing the utility of structure-from-motion photogrammetry reconstructions using small unmanned aerial vehicles and ground photography to estimate the extent of upland soil erosion. *Earth Surf. Process. Landforms* **2017**, *42*, 1860–1871, doi:10.1002/esp.4142.
72. Ashapure, A.; Jung, J.; Yeom, J.; Chang, A.; Maeda, M.; Maeda, A.; Landivar, J. A novel framework to detect conventional tillage and no-tillage cropping system effect on cotton growth and development using multi-temporal UAS data. *ISPRS J. Photogramm. Remote Sens.* **2019**, *152*, 49–64, doi:10.1016/j.isprsjprs.2019.04.003.
73. Primicerio, J.; Caruso, G.; Comba, L.; Crisci, A.; Gay, P.; Guidoni, S.; Genesio, L.; Aimonino, D. R.; Vaccari, F. P.; Ricauda Aimonino, D.; Vaccari, F. P. Individual plant definition and missing plant characterization in vineyards from high-resolution UAV imagery. *Eur. J. Remote Sens.* **2017**, *50*, 179–186, doi:10.1080/22797254.2017.1308234.
74. Zarco-Tejada, P. J.; Gonzlez-Dugo, V.; Berni, J. A. J. Fluorescence, temperature and narrow-band indices acquired from a UAV platform for water stress detection using a micro-hyperspectral imager and a thermal camera. *Remote Sens. Environ.* **2012**, *117*, 322–337, doi:10.1016/j.rse.2011.10.007.
75. Ahmed, O. S.; Shemrock, A.; Chabot, D.; Dillon, C.; Williams, G.; Wasson, R.; Franklin, S. E. Hierarchical land cover and vegetation classification using multispectral data acquired from an unmanned aerial vehicle. *Int. J. Remote Sens.* **2017**, *38*, 2037–2052, doi:10.1080/01431161.2017.1294781.
76. Whitehead, K.; Hugenholtz, C. H.; Myshak, S.; Brown, O.; LeClair, A.; Tamminga, A.; Barchyn, T. E.; Moorman, B.; Eaton, B. Remote sensing of the environment with small unmanned aircraft systems (UASs), part 1: a review of progress and challenges. *J. Unmanned Veh. Syst.* **2014**, *02*, 86–102, doi:10.1139/juvs-2014-0006.
77. Colomina, I.; Molina, P. Unmanned aerial systems for photogrammetry and remote sensing: A review. *ISPRS J. Photogramm. Remote Sens.* **2014**, *92*, 79–97, doi:10.1016/j.isprsjprs.2014.02.013.
78. Hugenholtz, C. H.; Moorman, B. J.; Riddell, K.; Whitehead, K. Small unmanned aircraft systems for remote sensing and Earth science research. *Eos, Trans. Am. Geophys. Union* **2012**, *93*, 236, doi:10.1029/2012EO250005.
79. Kelcey, J.; Lucieer, A. Sensor correction and radiometric calibration of a 6-band multispectral imaging sensor for UAV remote sensing. In *The 12th Congress of the International Society for Photogrammetry and Remote Sensing*; 2012; Vol. 39, pp. 393–398.

80. Lu, B.; He, Y. Species classification using Unmanned Aerial Vehicle (UAV)-acquired high spatial resolution imagery in a heterogeneous grassland. *ISPRS J. Photogramm. Remote Sens.* **2017**, *128*, 73–85, doi:10.1016/j.isprsjprs.2017.03.011.
81. Hueni, A.; Damm, A.; Kneubuehler, M.; Schläpfer, D.; Schaepman, M. E. Field and Airborne Spectroscopy Cross Validation - Some Considerations. *IEEE J. Sel. Top. Appl. Earth Obs. Remote Sens.* **2017**, *10*, 1117–1135, doi:10.1109/JSTARS.2016.2593984.
82. Del Pozo, S.; Rodrguez-Gonzlvez, P.; Hernndez-Lpez, D.; Felipe-Garca, B. Vicarious Radiometric Calibration of a Multispectral Camera on Board an Unmanned Aerial System. *Remote Sens.* 2014, *6*.
83. Zhang, J.; Yang, C.; Song, H.; Hoffmann, W. C.; Zhang, D.; Zhang, G. Evaluation of an Airborne Remote Sensing Platform Consisting of Two Consumer-Grade Cameras for Crop Identification. *Remote Sens.* **2016**, *8*, 257, doi:10.3390/rs8030257.
84. Gamba, P.; Dell'Acqua, F. 18 Spectral Resolution in the Context of Very High Resolution Urban Remote Sensing. In *Urban remote sensing*; Weng, Q., Quattrochi, D., Gamba, P. E., Eds.; CRC Press: Boca Raton, FL, USA, 2018; p. 377.
85. Laliberte, A. S.; Rango, A. Texture and Scale in Object-Based Analysis of Subdecimeter Resolution Unmanned Aerial Vehicle (UAV) Imagery. *IEEE Trans. Geosci. Remote Sens.* **2009**, *47*, 761–770, doi:10.1109/TGRS.2008.2009355.
86. Marcos, D.; Volpi, M.; Kellenberger, B.; Tuia, D. Land cover mapping at very high resolution with rotation equivariant CNNs: Towards small yet accurate models. *ISPRS J. Photogramm. Remote Sens.* **2018**, *in Press*, doi:10.1016/j.isprsjprs.2018.01.021.
87. Khatami, R.; Mountrakis, G.; Stehman, S. V. A meta-analysis of remote sensing research on supervised pixel-based land-cover image classification processes: General guidelines for practitioners and future research. *Remote Sens. Environ.* **2016**, *177*, 89–100, doi:10.1016/j.rse.2016.02.028.
88. Moser, G.; Serpico, S. B.; Benediktsson, J. A. Land-Cover Mapping by Markov Modeling of Spatial-Contextual Information in Very-High-Resolution Remote Sensing Images. *Proc. IEEE* 2013, *101*, 631–651.
89. Camps-Valls, G.; Tuia, D.; Bruzzone, L.; Benediktsson, J. A. Advances in Hyperspectral Image Classification: Earth Monitoring with Statistical Learning Methods. *Signal Process. Mag. IEEE* **2014**, *31*, 45–54, doi:10.1109/MSP.2013.2279179.
90. Haralick, R. M.; Shanmugam, K.; Dinstein, I. Textural Features for Image Classification. *Syst. Man Cybern. IEEE Trans.* **1973**, *SMC-3*, 610–621, doi:10.1109/TSMC.1973.4309314.

91. Woodcock, C. E.; Strahler, A. H.; Jupp, D. L. B. The use of variograms in remote sensing: I. Scene models and simulated images. *Remote Sens. Environ.* **1988**, *25*, 323–348, doi:http://dx.doi.org/10.1016/0034-4257(88)90108-3.
92. Gabor, D. Theory of communication. Part 1: The analysis of information. *J. Inst. Electr. Eng. - Part III Radio Commun. Eng.* **1946**, *93*, 429–441, doi:10.1049/ji-3-2.1946.0074.
93. Soille, P. *Morphological Image Analysis*; Springer Berlin Heidelberg: Berlin, Heidelberg, 2004; ISBN 978-3-642-07696-1.
94. Fauvel, M.; Tarabalka, Y.; Benediktsson, J. A.; Chanussot, J.; Tilton, J. C. Advances in Spectral-Spatial Classification of Hyperspectral Images. *Proc. IEEE* 2013, *101*, 652–675.
95. Tuia, D.; Pacifici, F.; Kanevski, M.; Emery, W. J. Classification of Very High Spatial Resolution Imagery Using Mathematical Morphology and Support Vector Machines. *IEEE Trans. Geosci. Remote Sens.* **2009**, *47*, 3866–3879, doi:10.1109/TGRS.2009.2027895.
96. Vincent, L. Morphological Grayscale Reconstruction in Image Analysis: Applications and Efficient Algorithms. *IEEE Trans. Image Process.* **1993**, *2*, 176–201, doi:10.1109/83.217222.
97. Breiman, L. Random Forests. *Mach. Learn.* **2001**, *45*, 5–32, doi:10.1023/A:1010933404324.
98. Fernndez-Delgado, M.; Cernadas, E.; Barro, S.; Amorim, D. Do we Need Hundreds of Classifiers to Solve Real World Classification Problems? *J. Mach. Learn. Res.* **2014**, *15*, 3133–3181.
99. Lyons, M. B.; Keith, D. A.; Phinn, S. R.; Mason, T. J.; Elith, J. A comparison of resampling methods for remote sensing classification and accuracy assessment. *Remote Sens. Environ.* **2018**, *208*, 145–153, doi:10.1016/j.rse.2018.02.026.
100. Böhler, J.; Schaepman, M.; Kneubühler, M. Crop Classification in a Heterogeneous Arable Landscape Using Uncalibrated UAV Data. *Remote Sens.* **2018**, *10*, doi:10.3390/rs10081282.
101. Congalton, R. *Assessing the Accuracy of Remotely Sensed Data*; Mapping Science; CRC Press, 2008; ISBN 978-1-4200-5512-2.
102. Cohen, J. Weighted kappa: Nominal scale agreement provision for scaled disagreement or partial credit. *Psychol. Bull.* 1968, *70*, 213–220.

Chapter

2

Crop Classification in a Heterogeneous Arable Landscape Using Uncalibrated UAV Data

This chapter is based on the peer-reviewed article:
***Böhler, J. E.**, Schaepman, M. E., Kneubühler, M. (2018) Crop Classification in a Heterogeneous Arable Landscape Using Uncalibrated UAV Data. Remote Sensing, 10(8), 1282. DOI:0.3390/rs10081282*

J.E.B. designed the research and analyzed the data with scientific advice of M.K. and M.E.S., J.E.B. wrote the manuscript and all co-authors thoroughly reviewed and edited the manuscript.

remote sensing

MDPI

Article

Crop Classification in a Heterogeneous Arable Landscape Using Uncalibrated UAV Data

Jonas E. Böhler *, Michael E. Schaepman and Mathias Kneubühler

Department of Geography, Remote Sensing Laboratories (RSL), University of Zürich, Winterthurerstrasse 190, 8057 Zürich, Switzerland; michael.schaepman@geo.uzh.ch (M.E.S.); mathias.kneubuehler@geo.uzh.ch (M.K.)
* Correspondence: jonas.boehler@geo.uzh.ch; Tel.: +41-446-355-249

Received: 22 June 2018; Accepted: 10 August 2018; Published: 14 August 2018

Abstract: Land cover maps are indispensable for decision making, monitoring, and management in agricultural areas, but they are often only available after harvesting. To obtain a timely crop map of a small-scale arable landscape in the Swiss Plateau, we acquired uncalibrated, very high-resolution data, with a spatial resolution of 0.05 m and four spectral bands, using a consumer-grade camera on an unmanned aerial vehicle (UAV) in June 2015. We resampled the data to different spatial and spectral resolutions, and evaluated the method using textural features (first order statistics and mathematical morphology), a random forest classifier for best performance, as well as number and size of the structuring elements. Our main findings suggest the overall best performing data consisting of a spatial resolution of 0.5 m, three spectral bands (RGB—red, green, and blue), and five different sizes of the structuring elements. The overall accuracy (OA) for the full set of crop classes based on a pixel-based classification is 66.7%. In case of a merged set of crops, the OA increases by ~7% (74.0%). For an object-based classification based on individual field parcels, the OA increases by ~20% (OA of 86.3% for the full set of crop classes, and 94.6% for the merged set, respectively). We conclude the use of UAV to be most relevant at 0.5 m spatial resolution in heterogeneous arable landscapes when used for crop classification.

Keywords: consumer-grade camera; land cover; very high resolution (VHR); random forest (RF) classifier; object-based classification; pixel-based classification; small-scaled agricultural fields; texture; spatial feature

1. Introduction

Agriculture reacts very sensitively to climate change [1]. Since the world population is expected to grow to 9.6 billion by the year 2050 [2], global food demand is increasing [3], and therefore, the availability of accurate and timely information about agriculture on a global [4], as well as on a local scale, is essential [5] to ensure that a growing world population can be fed. In order to address the problems of food insecurity or the volatility of the food market, remote sensing technologies provide a wide range of opportunities to assess these challenges [4,6].

Numerous aspects in agriculture and agronomy have been addressed for years with the support of remote sensing [6]. Among others are estimation of yield [7], biomass [8], seasonal plant development and stress monitoring [9,10], phenology and vigor [11], and land cover or land use change [12,13].

Accurate land cover assessments form the basis for such analyses in agricultural areas [14], and are particularly important for planning of water resources [15], automated short-term monitoring for yield estimation [16], sustainable land management [17], crop modeling before the end of season [18], or plot extraction for high-throughput phenotyping [19–21]. Further, current conditions and extent of land cover are needed as a basis for climate change modeling [22]. Often, information about arable land

cover is only available in administrative units, while detailed information on spatial distribution is lacking [23] or not accessible to the general public for reasons of data protection regulations [24].

In Switzerland, the agricultural landscape is mainly characterized by small structured farmland [25]. Support of farmers through direct payments plays a key role in Swiss agricultural policy. In 1996, the policy was changed from underwriting guarantee for most of the agricultural products towards compensation for provided services [26]. Today, the focus of direct payments to farmers in Switzerland is aligned with preservation of the cultural landscape, ensuring food supplies, sustainable production, enrichment of biodiversity, and contributions to the quality of the landscape. Small-scale subdivision of the arable area into portions of different crops guarantees an attractive landscape and fosters biodiversity [26,27]. Finally, direct payments are based on acreage, compensation for hilly terrain, individual crop plants, and their respective combinations [28]. Contributions for specific crops are paid, among others, for oilseed and sugar beet, while different types of cereals are not of specific interest.

The respective reporting is so far based on self-declaration, and likewise, the controlling is based on field visits. Accurate verification of crop types is important for subsidy control, to monitor biodiversity relevant land management practices, like crop rotation, soil protection and sustainable application of fertilizer, and to link up protected areas and ecological compensation areas [26].

Sharing information from reporting and controlling is often time consuming, and not straightforward. This is critical when it comes to the need for early warning [11], e.g., in case of water shortage, when sustainable planning is necessary [15]. Future predictions by climate models indicate that water will become a limited resource in Switzerland, as well [22,29]. Since water need for irrigation is crop dependent, accurate and timely information on crop allocation and acreage is required for planning purposes.

With the agricultural landscape in Switzerland being small structured, data of spatially very high resolution (VHR) are required to derive crop type and field extent [4,6,30]. Common sensors that acquire VHR data usually have the disadvantage of a limited number of spectral bands, which limits their capability when applying purely spectrally based classifications. Consequently, the incorporation of texture information contained in VHR data bears potential in data analysis [31–33]. In general, additional textural features result in the highest improvement of classification compared to other additional information sources like ancillary data, multitemporal datasets, or spectral indices [34].

Multispectral satellite data, e.g., stemming from RapidEye [35], SPOT 5 [36], QuickBird MS [16], IKONOS [16,37], WorldView-2 [38], or WorldView-3 [14], have been widely used to assess land cover in agricultural areas. These datasets have typical spatial resolutions between 0.5 m–6.5 m, and varying spectral bands (in terms of number, center wavelength and band width) mainly in the visible (VIS) and near-infrared (NIR) spectral range.

Nowadays, an increasing number of unmanned aerial vehicles (UAVs) provide the possibility to acquire VHR data. With such systems, it is possible to flexibly record data in an optimal spatial resolution. For agricultural mapping of small-scaled fields, a spatial resolution between 0.5 m–3 m is suggested to assess the infield variability [39]. Operating UAVs enables customized data acquisition in support of the definition and implementation of a dedicated processing chain for subsequent product generation.

Typical application fields of UAVs comprise vegetation, environmental, urban, or disaster monitoring [40], as well as precision agriculture, land cover mapping, and rangeland monitoring in the agricultural sector [41]. VHR data derived with a UAV have been used to determine land cover of small agricultural areas up to a few square kilometers [42]. Compared to satellite or airborne data acquisitions, UAVs are less expensive to operate [43,44], data acquisition needs less human interaction compared to destructive measurement methods [33], and is more flexible concerning weather conditions and flight planning [33,40]. Constraints are imposed by weather (e.g., rain and wind) and unfavorable solar illumination conditions. Nevertheless, since UAVs are usually operated at low flight altitude, data acquisition is also possible under cloudy conditions. In some countries, legal

restrictions for operating UAVs apply [43,45,46]. Apart from that, UAV data acquisition is more flexible throughout the day and not limited by given revisit times, as in the case of satellites, or potential flight restrictions with larger airborne platforms.

Although a wide range of sensors, ranging from consumer-grade cameras over multispectral sensors to imaging spectrometers [40], is available for UAVs today, their spectral calibration for sophisticated higher-level products requires additional effort [47,48]. On the one hand, sensors need to be calibrated while operated, e.g., by deploying a standard (white) reference in the field [49]. On the other hand, the exact spectral behavior of the sensor spectral bands must be known to eventually derive physical quantities [50].

In our study, we used a VHR dataset acquired with two uncalibrated consumer-grade cameras carried by a UAV for crop classification. While one camera captured the common red, green, and blue (RGB) bands, the other one recorded data with near-infrared, green, and blue (NirGB) bands. The data of the two cameras were combined into a NirRGB dataset. We present a novel method combining spectral and textural information to classify agricultural crops in a typical small structured arable landscape in the Swiss Plateau, using a random forest (RF) classifier [51] and VHR data from uncalibrated consumer-grade cameras. In this study, we analyze the influence of (i) spatial resolution, (ii) choice of spectral bands, and (iii) number of textural features, i.e., different sizes of the structuring element (SE), on the classification accuracy on a per-pixel basis and on the level of aggregated parcels.

2. Material

2.1. Study Area

The study area is situated in the Swiss Plateau within the Canton of Zurich (47.312°N, 8.733°E), Switzerland (Figure 1). The rural area is mainly covered by cropland and grassland. The elevation of the test site varies between 440 m–570 m above sea level (a.s.l.) and the climate can be described as warm temperate humid, with a yearly mean temperature around 9.3 °C and annual precipitation around 1134 mm [52]. Soils comprise mainly clay loam or loam, and Cambisol [53].

The predominant crop types in the study area are maize, sugar beet, and winter wheat (Table 1). Grassland comprises perennial (permanent) and annual (i.e., temporary) cover. Fields that were covered with hay during data acquisition and pure clover were treated as separate classes. The few and small spelt and winter barley fields were also taken into account. Rapeseed fields covered a minor area, and the bare soil fields were later planted with maize. Crop types present on less than three fields in the study area were excluded from our study. Additionally, the individual crop classes were grouped into generalized, merged classes to assess the performance of the subsequent classification (Table 1). Winter wheat, winter barley, and spelt were combined to cereals, the grassland class was merged with clover, and maize was extended to include pure soils, since maize was grown on these plots later during the year. Hay-covered fields were eventually excluded from our analysis, due to their heterogeneous appearance.

Remote Sens. **2018**, *10*, 1282

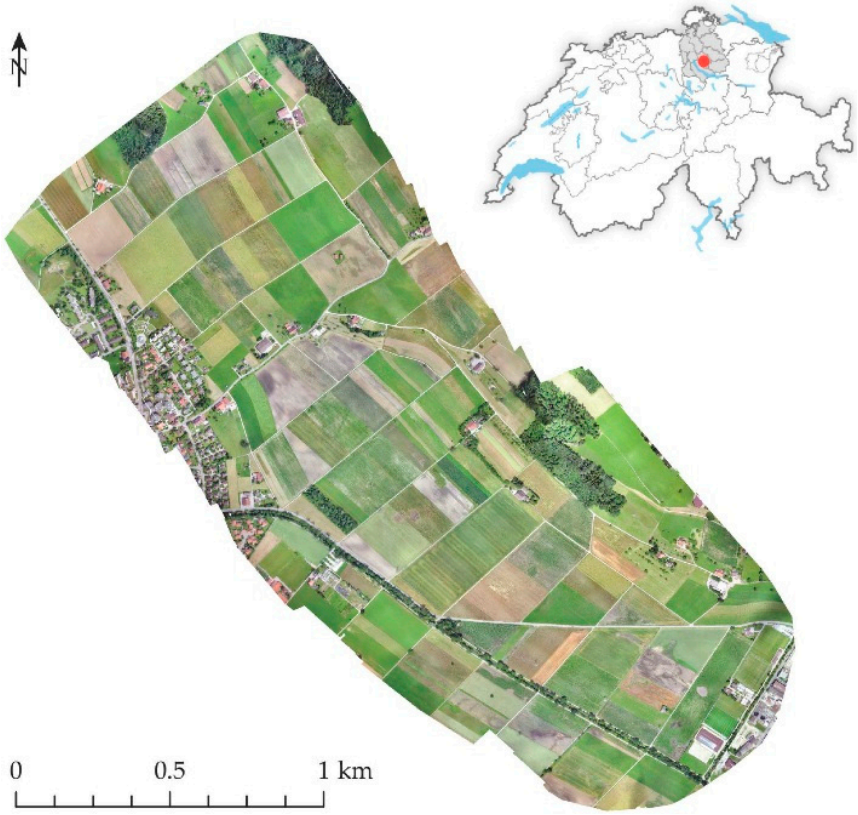

Figure 1. Outline of the study area (near Mönchaltorf, Switzerland). (See overview map of Switzerland, top right) in the Canton of Zurich, acquired with a spatial resolution of 0.05 m using a consumer-grade RGB (red, green, and blue) camera mounted on an unmanned aerial vehicle (UAV).

Table 1. Crop classes present in the study area and their respective field characteristics.

Crop Class		Total Area (ha)	Number of Fields	Spacing		Phenology (BBCH)
Full Set	Merged Set			Within-Row (cm)	Row (cm)	
Maize	Maize	19.6	15	14-16	75	0–33
Bare Soil		7.4	5	-	-	-
Sugar Beet	Sugar Beet	14.1	7	16	50	39
Winter Wheat	Cereals	24.4	13	5	14–15	75
Spelt		2.6	3	5	14–15	75
Winter Barley		2.5	3	5	14–15	99
Grassland	Grassland	15.0	17	-	-	-
Clover		5.4	3	-	10.5	-
Grass Hay	Excluded	3.6	5	-	-	-
Rapeseed	Rapeseed	7.6	6	10	30	80

2.2. Dataset

The entire study area comprises an extent of 170 ha, whereof 102 ha were taken into account. Data acquisition took place between 11:00–13:45 local time on 26 June 2015 in four flights of 30 min each. At this time of the year, all investigated crop types were present. The agricultural fields have an average size of 1.3 ha, ranging from 0.03 ha to 7.4 ha, with lengths of 140 m–200 m and widths of 23 m–180 m. Two larger fields have an extent of 183 $\times$ 437 m^2 (8 ha) and 465 $\times$ 87 m^2 (4 ha).

At the end of June 2015, the various crops were in different phenological stages. We determined the phenological code based on "Biologische Bundesanstalt, Bundessortenamt und CHemische Industrie"

(BBCH) [54] by non-destructive field inspections. Cereals were in maturity stage, with winter wheat and spelt in milk-ripe stage (BBCH 75), and winter barley in senescence (ready for harvest, BBCH 99). Maize included freshly sown to stem elongation stages (BBCH 0–33), rapeseed was just at the beginning of ripening (BBCH 80), and sugar beets had reached complete soil cover (BBCH 39). For grassland and clover, the exact phenological stages were not determined, since they were subject to a range of differing management. The phenological stages of pastures were heterogeneous due to grazing, whereas in the case of perennial and annual grasslands, phenological differences were linked to differing cutting strategies, reaching from complete mowing of the entire field to daily cuts of small parts for fresh forage.

Data acquisition was performed under clear sky conditions with a few condensation trails present. As the typical flight time of the deployed eBee UAV (Sensefly, Cheseaux-Lausanne, Switzerland) is limited to approximately 30 min, the total study area was divided into two parts in order for each subarea to be recorded in a single flight. For each subarea, both a 16.1 megapixel Canon IXUS 125HS camera with red, green, and blue (RGB) bands (center wavelengths at 660, 520, and 450 nm) and a modified camera of the same type with near infrared (NIR), green, and blue (NirGB) bands (center wavelengths at 720, 520, and 450 nm) were used consecutively. Flight planning and subsequent image acquisition were performed using the eMotion2 software (Sensefly, Cheseaux-Lausanne, Switzerland). The flight altitude was 150 m above ground, resulting in a spatial resolution of approximately 0.05 m. The images were acquired in parallel flight paths with a lateral overlap of 60% and a longitudinal overlap of 75%.

A total of 1092 single images were geo-tagged based on their respective GPS and IMU measurements on board the UAV during flight. The images were subsequently processed in Pix4D Mapper (Pix4D SA, Lausanne, Switzerland). The software uses the structure from motion (SfM) technique to generate a dense point cloud, a digital elevation model, and a mosaicked and rectified image product with a predefined spatial resolution of 0.05 m. During processing, five ground control points (GCP) that were measured with a differential GPS (dGPS) device on the ground were added for improved geo-rectification of the camera-wise image mosaics. The RGB mosaic and the NIR band was eventually stacked together with the RGB bands of the RGB camera, resulting in a VHR dataset consisting of four bands.

A crop type reference dataset of the study area was built based on a concurrent field survey and identified parcel boundaries (Figure 2). In order to avoid mixing effects at field borders, a buffer of 2 m was applied for classification training and validation (see Section 3).

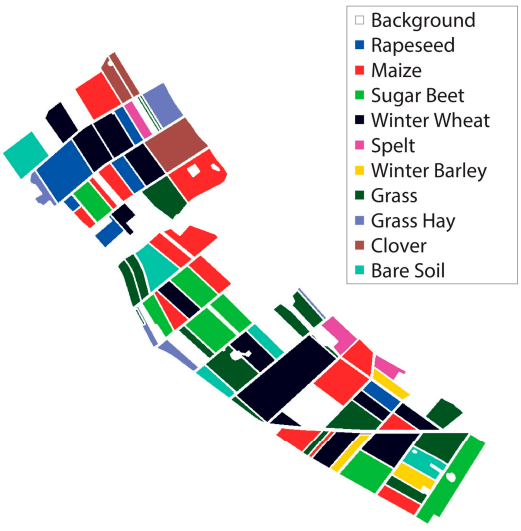

Figure 2. Reference map for all crop classes.

Remote Sens. **2018**, *10*, 1282

3. Method

We applied a robust classification and accuracy assessment workflow that consists of several steps (Figure 3). First, the VHR dataset was resampled to a range of spatial resolutions from which textural features were subsequently extracted. The features of these datasets were compiled to six different settings, based on spectral properties and amount of SE sizes. The data of these settings were then split into three parts for (i) training of the random forest (RF) model, (ii) validation of the model parameters, and (iii) testing of the final model classification performance. For the classification, we used an RF approach [51], having been widely used in previous studies and successfully applied [55]. The validated classification model was eventually applied to the test dataset, and an accuracy assessment was performed on both spatial supports (i.e., pixel- and parcel-based classification). The individual steps of our approach are described in detail below.

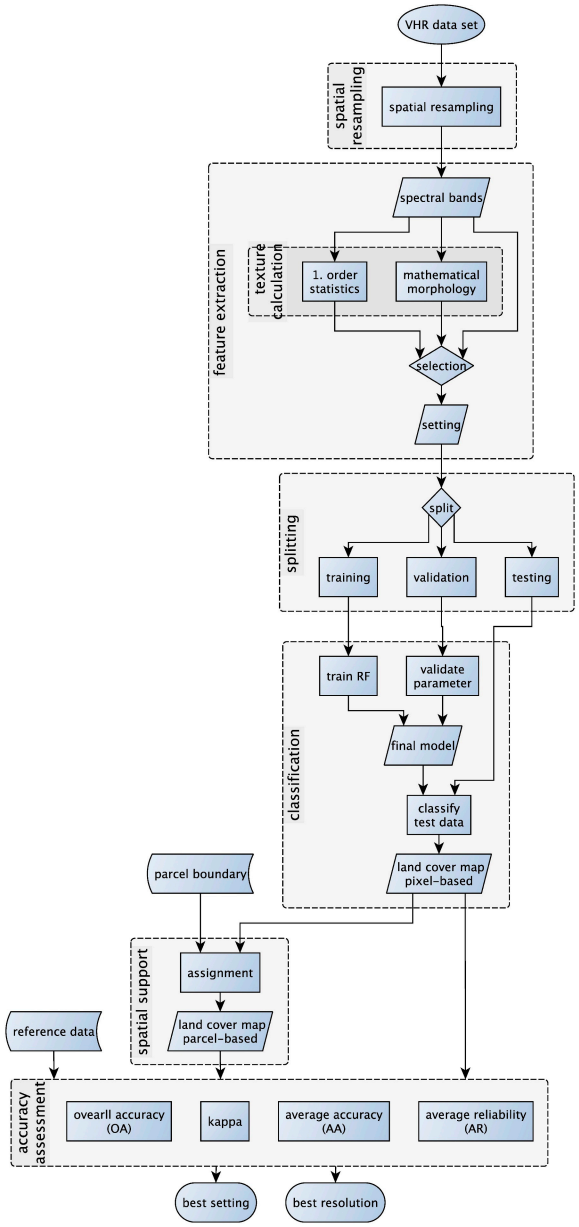

Figure 3. Flowchart of the method.

3.1. Resampling

To evaluate the influence of the spatial resolution on the classification accuracy, we resampled the VHR dataset to 0.1 m, 0.25 m, 0.5 m, 0.75 m, 1 m, and 2 m using a bicubic transformation. The reference dataset was resampled to the same spatial resolutions by applying a nearest neighbor method.

3.2. Feature Extraction

In order to incorporate spatial information into the classification chain, two types of textual features, i.e., first-order statistics and mathematical morphology, were calculated. The following statistical characteristics were used: mean, standard deviation, range, and entropy. Morphological operations comprised dilatation/erosion, opening/closing, opening/closing top hat, opening/closing by reconstruction, and opening/closing by reconstruction top hat [56–59]. The respective formulas can be found in Table 2.

These features were calculated based on a SE, i.e., a moving window. Since its shape and size are decisive, an SE is usually pre-selected based on expert knowledge. With some agricultural crops (in particular maize and sugar beet) in our dataset being cultivated in rows, their orientation has a major impact on the analyzed texture in an SE. Consequently, resulting feature values depend on the angle between plant rows and SE, especially in the case of a linear, but also a rectangular SE. To be rotation-invariant, all features were calculated in a disk-shaped SE.

The SE size, i.e., the diameter of the disk, was selected according to the measured distances between the plant rows in the study area, with the goal to include at least two rows of plants, in case of 5 cm spatial resolution. The distance between two rows for clover was 10.5 cm, for cereals 14 cm–15 cm, for rapeseed 30 cm, for sugar beet 50 cm, and for maize 75 cm (Table 1). To assess the texture of at least two crop rows, diameters of 3, 5, 9, 13, and 29 pixels were thus chosen as SE sizes. We applied the same SE sizes to all spatially resampled datasets.

For the subsequent analysis, six combinations of spectral bands and amount of SE sizes, so-called settings, were formed in total (Table 3). They are based on three sets of spectral bands, i.e., a set of all available bands of the two cameras (NIR, R, G, B), and two spectral subsets, representing the two cameras (NirGB and RGB) individually. Each of these spectral datasets was applied once to all SE sizes (5SE) and once to a reduced number of two SE sizes (2SE), with diameters of 3 and 5 pixels [38,60]. The added textural features were specifically built on the corresponding spectral subset. The settings are named according to the respective spectral bands and SE sizes (e.g., 5SE-NirRGB, comprising all spectral bands and all textural features with all SE sizes).

Table 2. Mathematical morphology formulae for image f and structuring element (SE) B for a pixel x. For further details see [56–59].

Name	Formula
Dilatation	$[\varepsilon Bf]x = \min b \in Bf\ (x + b)$
Erosion	$[\delta Bf]x = \max b \in Bf\ (x + b)$
Opening	$\Gamma Bf = \delta B \circ \varepsilon B(f)$
Closing	$\varphi Bf = \varepsilon B \circ \delta B(f)$
Opening by top hat	$OTH = f - \gamma Bf$
Closing by top hat	$CTH = \varphi Bf - f$
Opening by reconstruction	$\gamma R(n) = Rf\delta[\varepsilon nf]$
Closing by reconstruction	$\varphi R(n) = Rf\varepsilon[\delta n(f)]$
Opening by reconstruction top hat	$ORTH = f - \gamma Rn(f)$
Closing by reconstruction top hat	$CRTH = \varphi Rnf - f$

Table 3. Composition of spectral and textural settings.

Setting	Spectral Bands	SE Sizes (Diameter (Pixel))
5SE-NirRGB	NIR-R-G-B	5SE (3, 5, 9, 13, 29)
5SE-RGB	R-G-B	5SE (3, 5, 9, 13, 29)
5SE-NirGB	NIR-G-B	5SE (3, 5, 9, 13, 29)
2SE-NirRGB	NIR-R-G-B	2SE (3, 5)
2SE-RGB	R-G-B	2SE (3, 5)
2SE-NirGB	NIR-G-B	2SE (3, 5)

3.3. Data Splitting for Validation

The dataset was split in three parts to perform a 3-fold cross validation, whereby one split was used for training of the RF classifier, one for validation of RF parameters, and the last one for testing to determine the classification accuracy. This ensures that only data that were not used for training and validation were used for classification [61]. Therefore, entire fields were assigned randomly to one of these data subsets, such that one third of the fields of a crop class was assigned to a split. In order to avoid these split specific assignments that influence the classification, all six possible permutations, called folds, were exercised.

3.4. Classification

To train the RF and to validate the model parameters, a set of 1000 stratified, randomly sampled pixels per class were selected from the respective training and validation datasets. The native TreeBagger implementation in MATLAB Version 2016a was used for the RF classifier. Usually, the number of trees is preselected by preliminary tests [38], or default values may be used [18]. In our case, we trained the RF with 20 logarithmically evenly spaced values between 10 and 1000 trees to determine the best amount of trees. A minimal leaf size of 3 was chosen to avoid overfitting. For all other parameters, default settings were kept, in particular, the square root of all features at each split.

In a first step (Equation (1)), we calculated the proportion of the correctly classified validation pixels and fitted them to an exponential function of the form

$$y = a * e^{-b*x} + c, \tag{1}$$

using a nonlinear least squares method with starting values of 0 for a and b, and 1 for c. A pre-study showed that this model and these parameters were the most suitable.

Then, we chose the number of trees with an accuracy loss of 0.1% compared to the best accuracy achieved with the fitted function in 1000 trees. However, in order to ensure stability, we set a threshold of at least 100 trees. Eventually, we trained the final model for classification with the determined number of trees, and all training and validation pixels. For the pixel-based classification, this final model was applied to all pixels of test data in the respective fold.

3.5. Spatial Support

Data smoothing at parcel level is commonly applied to agricultural classification results [16]. Parcels were resampled to the respective spatial resolutions using a nearest neighbor approach. The pixel-based classification was followed by the assignment of the most frequent label within a parcel to each pixel of the respective parcel, producing, thus, the parcel-based classification result.

3.6. Accuracy Assessment

The confusion matrix for the test dataset of each fold forms the basis for calculating the overall accuracy [62], kappa coefficient [63], as well as user and producer accuracy [62]. In order to get a better overall view, we averaged the values achieved for each fold. Overall accuracy (OA) refers to the average of the overall accuracy values of the six folds weighted by the number of total test pixels in

the corresponding fold. It is a very frequently used accuracy measure, and allows the comparison to other studies [34]. Kappa refers to the kappa coefficient, average accuracy (AA) refers to the mean of the user accuracies, and average reliability (AR) to the mean of the producer accuracies, respectively.

4. Results

We first present the overall best performing setting (i.e., 5SE-RGB) and then the influence of spatial resampling, selection of spectral bands, and amount of features, i.e., SE sizes. We show the results for the spatial support of pixels and parcels, as well as the full and merged sets of crop classes. All results over all classes are presented and discussed based on OA. Obtained kappa, AA, and AR are not described here in detail, although the corresponding values can be found in Tables S1–S4, and condensed summaries of accuracy values are given in Tables 4 and 5. Subsequently, we also present the class specific UA and PA values.

Table 4. Overall accuracy (OA (%)) for 5SE-RGB for all tested spatial supports (i.e., pixel- and parcel-based) and crop classes at different spatial resolutions.

Resolution (m)	Pixel-Based		Parcel-Based	
	Full Set	Merged Set	Full Set	Merged Set
0.1	61.1	80.2	76.1	94.7
0.25	60.5	86.5	69.9	96.7
0.5	66.7	86.3	74.0	94.6
0.75	63.7	86.5	65.7	96.2
1	62.6	86.0	61.9	94.3
2	60.0	82.7	67.8	92.2

Table 5. OA (%) for all settings, spatial supports and sets of crop classes at 0.5 m spatial resolution.

Settings	Pixel-Based		Parcel-Based	
	Full Set	Merged Set	Full Set	Merged Set
2SE-NirGB	53.5	72.4	68.0	79.4
2SE-NirRGB	60.5	77.1	75.6	83.5
2SE-RGB	60.1	81.5	65.0	92.6
5SE-NirGB	62.1	79.8	73.0	93.0
5SE-NirRGB	65.5	83.5	76.7	95.0
5SE-RGB	66.7	86.3	74.0	94.6

The best accuracy values are achieved for the 5SE-RGB setting at a spatial resolution of 0.5 m (Figure 4). In case of pixel-based classification the OA reaches 66.7%, whereas in the parcel-based case, an OA of 74.0% is achieved for the full set of crop classes (Table 4). The corresponding land cover maps can be found in Figure 5.

Remote Sens. **2018**, *10*, 1282

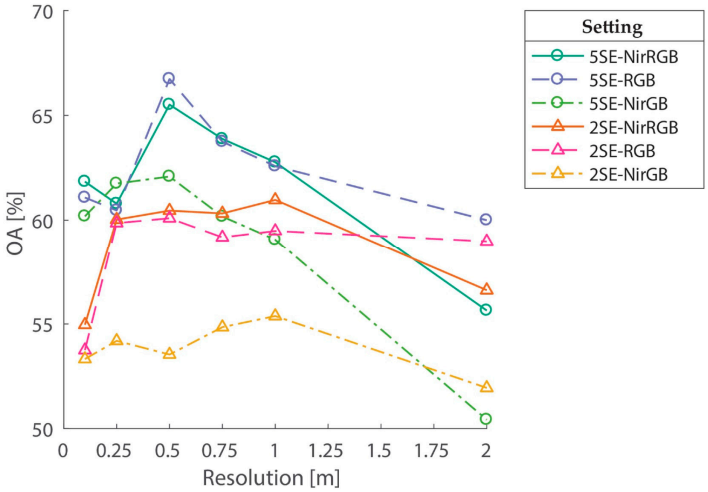

Figure 4. Overall accuracy (OA) for the full set of crop classes for all tested spatial resolutions and settings of the dataset for a pixel-based classification. Circles mark five structuring element (SE) sizes at evaluated resolutions and triangles two SEs, respectively. The line styles correspond to the applied spectral band selection.

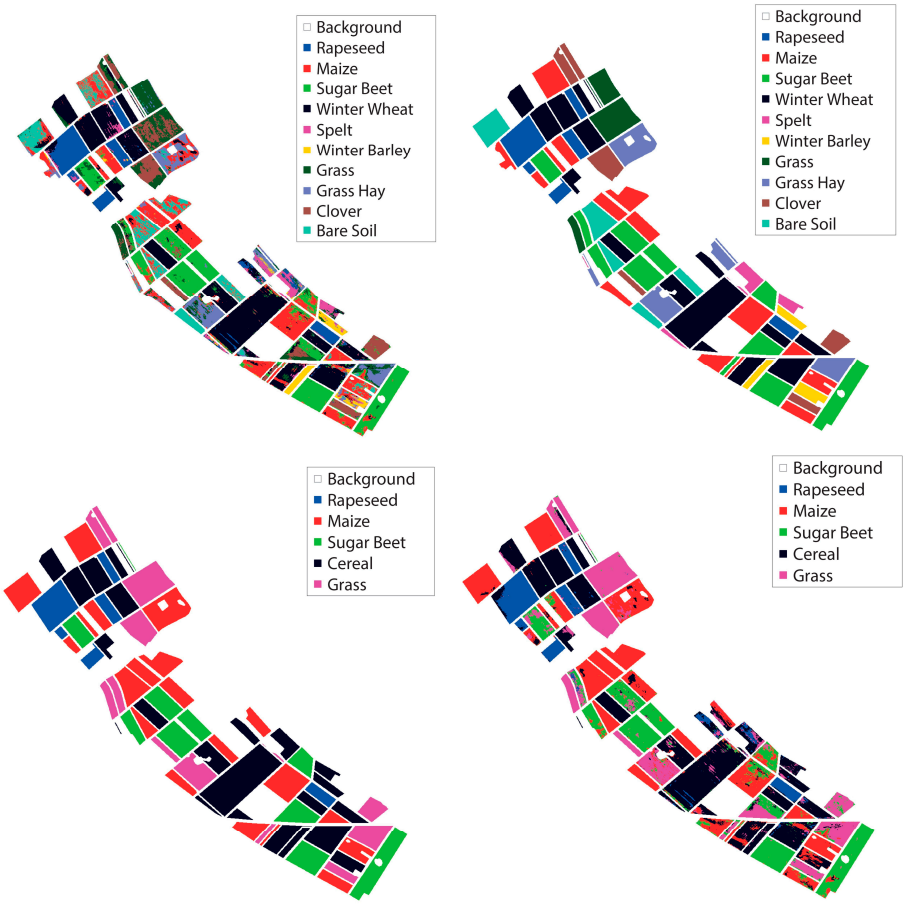

Figure 5. Land cover maps for the 5SE-RGB setting at 0.5 m spatial resolution. Full set of crop classes (**top**), merged set of crop classes (**bottom**), pixel-based classification (**left**), and parcel-based classification (**right**).

For the merged set of classes, the best values are achieved for 0.75 m spatial resolution for a pixel-based classification in terms of OA and AA (OA 86.5%, kappa 0.823, AA 85.8%, AR 87.9%), and for 0.25 m in terms of kappa and AR (OA 86.5%, kappa 0.823, AA 85.4.7%, AR 88.1%) (Table S3). However, the differences between the calculated accuracy measurements are small. The difference between the spatial resolution of 0.75 m and 0.5 m is 0.050% in terms of OA (differences in kappa: 0.000%, AA: 0.204%, AR: −0.127%). For the parcel-based classification, the best performance was achieved for a spatial resolution of 0.25 m with an OA of 96.7%, which is 2.1% better than for 0.5 m (Table S4).

4.1. Spatial Resampling

Concerning OA values for the tested spatial resolutions, most settings show a similar pattern for pixel-based classification of the full set of crop classes (Figure 4). The maximum OA is reached around 0.5 m, with decreasing values for higher or lower spatial resolution (Table 4).

In the case of pixel-based classification, the OA of the best performing setting (5SE-RGB) rises from 60.0% at a spatial resolution of 2 m, to 66.7% at 0.5 m for the full set of crop classes (Table 4). Then, it decreases to 61.1% at 0.1 m. For the set of merged classes, the OA raises from 82.7% at 2 m up to 86.3% at 0.5 m, and decreases to 80.2% at 0.1 m.

For parcel-based classifications, different spatial resolutions perform best for the full and merged set of crop classes (Figures S2 and S3). For the full set, a spatial resolution of 0.5 m yields the best classification accuracy, except for some settings that perform slightly better at 0.1 m spatial resolution. For the merged set of classes, highest accuracies are achieved at 0.25 m or 0.75 m spatial resolution, with slightly lower values at 0.5 m.

4.2. Spectral Resolution

Regarding spectral resolution of pixel-based classification, RGB settings generally lead to a better performance than settings with the additional NIR band (Figure 4 and Table 5). Settings without the red band (i.e., NirGB) perform worse. In the case of the full set of crop classes and the settings with five SE (5SE), this is only true for a spatial resolution of 0.5 m and 2 m (Table S1). For the other considered spatial resolutions, 5SE-NirRGB performs slightly better than 5SE-RGB in terms of OA. OA values for 5SE-NirGB are always lower than in the case of 5SE-NirRGB and 5SE-RGB, except for a spatial resolution of 0.25 m, where a 5SE-NirGB setting performs best. For settings with less SE sizes, 2SE-NirRGB outperforms 2SE-RGB, except for a resolution of 2 m. The OA values for classification of a 2SE-NirGB setting are always lower than for the other settings. In the case of the merged set of crop classes, the above statement applies to all spatial resolutions and amount of SE sizes (Figure S1).

Settings with RGB bands lead to better classification results than NirRGB and NirGB settings, irrespective of the spatial resolution and the amount of SE sizes (Table 5). On average, RGB settings show a 6% better OA compared to NIR-RGB, and 9% compared to NirGB for the full set of crop classes, and 7% and 10% in the case of the merged set, respectively.

In the parcel-based classification of the full set of crop classes, four-band settings perform best, followed by RGB and NirGB settings, with some exceptions for 0.1 m and 2 m spatial resolution (Table S2). Independent of the amount of SE sizes, 2SE-RGB and 5SE-RGB settings achieve better accuracies at a spatial resolution of 2 m than NirRGB settings. In addition, 5SE-RGB performs best at a spatial resolution of 0.1 m. In case of merged crop classes, RGB settings perform best, followed by NirRGB and NirGB settings.

4.3. Number of SE Sizes

In general, a higher number of SE sizes (5SE), and therefore, more textural features, lead to higher classification accuracies compared to a reduced amount (2SE) for the same spectral and spatial resolutions (Table 5). Nevertheless, 2SE settings outperform 5SE settings for parcel-based classification of the full set of crop classes at a spatial resolution of 0.75 and 1 m (Figure S1), and of the merged set of classes at 2 m (Figure S3), respectively.

4.4. Number of Classes and Spatial Support

In case of the best overall setting (i.e., 5SE-RGB, at 0.5 m), the classification result of the merged set of crop classes yields a 19.6% better OA compared to the full set for the pixel-based classification, and a 20.6% better OA for the parcel-based case (Table 5). The difference in OA between the two spatial supports is 7.3% for the full set of crop classes, and 8.3% for the merged set, respectively.

4.5. Class Specific Accuracy

For the full set of crop classes, the class specific accuracies range between 7.4% (UA of hay) and 100% (PA of various crops, e.g., sugar beet) for the best performing setting, i.e., 5SE-RGB at 0.5 spatial resolution, and a parcel-based classification (Tables S5 and S6). For the pixel-based classification, the range is slightly smaller and lies between 10.8% (UA of hay) and 91.8% (PA of rapeseed). Main mixtures occurred between maize and bare soil on the one hand and grassland, maize, and sugar beet on the other hand. The three cereal types mainly mixed up with each other. The same was true for grassland, clover and hay.

The class specific accuracies are slightly better with the additional NIR band in the NirRGB setting. Consequently, AA slightly increases to 60.0% and AR to 64.7% for the pixel-based classification (Table S1), and to 70.3% (AA) and 78.0% (AR) for the parcel-based classification (Table S1), compared to the 5SE-RGB setting. The mixtures between classes remain the same, but could be reduced. In particular, UA and PA of the cereals and bare soil could be improved by approximately 10%.

For the merged set of classes, the range of UA is 17.0% for the pixel-based classification and 14.8% for the parcel-based case, respectively. The range of PA is 15.5% for the pixel-based classification and 17.5% for the parcel-based case (Table S6). The primary mixtures occurred between grassland, maize, and sugar beet. In addition, rapeseed was mixed up with cereals, and the cereals with maize and grassland.

For some of the crop classes, a slight improvement of UA and/or PA could be achieved with the additional NIR band combined with a finer spatial resolution. For a spatial resolution of 0.25 m, AR increased by 1.5% for the parcel-based classification. The increase of AA with other settings and resolutions is negligible, as well as the increase of AA and AR for the pixel-based classification for the merged set of crops.

5. Discussion

A random forest-based classification method incorporating textural features was developed to assess the influence of spatial resolution, the choice of spectral bands, as well as the amount of different SE sizes on the classification accuracy of an uncalibrated, UAV-based VHR dataset. Overall, the best performing setting is 5SE-RGB at a spatial resolution of 0.5 m (Figure 4). For the full set of crop classes, an OA of 66.7% is achieved with a pixel-based classification. For a parcel-based classification, the OA increased by 7.3% to 74.0%. In the case of the merged set of crop classes, a similar behavior can be observed, with the OA for the pixel-based classification being 86.3%, and increasing by 8.3% to 94.6% for the parcel-based classification.

5.1. Influence of Spatial Resolution

Additional textural features, along with spectral data, improve the classification result, but these features depend on the spatial resolution of the sensor and SE size and number. This is consistent with [34], who found that additional textural features resulted in the highest improvement of a classification. In case of coarse resolutions, however, texture does not always improve the results, as was shown for mapping crops in an agricultural area in Austria with spatial structures similar to our study area and using Sentinel-2 data of 10 m resolution [18].

The spatial resolution of the dataset is crucial, because it determines the degree of detail. The elements that cause texture effects in crops are, on the one hand, the row spacing and the

within-row spacing of plants and, on the other hand, the visible bare soil in between the plants. At full canopy closure, the effects are mainly caused by shading of leaves and varying reflectance properties at different leaf angles [64]. In coarse resolution datasets (several meters), all these effects are integrated in the measurement of a single pixel, whereas in high-resolution data (few centimeters) the different leaf angles or even pebbles on the soil in the background are captured by a single pixel. Consequently, the optimal spatial resolution is driven by the fact that the between-class variability of pixels allows for the discrimination of the crop type, while not hampering the classification algorithm by within-class variation.

For industrially managed crops, the texture effects depend largely on the spacing between both the within-row and the row spacing [37]. Usually, single plants (or seeds) are placed at an optimal mutual distance in order to achieve the maximal possible yield [65], or rather, profit [66]. Therefore, best classification accuracies are achieved at an optimal spatial resolution where within-class variability of (texture) features is smaller than between-class variability [60].

In case of crops, both the within-class variability and the between-class variability decline with coarser spatial resolution. Consequently, the best performing spatial resolution is a trade-off in within- and between-class variability [67]. On the one hand, the within-class variability needs to be minimized. This is achieved when multiple plants are covered by a single pixel. On the other hand, the between-class variability should be as large as possible. For coarser resolutions, neighboring pixels in a class become more similar, and as a consequence, texture properties of different classes converge.

Within-row and row spacing influence the textural features of crops. In our study site, only sugar beet and maize are not yet in a stage of complete canopy closure at the end of June. Hence, the best spatial resolution is in the same range as the row spacing of these two classes. With a row spacing of 0.5 m for sugar beet, this value is equal to the best performing spatial resolution. Since maize fields are in (i) very early and (ii) heterogeneous phenological stages (Table 1), their row spacing does not have a dominant effect on the best spatial resolution.

Nevertheless, the optimal spatial resolution is also dependent on the spatial support, and number and kind of crop classes. For the pixel-based classification with a merged set of crop classes, the optimal spatial resolution is slightly coarser, i.e., a spatial resolution of 0.75 m performs best (Table 4). In contrast to the full set of crop classes, discrimination of grassland and clover, as well as among different cereals, is no longer performed. In case of parcel-based classification, a dataset based on 0.25 m spatial resolution yields higher classification accuracies than a dataset of 0.5 m pixel size (Figure S3).

In summary, a spatial resolution of 0.5 m performs best, in general, despite small accuracy losses for some classes or spatial supports. This is consistent with the findings of [39], where a spatial resolution of 0.5 m was found to be optimal to analyze the in-field variability of pasture using the red band of a multispectral sensor.

Numerous studies have been based on datasets of coarser spatial resolution acquired e.g., by the Moderate Resolution Imaging Spectrometer (MODIS) or Landsat, and providing sufficient spatial, spectral, and temporal resolution for large scale field monitoring [6]. Their main difference to our study relates to the prevalent field sizes in the Swiss Plateau, being smaller than elsewhere. In agricultural areas like, for instance, the US Central Great Plains, single fields are larger, with field sizes of more than 30 ha [13]. These areas are not as small-scaled as in Switzerland. Consequently, data of higher spatial resolution is necessary to analyze crop types in study areas like ours [4].

5.2. Impact of Spectral Characteristics

In general, remotely sensed data of spaceborne instruments are of more favorable spectral and radiometric specifications than VHR data obtained with an uncalibrated consumer-grade camera carried on a UAV, as in our study. Unlike our system that only acquires data in RGB bands and in an additional NIR band, datasets of e.g., Landsat 8 or MODIS provide a broader spectral range, with a number of bands in the NIR and SWIR spectral region. In addition, the spectral characteristics of spaceborne instruments are better defined in terms of spectral band width, and full width at

half maximum (FWHM). Nevertheless, our study demonstrates the feasibility to generate crop maps of documented accuracy, based on the respective VHR data and following the proposed classification method.

A number of studies document the benefits of using a NIR band [33,37] or a band in the red edge region [35] for crop classification. However, in our study, the NIR band does not improve the OA, in general. The NIR band of the modified Canon IXUS 125HS camera covers the wavelength region of approximately 690–730 nm, where the data values of vegetation and bare soil occur to be very similar in the acquired dataset. Further, the red band with its spectral range of approximately 640–680 nm is closely situated to the NIR band. Highest accuracies were thus achieved with an RGB band configuration. The fact that NirGB performs worst in general demonstrates the importance of the red band in our constellation. Indeed, we find that the differences in remotely sensed data values of vegetation and bare soil are most pronounced in this band. Consequently, RGB settings without a NIR band perform better overall. Only in the case of the merged set of crop classes on a parcel-based classification the 5SE-NirRGB setting achieves a slightly better OA than the 5SE-RGB setting. However, the classification of sugar beet and grassland would profit from the additional NIR band in terms of class specific accuracy (UA and PA, as mentioned in Section 4.5), but only in combination with a higher spatial resolution. Due to very similar spectral behavior of the three cereal crops (i.e., winter wheat, winter barley, and spelt) any additional spectral information may improve a classification performance.

5.3. Effect of Different SE sizes

Besides the spatial and spectral resolution having an influence on the classification result, more and larger SE sizes improve the classification accuracy. Morphological features keep or erase the elements in the SE that cause the texture by enlarging or erasing dark or bright elements [56]. As mentioned in Section 5.1, the main textural elements in crops are plants and bare soil. Depending on the sun position, shade causes dark parts. Since the different crops were tilled with different within-row and row spacing, the SE sizes must be defined in a way that they capture all present gaps [60]. Therefore, settings using five SE sizes (5SE) perform better than those taking only two SE sizes (2SE) into account, since the SE sizes should correspond to the present crops and their spacing.

5.4. Influence of Spatial Support

Object-based, i.e., parcel-based, classification improves the classification result [33], and is considered as the state-of-the-art in crop mapping [16]. In our case, it improves the pixel-based classification by 20% in terms of OA. The required field boundaries originate either from an additional data source [16], manual digitalization from scratch [38], or unsupervised segmentation [42]. For rural areas in the Swiss Plateau, a manual digitalization of individual parcels is feasible, since the field boundaries usually remain stable over several years.

5.5. Considerations about Acquisition Date and Temporal Resolution

An accurate classification of agricultural crops depends on a suitable point in time for data acquisition, since phenological stages of crops are changing rapidly [4]. By the end of June, all crops present in our study area were accrued, apart from maize. At this time of the year, most cultures are in their final stage of maturation, except for maize and sugar beet. Other studies also considered earlier and later acquisition dates, but concluded that maturity is the most promising phenological stage for a monotemporal analysis [16]. A later acquisition date (e.g., 30 August) leads to confusion, as some of the winter crops have already been harvested [18], while earlier dates may affect differentiation between bare soil and small plants [16,18]. In our dataset, this issue applies to maize being in an early phenological stage, and therefore, mixing up with bare soil. Additionally, the phenological variability among individual maize fields is large. In multitemporal analyses, datasets acquired before the end of July are reported to be the most important, with later datasets leading only to a minor improvement of

the classification result [15]. However, classification of a monotemporal dataset can achieve similar accuracies as in the case of a multitemporal dataset [18].

5.6. Comparison to Other Studies

When comparing our findings on the best performing spatial resolution of 0.5 m to other studies, not only spatial and spectral properties of the dataset and amount of different SE sizes for the textural features need to be considered. As could be seen in the differences in classification accuracy for the full and merged set of crop classes, the result depends as well on the actual classes, and the spatial support.

A recent study based on a multilevel classification in central Ontario, Canada, mainly aimed to differentiate tree species [42]. Maize, wheat, soybean, and alfalfa were classified as a side product in a parcel-based classification. The dataset was obtained using an eBee UAV as well, but with different cameras acquiring spectrally calibrated data. The study achieved an OA of 89% using a dataset acquired with the Parrot Sequoia sensor (green, red, NIR, and red edge bands, spatial resolution of 12.9 cm). Simultaneously, an RGB true color dataset was acquired (spatial resolution of 3.42 cm), serving as the basis to classify the crops with an OA of 83%. Finally, a Sony DSC-WX220 RGB camera was deployed (successor of the camera used in our study) to acquire a dataset with a spatial resolution of 3.52 cm. With this dataset, crop classification resulted in an OA of 81%. In addition to the spectral bands, the authors used texture and normalized difference vegetation index (NDVI) features, as well. With the method presented in our study and the 5SE-RGB setting, we achieve an OA of 94.6% at a spatial resolution of 0.5 m for the parcel-based classification of the merged classes. Based on a spatial resolution of 0.1 m, we still achieve an OA of 92.8%. Our approach performs slightly better, most likely due to the resampling to a coarser spatial resolution. Despite the additional calibration and NDVI feature, the OA accuracy of the aforementioned study is slightly lower.

Another classification study on simulated Sentinel-2 data from the Marchfeld region in Lower Austria achieved an OA of 76.5% [18]. The authors used an object-based method to classify seven agricultural cultures (carrots, maize, onions, soya, sugar beet, sunflower, and winter crops) based on spectral features only. The lower accuracy compared to our study was likely due to the unfavorable data acquisition date (30 August). At that point in time, winter crops were already harvested, and were therefore classified based on the spectral signature of bare soil and crop residuals. The high soil proportions in the harvested fields led to confusion with onion fields. Their pixel-based classification, however, performed better (OA of 83.2%), although with a higher variability in class specific accuracy, than in our case.

A further monotemporal study analyzed an Ikonos dataset of a rural area in Bursa, northwest Turkey, with a spatial resolution of 4 m acquired on 13 June [16]. Only R, G, B, and NIR bands of the dataset were used. An OA of 83.6% was achieved for a pixel-based classification of maize, pasture, rice, sugar beet, wheat, and tomato using an SVM-based method. A parcel-based classification leads to an improvement of 12.5% in OA. In comparison to our proposed method applied to the merged set of crop classes, this study achieved a slightly lower OA for the pixel-based classification, and a slightly better OA for the parcel-based classification approach.

Crop height is an additional parameter that can be derived from UAV data. In [68], the authors used the difference of the surface height between two acquisitions of RGB and NIR data with a spatial resolution of 0.8 m on 30 June and 21 October in Texas, USA. It could be shown that with crop height alone, the classification quality was limited, due to high variance even in single fields. Therefore, the authors used spectral, textural, and spatial features in addition, and reached an OA of 97.50% for an object-based method, and an OA of 78.52% for a pixel-based maximum likelihood (ML) classification. The OA accuracy was 2.5% lower when height information was not used. The reported land cover consisted of corn, cotton, sorghum, grass, bare soil, and wheat, being well comparable to our merged setting of crop types. The OA of our parcel-based classification is similar to the reported case without crop height information. In the pixel-based case, we achieved a roughly 10% better OA.

A further study was performed in July 2015 in the same area, using an RGB and a NIR camera to acquire data of five crop classes (i.e., cotton, corn, sorghum, soybean and watermelon) and five non-crop classes (i.e., impervious ground, bare soil, fallow, water, grass, and forest) at a spatial resolution of 0.35 m [69]. The authors tested a variety of groupings with pixel- and parcel-based classifications. The pixel-based classifications were based on a three-band setting (RGB) or a four-band setting (NirRGB). Based solely on spectral bands, the pixel-based classifications achieved OAs between 62% and 69% for the most comparable grouping containing all crops, and a single class for non-crops. In our setting, with textural features and the full set of crop classes, we achieved a comparable accuracy (OA of 66.7%). However, our merged set of crop classes outperformed all groupings of [69] with an OA of 86.3%. For the parcel-based classification, the authors additionally used vegetation indices (VIs), and statistical, geometrical, and textural features. In contrast to our study, they found an improvement of OA with an additional NIR band, which could be caused by the VIs that are based on the NIR band. They achieved OAs between 73% and 91%, depending on the setting and number of bands. Hence, their parcel-based results are slightly better when compared to our full set of crop classes (OA 74.0%), but slightly less accurate than our merged set (94.6%).

In another study at the same location, a NirRGB dataset of 0.4 m spatial resolution was upscaled to 1, 2, 4, 10, 15, and 30 m pixel sizes [70]. The authors classified cotton, sorghum, soybean, watermelon, non-crop vegetation, and non-vegetated area in the RGB dataset with an OA of 83.3%, and in the NirRGB dataset with an OA of 90.42% at a spatial resolution of 0.4 m. For coarser pixel sizes, the OA decreased to less than 70%. Compared to our best performing setting (5SE-RGB at 0.5 m spatial resolution) with an OA of 86.3%, they achieved similar accuracies in the RGB case. Again, with the additional NIR band and the implementation of VIs, their performance increased by 7%.

5.7. Limitations of Our Method

Both our method and the employed dataset have some limitations. Besides the spectral bands, the current approach relies mostly on textural features. Additional spectral or multitemporal features could improve the classification [34]. So far, there are only the spectral bands themselves incorporated, but further spectral features, such as spectral indices, could lead to performance improvements [31].

Since parcel-based classifications lead to higher accuracies, ancillary information about field borders is required. With this information not always being available, a conditional random field (CRF) smoothing to homogenize class assignments of a pixel-based classification for a certain field could alternatively be applied, leading to only slightly lower accuracies, but not being dependent on additional information sources [16]. Alternatively, a classification of segments within fields could improve the results as well [42].

A NIR band at ~800 nm instead of 720 nm would most likely improve the classification, as can be seen from the comparison of a Sequoia Parrot sensor and our modified Canon IXUS 125HS camera containing a NIR band [42]. This would allow an appropriate incorporation of vegetation indices (e.g., NDVI, generalized difference vegetation index (GDVI), or soil-adjusted vegetation index (SAVI)). Moreover, the spatial resolution of individual bands should be further analyzed, since a coarser resolution for NIR bands compared to a red band could lead to similar results [39].

6. Conclusions

We presented a classification method for crops on a dataset obtained by uncalibrated consumer-grade cameras mounted on a UAV. We analyzed different spatial and spectral resolutions, as well as different SE sizes for textural features. We investigated pixel and parcel-based spatial support and two sets of crop classes. On the one hand, we analyzed nine individual crop classes, and on the other hand, we pooled maize and bare soil, the three cereals types, and grassland and clover together.

Overall, the best performance was achieved with a dataset consisting of RGB bands and textural features of five structuring element (SE) sizes at a spatial resolution of 0.5 m. We were able to show that both a finer and a coarser spatial resolution perform worse. Settings that take the RGB bands into

account outperform such with the additional NIR band. Nevertheless, the NIR band leads partially to class specific improvements, but to slightly less accurate crop maps when all crops are classified together. SE sizes that cover the entire range of both within-row and row spacing of crops perform better. Consequently, our tested settings with five SE sizes outperform settings with two SE sizes.

A reduced set of crop classes led to better classification results (increase of ~7% in OA). As in other studies, we were not able to properly discriminate clover from grassland and the different cereal types from each other. Maize was in heterogeneous phenological stages ranging from fresh sown to stem elongation and could, therefore, not be distinguished from bare soil. As expected, parcel-based classification led to an improvement of ~20% in terms of OA compared to a pixel-based classification.

We conclude that a dataset with a spatial resolution of 0.5 m, consisting of spectrally poorly characterized and uncalibrated RGB bands, can provide sufficient information to differentiate between agricultural crop classes, given a set of SE sizes to describe textural features is taken into account in an appropriate manner. With an increasing availability of spaceborne VHR imagery becoming operationally available in the near future, the classification method presented and evaluated in this study contributes to the generation of crop maps of documented accuracy in small-scaled agricultural areas.

Supplementary Materials: The following are available online at http://www.mdpi.com/2072-4292/10/8/1282/s1. Figure S1: Overall accuracy (OA) for the merged set of crop classes for all tested spatial resolutions and settings of the data set for a pixel-based classification. Circles mark five structuring element (SE) sizes at evaluated resolutions and triangles two SE, respectively. The line styles correspond to the applied spectral band selection. Figure S2: Overall accuracy (OA) for the full set of crop classes for all tested spatial resolutions and settings of the data set for a parcel-based classification. Circles mark five structuring element (SE) sizes at evaluated resolutions and triangles two SE, respectively. The line styles correspond to the applied spectral band selection. Figure S3: Overall accuracy (OA) for the merged set of crop classes for all tested spatial resolutions and settings of the data set for a parcel-based classification. Circles mark five structuring element (SE) sizes at evaluated resolutions and triangles two SE, respectively. The line styles correspond to the applied spectral band selection. Table S1: Accuracy values for all tested spatial resolutions and settings of the full set of crop classes for a pixel-based classification. Table S2: Accuracy values for all tested spatial resolutions and settings of the full set of crop classes for a parcel-based classification. Table S3: Accuracy values for all tested spatial resolutions and settings of the merged set of crop classes for a pixel-based classification. Table S4: Accuracy values for all tested spatial resolutions and settings of the merged set of crop classes for a parcel-based classification. Table S5: User Accuracy (UA) and Producer Accuracy (PA) for the full set of crop classes in a pixel- and parcel-based classification at a spatial resolution of 0.5 m and the 5SE-RGB setting. Table S6: User Accuracy (UA) and Producer Accuracy (PA) for the merged set of crop classes in a pixel- and parcel-based classification at a spatial resolution of 0.5 m and the 5SE-RGB setting.

Author Contributions: J.E.B. designed the research and analyzed the data with scientific advice of M.K. and M.E.S., J.E.B. wrote the manuscript and all co-authors thoroughly reviewed and edited the manuscript.

Funding: This research received no external funding.

Acknowledgments: The contribution of M.E.S. is supported by the University of Zurich Research Priority Program on 'Global Change and Biodiversity' (URPP GCB). We thank staff from RSL and GRS (Wageningen University) supporting fieldwork and providing background information.

Conflicts of Interest: The authors declare no conflict of interest.

References

1. Rosenzweig, C.; Elliott, J.; Deryng, D.; Ruane, A.C.; Müller, C.; Arneth, A.; Boote, K.J.; Folberth, C.; Glotter, M.; Khabarov, N.; et al. Assessing agricultural risks of climate change in the 21st century in a global gridded crop model intercomparison. *Proc. Natl. Acad. Sci. USA* **2014**, *111*, 3268–3273. [CrossRef] [PubMed]
2. Gerland, P.; Raftery, A.E.; Ševčíková, H.; Li, N.; Gu, D.; Spoorenberg, T.; Alkema, L.; Fosdick, B.K.; Chunn, J.; Lalic, N.; et al. World population stabilization unlikely this century. *Science* **2014**, *346*, 234–237. [CrossRef] [PubMed]
3. Tilman, D.; Balzer, C.; Hill, J.; Befort, B.L. Global food demand and the sustainable intensification of agriculture. *Proc. Natl. Acad. Sci. USA* **2011**, *108*, 20260–20264. [CrossRef] [PubMed]

4. Whitcraft, A.K.; Becker-Reshef, I.; Justice, C.O. A framework for defining spatially explicit earth observation requirements for a global agricultural monitoring initiative (GEOGLAM). *Remote Sens.* **2015**, *7*, 1461–1481. [CrossRef]
5. Fuhrer, J.; Gregory, P.J. *Climate Change Impact and Adaptation in Agricultural Systems*; CABI: Wallingford, CT, USA, 2014; ISBN 9781780642895.
6. Atzberger, C. Advances in Remote Sensing of Agriculture: Context Description, Existing Operational Monitoring Systems and Major Information Needs. *Remote Sens.* **2013**, *5*, 949–981. [CrossRef]
7. Kastens, J.H.; Kastens, T.L.A.; Kastens, D.L.A.; Price, K.P.; Martinko, E.A.; Lee, R.Y. Image masking for crop yield forecasting using AVHRR NDVI time series imagery. *Remote Sens. Environ.* **2005**, *99*, 341–356. [CrossRef]
8. Zhang, P.; Anderson, B.; Tan, B.; Huang, D.; Myneni, R. Potential monitoring of crop production using a satellite-based Climate-Variability Impact Index. *Agric. For. Meteorol.* **2005**, *132*, 344–358. [CrossRef]
9. Mueller, N.D.; Gerber, J.S.; Johnston, M.; Ray, D.K.; Ramankutty, N.; Foley, J.A. Closing yield gaps through nutrient and water management. *Nature* **2012**, *490*, 254–257. [CrossRef] [PubMed]
10. Verbesselt, J.; Hyndman, R.; Newnham, G.; Culvenor, D. Detecting trend and seasonal changes in satellite image time series. *Remote Sens. Environ.* **2010**, *114*, 106–115. [CrossRef]
11. Rembold, F.; Atzberger, C.; Savin, I.; Rojas, O. Using low resolution satellite imagery for yield prediction and yield anomaly detection. *Remote Sens.* **2013**, *5*, 1704–1733. [CrossRef]
12. Galford, G.L.; Mustard, J.F.; Melillo, J.; Gendrin, A.; Cerri, C.C.; Cerri, C.E.P. Wavelet analysis of MODIS time series to detect expansion and intensification of row-crop agriculture in Brazil. *Remote Sens. Environ.* **2008**, *112*, 576–587. [CrossRef]
13. Wardlow, B.D.; Egbert, S.L.; Kastens, J.H. Analysis of time-series MODIS 250 m vegetation index data for crop classification in the U.S. Central Great Plains. *Remote Sens. Environ.* **2007**, *108*, 290–310. [CrossRef]
14. Palchowdhuri, Y.; Valcarce-Diñeiro, R.; King, P.; Sanabria-Soto, M. Classification of multi-temporal spectral indices for crop type mapping: A case study in Coalville, UK. *J. Agric. Sci.* **2018**, *156*, 24–36. [CrossRef]
15. Azar, R.; Villa, P.; Stroppiana, D.; Crema, A.; Boschetti, M.; Brivio, P.A. Assessing in-season crop classification performance using satellite data: A test case in Northern Italy. *Eur. J. Remote Sens.* **2016**, *49*, 361–380. [CrossRef]
16. Ozdarici-Ok, A.; Ok, A.; Schindler, K. Mapping of Agricultural Crops from Single High-Resolution Multispectral Images–Data-Driven Smoothing vs. Parcel-Based Smoothing. *Remote Sens.* **2015**, *7*, 5611–5638. [CrossRef]
17. Inglada, J.; Arias, M.; Tardy, B.; Hagolle, O.; Valero, S.; Morin, D.; Dedieu, G.; Sepulcre, G.; Bontemps, S.; Defourny, P.; et al. Assessment of an operational system for crop type map production using high temporal and spatial resolution satellite optical imagery. *Remote Sens.* **2015**, *7*, 12356–12379. [CrossRef]
18. Immitzer, M.; Vuolo, F.; Atzberger, C. First experience with Sentinel-2 data for crop and tree species classifications in central Europe. *Remote Sens.* **2016**, *8*, 166. [CrossRef]
19. Shi, Y.; Thomasson, J.A.; Murray, S.C.; Pugh, N.A.; Rooney, W.L.; Shafian, S.; Rajan, N.; Rouze, G.; Morgan, C.L.S.; Neely, H.L.; et al. Unmanned Aerial Vehicles for High-Throughput Phenotyping and Agronomic Research. *PLoS ONE* **2016**, *11*, e0159781. [CrossRef] [PubMed]
20. Tattaris, M.; Reynolds, M.P.; Chapman, S.C. A Direct Comparison of Remote Sensing Approaches for High-Throughput Phenotyping in Plant Breeding. *Front. Plant Sci.* **2016**, *7*, 1131. [CrossRef] [PubMed]
21. Holman, F.H.; Riche, A.B.; Michalski, A.; Castle, M.; Wooster, M.J.; Hawkesford, M.J. High Throughput Field Phenotyping of Wheat Plant Height and Growth Rate in Field Plot Trials Using UAV Based Remote Sensing. *Remote Sens.* **2016**, *8*, 1031. [CrossRef]
22. Fuhrer, J.; Tendall, D.; Klein, T.; Lehmann, N.; Holzkämper, A. *Water Demand in Swiss Agriculture—Sustainable Adaptive Options for Land and Water Management to Mitigate Impacts of Climate Change*; Art-Schriftenreihe: Ettenhausen, Switzerland, 2013; Volume 59, Available online: https://www.agroscope.admin.ch/agroscope/de/home/publikationen/suchen/reihen-bis-2013/art-schriftenreihe.html (accessed on 14 August 2018).
23. De Wit, A.J.W.; Clevers, J.G.P.W. Efficiency and accuracy of per-field classification for operational crop mapping. *Int. J. Remote Sens.* **2004**, *25*, 4091–4112. [CrossRef]
24. Waldhoff, G.; Lussem, U.; Bareth, G. Multi-Data Approach for remote sensing-based regional crop rotation mapping: A case study for the Rur catchment, Germany. *Int. J. Appl. Earth Obs. Geoinf.* **2017**, *61*, 55–69. [CrossRef]

25. Long, T.B.; Blok, V.; Coninx, I. Barriers to the adoption and diffusion of technological innovations for climate-smart agriculture in Europe: Evidence from the Netherlands, France, Switzerland and Italy. *J. Clean. Prod.* **2016**, *112*, 9–21. [CrossRef]
26. Swiss Federal Office for Agriculture (FOAG). *Swiss Agricultural Policy*; FOAG: Berne, Switzerland, 2004; Available online: https://www.cbd.int/financial/pes/swiss-pesagriculturalpolicy.pdf (accessed on 14 August 2018).
27. Benton, T.G.; Vickery, J.A.; Wilson, J.D. Farmland biodiversity: Is habitat heterogeneity the key? *Trends Ecol. Evol.* **2003**, *18*, 182–188. [CrossRef]
28. Bundesrat, D.S. Verordnung über die Direktzahlungen an die Landwirtschaft. 2017, Volume 2013, pp. 1–152. Available online: https://www.admin.ch/opc/de/classified-compilation/20130216/index.html (accessed on 14 August 2018).
29. Akademien der Wissenschaften Schweiz Brennpunkt Klima Schweiz. *Grundlagen, Folgen, Perspektiven*; Swiss Academies Reports; 2016; Volume 11, pp. 1–128. Available online: http://www.akademien-schweiz.ch (accessed on 14 August 2018).
30. Vuolo, F.; Neugebauer, N.; Bolognesi, S.; Atzberger, C.; D'Urso, G. Estimation of Leaf Area Index Using DEIMOS-1 Data: Application and Transferability of a Semi-Empirical Relationship between two Agricultural Areas. *Remote Sens.* **2013**, *5*, 1274–1291. [CrossRef]
31. Laliberte, A.S.; Rango, A. Texture and Scale in Object-Based Analysis of Subdecimeter Resolution Unmanned Aerial Vehicle (UAV) Imagery. *IEEE Trans. Geosci. Remote Sens.* **2009**, *47*, 761–770. [CrossRef]
32. Marcos, D.; Volpi, M.; Kellenberger, B.; Tuia, D. Land cover mapping at very high resolution with rotation equivariant CNNs: Towards small yet accurate models. *ISPRS J. Photogramm. Remote Sens.* **2018**, in press. [CrossRef]
33. Whitehead, K.; Hugenholtz, C.H.; Myshak, S.; Brown, O.; LeClair, A.; Tamminga, A.; Barchyn, T.E.; Moorman, B.; Eaton, B. Remote sensing of the environment with small unmanned aircraft systems (UASs), Part 1: A review of progress and challenges. *J. Unmanned Veh. Syst.* **2014**, *2*, 69–85. [CrossRef]
34. Khatami, R.; Mountrakis, G.; Stehman, S.V. A meta-analysis of remote sensing research on supervised pixel-based land-cover image classification processes: General guidelines for practitioners and future research. *Remote Sens. Environ.* **2016**, *177*, 89–100. [CrossRef]
35. Zhang, H.; Li, Q.; Liu, J.; Shang, J.; Du, X.; McNairn, H.; Champagne, C.; Dong, T.; Liu, M. Image Classification Using RapidEye Data: Integration of Spectral and Textual Features in a Random Forest Classifier. *IEEE J. Sel. Top. Appl. Earth Obs. Remote Sens.* **2017**, *10*, 5334–5349. [CrossRef]
36. Topaloglou, C.A.; Mylonas, S.K.; Stavrakoudis, D.G.; Mastorocostas, P.A.; Theocharis, J.B. Accurate crop classification using hierarchical genetic fuzzy rule-based systems. In Proceedings of the SPIE— Remote Sensing for Agriculture, Ecosystems, and Hydrology, Amsterdam, The Netherlands, 22–23 September 2014; Volume 9239.
37. Helmholz, P.; Rottensteiner, F.; Heipke, C. Semi-automatic verification of cropland and grassland using very high resolution mono-temporal satellite images. *ISPRS J. Photogramm. Remote Sens.* **2014**, *97*, 204–218. [CrossRef]
38. Debats, S.R.; Luo, D.; Estes, L.D.; Fuchs, T.J.; Caylor, K.K. A generalized computer vision approach to mapping crop fields in heterogeneous agricultural landscapes. *Remote Sens. Environ.* **2016**, *179*, 210–221. [CrossRef]
39. Atkinson, P.M. Selecting the spatial resolution of airborne MSS imagery for small-scale agricultural mapping. *Int. J. Remote Sens.* **1997**, *18*, 1903–1917. [CrossRef]
40. Pajares, G. Overview and Current Status of Remote Sensing Applications Based on Unmanned Aerial Vehicles (UAVs). *Photogramm. Eng. Remote Sens.* **2015**, *81*, 281–330. [CrossRef]
41. Shahbazi, M.; Théau, J.; Ménard, P. Recent applications of unmanned aerial imagery in natural resource management. *GISci. Remote Sens.* **2014**, *51*, 339–365. [CrossRef]
42. Ahmed, O.S.; Shemrock, A.; Chabot, D.; Dillon, C.; Williams, G.; Wasson, R.; Franklin, S.E. Hierarchical land cover and vegetation classification using multispectral data acquired from an unmanned aerial vehicle. *Int. J. Remote Sens.* **2017**, *38*, 2037–2052. [CrossRef]
43. Colomina, I.; Molina, P. Unmanned aerial systems for photogrammetry and remote sensing: A review. *ISPRS J. Photogramm. Remote Sens.* **2014**, *92*, 79–97. [CrossRef]

44. Hugenholtz, C.H.; Moorman, B.J.; Riddell, K.; Whitehead, K. Small unmanned aircraft systems for remote sensing and Earth science research. *Eos Trans. Am. Geophys. Union* **2012**, *93*, 236. [CrossRef]
45. Whitehead, K.; Hugenholtz, C.H.; Myshak, S.; Brown, O.; LeClair, A.; Tamminga, A.; Barchyn, T.E.; Moorman, B.; Eaton, B. Remote sensing of the environment with small unmanned aircraft systems (UASs), Part 2: Scientific and commercial applications 1. *J. Unmanned Veh. Syst.* **2014**, *2*, 86–102. [CrossRef]
46. Stöcker, C.; Bennett, R.; Nex, F.; Gerke, M.; Zevenbergen, J. Review of the Current State of UAV Regulations. *Remote Sens.* **2017**, *9*, 459. [CrossRef]
47. Kelcey, J.; Lucieer, A. Sensor correction and radiometric calibration of a 6-band multispectral imaging sensor for UAV remote sensing. In Proceedings of the 12th Congress of the International Society for Photogrammetry and Remote Sensing, Melbourne, Australia, 25 August–1 September 2012; Volume 39, pp. 393–398.
48. Lu, B.; He, Y. Species classification using Unmanned Aerial Vehicle (UAV)-acquired high spatial resolution imagery in a heterogeneous grassland. *ISPRS J. Photogramm. Remote Sens.* **2017**, *128*, 73–85. [CrossRef]
49. Hueni, A.; Damm, A.; Kneubuehler, M.; Schläpfer, D.; Schaepman, M.E. Field and Airborne Spectroscopy Cross Validation—Some Considerations. *IEEE J. Sel. Top. Appl. Earth Obs. Remote Sens.* **2017**, *10*, 1117–1135. [CrossRef]
50. Del Pozo, S.; Rodríguez-Gonzálvez, P.; Hernández-López, D.; Felipe-García, B. Vicarious Radiometric Calibration of a Multispectral Camera on Board an Unmanned Aerial System. *Remote Sens.* **2014**, *6*, 1918–1937. [CrossRef]
51. Breiman, L. Random Forests. *Mach. Learn.* **2001**, *45*, 5–32. [CrossRef]
52. MeteoSwiss Climate Normals Zürich/Fluntern Climate Normals Zürich/Fluntern. Available online: http://www.meteoswiss.admin.ch/product/output/climate-data/climate-diagrams-normal-values-station-processing/SMA/climsheet_SMA_np8110_e.pdf (accessed on 19 March 2018).
53. Diek, S.; Schaepman, M.; de Jong, R. Creating Multi-Temporal Composites of Airborne Imaging Spectroscopy Data in Support of Digital Soil Mapping. *Remote Sens.* **2016**, *8*, 906. [CrossRef]
54. Meier, U. Entwicklungsstadien mono-und dikotyler Pflanzen. *Die erweiterte BBCH Monogr.* **2001**, *2*. Available online: http://www.agrometeo.ch/sites/default/files/u10/bbch-skala_deutsch.pdf (accessed on 14 August 2018).
55. Fernández-Delgado, M.; Cernadas, E.; Barro, S.; Amorim, D. Do we Need Hundreds of Classifiers to Solve Real World Classification Problems? *J. Mach. Learn. Res.* **2014**, *15*, 3133–3181.
56. Fauvel, M.; Tarabalka, Y.; Benediktsson, J.A.; Chanussot, J.; Tilton, J.C. Advances in Spectral-Spatial Classification of Hyperspectral Images. *Proc. IEEE* **2013**, *101*, 652–675. [CrossRef]
57. Tuia, D.; Pacifici, F.; Kanevski, M.; Emery, W.J. Classification of Very High Spatial Resolution Imagery Using Mathematical Morphology and Support Vector Machines. *IEEE Trans. Geosci. Remote Sens.* **2009**, *47*, 3866–3879. [CrossRef]
58. Vincent, L. Morphological Grayscale Reconstruction in Image Analysis: Applications and Efficient Algorithms. *IEEE Trans. Image Process.* **1993**, *2*, 176–201. [CrossRef] [PubMed]
59. Soille, P. *Morphological Image Analysis*; Springer: Berlin/Heidelberg, Germany, 2004; ISBN 978-3-642-07696-1.
60. Ferro, C.J.S.; Warner, T.A. Scale and texture in digital image classification. *Photogramm. Eng. Remote Sens.* **2002**, *68*, 51–63.
61. Lyons, M.B.; Keith, D.A.; Phinn, S.R.; Mason, T.J.; Elith, J. A comparison of resampling methods for remote sensing classification and accuracy assessment. *Remote Sens. Environ.* **2018**, *208*, 145–153. [CrossRef]
62. Congalton, R. *Assessing the Accuracy of Remotely Sensed Data*; Mapping Science; CRC Press: Boca Raton, FL, USA, 2008; ISBN 978-1-4200-5512-2.
63. Cohen, J. Weighted kappa: Nominal scale agreement provision for scaled disagreement or partial credit. *Psychol. Bull.* **1968**, *70*, 213–220. [CrossRef] [PubMed]
64. Norman, J.; Welles, J. Radiative transfer in an array of canopies. *Agron. J.* **1983**, *75*, 481–488. [CrossRef]
65. Flénet, F.; Kiniry, J.R.; Board, J.E.; Westgate, M.E.; Reicosky, D.A. Row spacing effects on light extinction coefficiencts of corn, sorghum, soybena, and sunflower. *Agron. J.* **1996**, *88*, 185–190. [CrossRef]
66. Seginer, I.; Ioslovich, I. Optimal spacing and cultivation intensity for an industrialized crop production system. *Agric. Syst.* **1999**, *62*, 143–157. [CrossRef]
67. Tokarczyk, P.; Wegner, J.D.; Walk, S.; Schindler, K. Features, Color Spaces, and Boosting: New Insights on Semantic Classification of Remote Sensing Images. *IEEE Trans. Geosci. Remote Sens.* **2015**, *53*, 280–295. [CrossRef]

68. Wu, M.; Yang, C.; Song, X.; Hoffmann, W.C.; Huang, W.; Niu, Z.; Wang, C.; Li, W. Evaluation of orthomosics and digital surface models derived from aerial imagery for crop type mapping. *Remote Sens.* **2017**, *9*, 239. [CrossRef]
69. Zhang, J.; Yang, C.; Song, H.; Hoffmann, W.C.; Zhang, D.; Zhang, G. Evaluation of an Airborne Remote Sensing Platform Consisting of Two Consumer-Grade Cameras for Crop Identification. *Remote Sens.* **2016**, *8*, 257. [CrossRef]
70. Zhang, J.; Yang, C.; Zhao, B.; Song, H.; Hoffmann, W.C.; Shi, Y.; Zhang, D.; Zhang, G. Crop classification and LAI estimation using original and resolution-reduced images from two consumer-grade cameras. *Remote Sens.* **2017**, *9*, 2054. [CrossRef]

Crop Classification in a Heterogeneous Arable Landscape Using Uncalibrated UAV Data

Jonas E. Böhler *, Michael E. Schaepman and Mathias Kneubühler

This supplementary material supports the main text as follows:

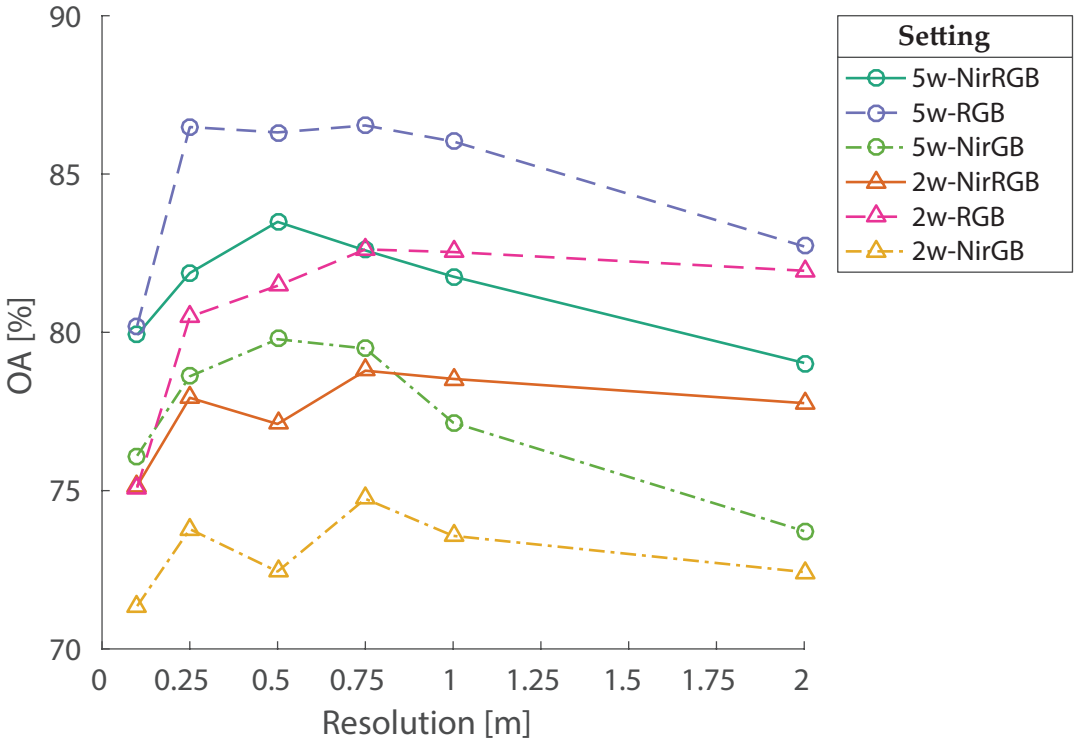

Figure S1. Overall accuracy (OA) for the merged set of crop classes for all tested spatial resolutions and settings of the data set for a pixel-based classification. Circles mark five structuring element (SE) sizes at evaluated resolutions and triangles two SE, respectively. The line styles correspond to the applied spectral band selection.

Remote Sens. **2018**, 11, x; doi: FOR PEER REVIEW

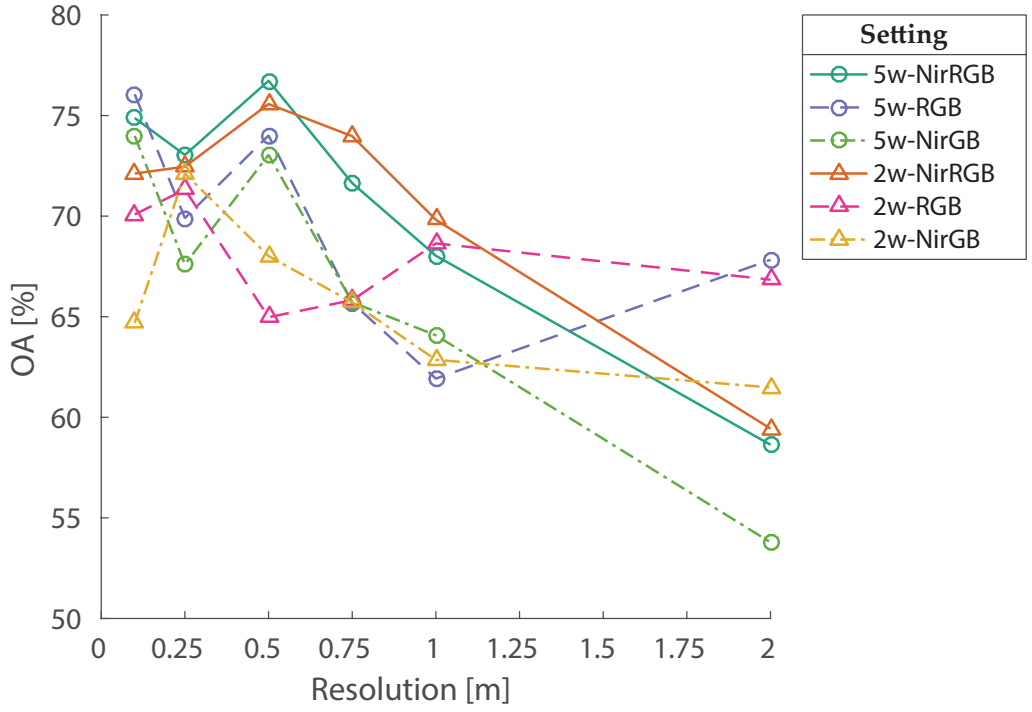

Figure S2. Overall accuracy (OA) for the full set of crop classes for all tested spatial resolutions and settings of the data set for a parcel-based classification. Circles mark five structuring element (SE) sizes at evaluated resolutions and triangles two SE, respectively. The line styles correspond to the applied spectral band selection.

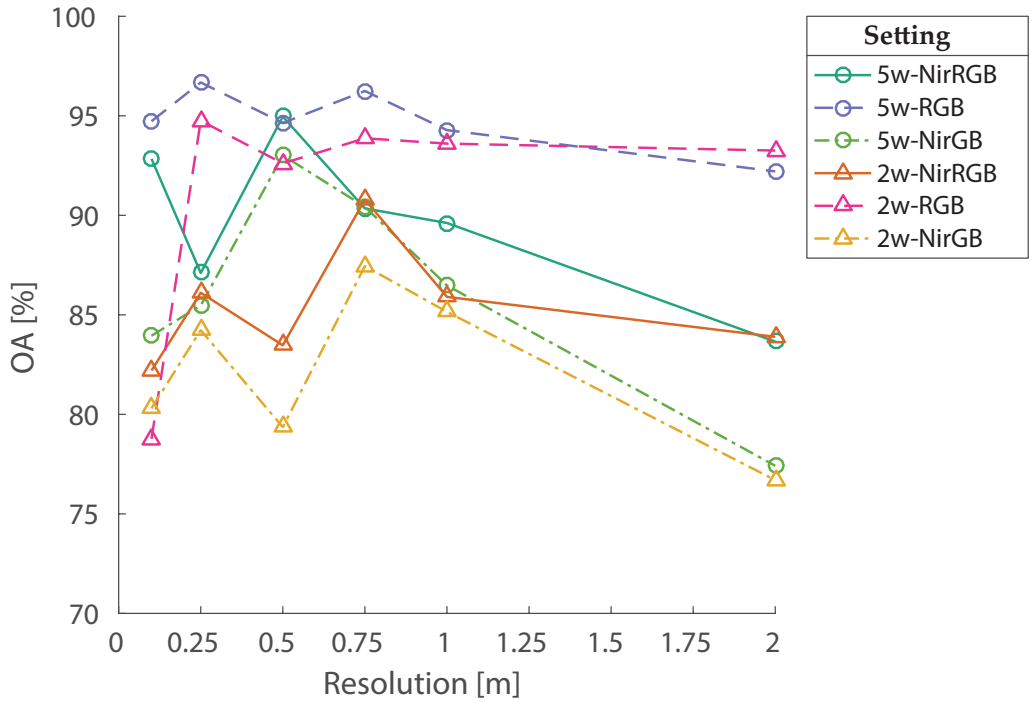

Figure S3. Overall accuracy (OA) for the merged set of crop classes for all tested spatial resolutions and settings of the data set for a parcel-based classification. Circles mark five structuring element (SE) sizes at evaluated resolutions and triangles two SE, respectively. The line styles correspond to the applied spectral band selection.

Remote Sens. **2018**, 11, x; doi: FOR PEER REVIEW

Table S1. Accuracy values for all tested spatial resolutions and settings of the full set of crop classes for a pixel-based classification.

Resolution (m)	Setting	OA (%)	Kappa	AA (%)	AR (%)
0.1	2SE-NirGB	53.3	0.466	53.0	57.0
0.25	2SE-NirGB	54.2	0.473	49.8	56.4
0.5	2SE-NirGB	53.5	0.461	48.7	53.9
0.75	2SE-NirGB	54.8	0.474	48.5	53.8
1	2SE-NirGB	55.4	0.479	48.2	54.0
2	2SE-NirGB	51.9	0.440	47.2	51.5
0.1	2SE-NirRGB	55.0	0.483	52.9	56.9
0.25	2SE-NirRGB	60.0	0.539	56.2	63.5
0.5	2SE-NirRGB	60.5	0.540	55.5	61.9
0.75	2SE-NirRGB	60.3	0.536	54.8	60.6
1	2SE-NirRGB	61.0	0.543	54.8	60.8
2	2SE-NirRGB	56.6	0.494	54.2	57.6
0.1	2SE-RGB	53.8	0.468	50.9	55.6
0.25	2SE-RGB	59.9	0.534	54.1	59.0
0.5	2SE-RGB	60.1	0.534	52.8	58.5
0.75	2SE-RGB	59.2	0.523	51.1	57.2
1	2SE-RGB	59.5	0.526	51.3	57.6
2	2SE-RGB	59.0	0.520	51.4	56.1
0.1	5SE-NirGB	60.2	0.540	57.8	62.4
0.25	5SE-NirGB	61.8	0.557	56.4	62.9
0.5	5SE-NirGB	62.1	0.555	55.0	59.5
0.75	5SE-NirGB	60.2	0.531	52.8	56.9
1	5SE-NirGB	59.1	0.517	52.0	55.9
2	5SE-NirGB	50.4	0.420	47.4	48.5
0.1	5SE-NirRGB	61.8	0.558	58.3	61.9
0.25	5SE-NirRGB	60.8	0.544	55.0	60.0
0.5	5SE-NirRGB	65.5	0.596	60.0	64.7
0.75	5SE-NirRGB	63.9	0.575	58.5	62.0
1	5SE-NirRGB	62.8	0.562	57.1	60.7
2	5SE-NirRGB	55.6	0.482	54.1	55.4
0.1	5SE-RGB	61.1	0.548	56.1	60.0
0.25	5SE-RGB	60.5	0.538	54.2	55.9
0.5	5SE-RGB	66.7	0.608	59.3	62.9
0.75	5SE-RGB	63.7	0.573	56.1	59.1
1	5SE-RGB	62.6	0.559	55.5	57.8
2	5SE-RGB	60.0	0.526	52.2	53.7

Remote Sens. **2018**, 11, x; doi: FOR PEER REVIEW

Table S2. Accuracy values for all tested spatial resolutions and settings of the full set of crop classes for a parcel-based classification.

Resolution (m)	Setting	OA (%)	Kappa	AA (%)	AR (%)
0.1	2SE-NirGB	64.7	0.601	61.9	72.3
0.25	2SE-NirGB	72.1	0.676	67.0	74.7
0.5	2SE-NirGB	68.0	0.625	62.4	69.0
0.75	2SE-NirGB	65.7	0.597	58.5	65.6
1	2SE-NirGB	62.9	0.562	55.7	60.8
2	2SE-NirGB	61.5	0.546	54.1	61.3
0.1	2SE-NirRGB	72.1	0.678	62.7	71.1
0.25	2SE-NirRGB	72.5	0.676	66.7	71.0
0.5	2SE-NirRGB	75.6	0.715	72.1	77.2
0.75	2SE-NirRGB	74.0	0.694	66.9	73.7
1	2SE-NirRGB	69.8	0.644	64.2	69.8
2	2SE-NirRGB	59.4	0.530	58.2	65.1
0.1	2SE-RGB	70.1	0.655	60.7	69.5
0.25	2SE-RGB	71.3	0.667	60.4	64.7
0.5	2SE-RGB	65.0	0.593	56.8	64.4
0.75	2SE-RGB	65.8	0.601	60.8	67.8
1	2SE-RGB	68.6	0.634	63.8	70.5
2	2SE-RGB	66.8	0.614	59.0	65.0
0.1	5SE-NirGB	74.0	0.702	69.6	77.2
0.25	5SE-NirGB	67.6	0.625	66.4	72.5
0.5	5SE-NirGB	73.0	0.683	65.5	71.7
0.75	5SE-NirGB	65.7	0.594	60.7	64.5
1	5SE-NirGB	64.1	0.577	57.4	63.2
2	5SE-NirGB	53.8	0.459	50.2	54.1
0.1	5SE-NirRGB	74.9	0.709	69.8	73.2
0.25	5SE-NirRGB	73.0	0.687	68.4	71.9
0.5	5SE-NirRGB	76.7	0.728	70.3	78.0
0.75	5SE-NirRGB	71.6	0.667	66.0	72.4
1	5SE-NirRGB	68.0	0.625	61.9	66.9
2	5SE-NirRGB	58.6	0.520	58.0	62.2
0.1	5SE-RGB	76.1	0.721	67.8	72.4
0.25	5SE-RGB	69.9	0.648	61.7	64.4
0.5	5SE-RGB	74.0	0.696	69.1	77.3
0.75	5SE-RGB	65.7	0.598	58.0	64.2
1	5SE-RGB	61.9	0.554	54.4	59.3
2	5SE-RGB	67.8	0.615	54.8	58.1

Remote Sens. **2018**, 11, x; doi: FOR PEER REVIEW

Table S3. Accuracy values for all tested spatial resolutions and settings of the merged set of crop classes for a pixel-based classification.

Resolution (m)	Setting	OA (%)	Kappa	AA (%)	AR (%)
0.1	2SE-NirGB	71.4	0.635	71.8	77.2
0.25	2SE-NirGB	73.8	0.663	74.6	78.4
0.5	2SE-NirGB	72.4	0.644	74.4	76.9
0.75	2SE-NirGB	74.7	0.671	75.8	77.5
1	2SE-NirGB	73.6	0.657	75.0	76.3
2	2SE-NirGB	72.4	0.645	73.9	76.4
0.1	2SE-NirRGB	75.1	0.682	75.0	80.1
0.25	2SE-NirRGB	77.9	0.717	78.4	82.3
0.5	2SE-NirRGB	77.1	0.706	78.3	81.1
0.75	2SE-NirRGB	78.8	0.725	79.2	81.4
1	2SE-NirRGB	78.5	0.722	79.6	81.2
2	2SE-NirRGB	77.8	0.714	79.3	81.3
0.1	2SE-RGB	75.1	0.681	74.8	79.6
0.25	2SE-RGB	80.5	0.748	78.8	83.4
0.5	2SE-RGB	81.5	0.759	80.2	83.2
0.75	2SE-RGB	82.6	0.773	81.0	84.1
1	2SE-RGB	82.5	0.772	81.1	83.9
2	2SE-RGB	81.9	0.764	80.8	83.2
0.1	5SE-NirGB	76.1	0.694	76.5	81.1
0.25	5SE-NirGB	78.6	0.724	80.6	83.1
0.5	5SE-NirGB	79.8	0.736	80.9	82.6
0.75	5SE-NirGB	79.5	0.732	80.3	82.4
1	5SE-NirGB	77.1	0.703	78.0	80.6
2	5SE-NirGB	73.7	0.661	76.8	78.0
0.1	5SE-NirRGB	79.9	0.741	79.3	83.8
0.25	5SE-NirRGB	81.9	0.767	83.2	86.2
0.5	5SE-NirRGB	83.5	0.785	84.0	86.1
0.75	5SE-NirRGB	82.6	0.774	83.7	85.5
1	5SE-NirRGB	81.8	0.763	83.0	84.7
2	5SE-NirRGB	79.0	0.730	81.7	82.5
0.1	5SE-RGB	80.2	0.745	78.8	83.6
0.25	5SE-RGB	86.5	0.823	85.4	88.1
0.5	5SE-RGB	86.3	0.820	85.7	87.5
0.75	5SE-RGB	86.5	0.823	85.8	87.9
1	5SE-RGB	86.0	0.816	85.4	87.2
2	5SE-RGB	82.7	0.773	83.0	83.6

Remote Sens. **2018**, 11, x; doi: FOR PEER REVIEW

Table S4. Accuracy values for all tested spatial resolutions and settings of the merged set of crop classes for a parcel-based classification.

Resolution (m)	Setting	OA (%)	Kappa	AA (%)	AR (%)
0.1	2SE-NirGB	80.3	0.751	83.8	87.1
0.25	2SE-NirGB	84.2	0.799	89.8	90.6
0.5	2SE-NirGB	79.4	0.735	84.9	86.5
0.75	2SE-NirGB	87.5	0.837	90.1	91.3
1	2SE-NirGB	85.2	0.807	88.4	89.2
2	2SE-NirGB	76.7	0.705	82.8	83.9
0.1	2SE-NirRGB	82.2	0.775	84.1	88.6
0.25	2SE-NirRGB	86.1	0.823	91.0	92.0
0.5	2SE-NirRGB	83.5	0.789	88.5	89.7
0.75	2SE-NirRGB	90.8	0.880	91.5	93.8
1	2SE-NirRGB	85.9	0.819	88.6	90.6
2	2SE-NirRGB	83.9	0.798	89.2	90.1
0.1	2SE-RGB	78.8	0.734	81.3	85.8
0.25	2SE-RGB	94.8	0.931	91.7	95.9
0.5	2SE-RGB	92.6	0.903	92.2	94.4
0.75	2SE-RGB	93.9	0.920	93.4	95.1
1	2SE-RGB	93.6	0.916	93.2	94.8
2	2SE-RGB	93.3	0.912	92.7	94.7
0.1	5SE-NirGB	83.9	0.796	88.1	89.5
0.25	5SE-NirGB	85.5	0.815	90.9	91.5
0.5	5SE-NirGB	93.0	0.908	94.7	95.1
0.75	5SE-NirGB	90.4	0.875	92.9	92.7
1	5SE-NirGB	86.5	0.823	88.6	89.9
2	5SE-NirGB	77.4	0.716	84.8	84.9
0.1	5SE-NirRGB	92.8	0.907	93.8	95.3
0.25	5SE-NirRGB	87.1	0.836	92.0	92.7
0.5	5SE-NirRGB	95.0	0.934	95.3	96.9
0.75	5SE-NirRGB	90.3	0.876	93.1	94.4
1	5SE-NirRGB	89.6	0.867	92.2	93.8
2	5SE-NirRGB	83.7	0.795	89.1	89.7
0.1	5SE-RGB	94.7	0.931	92.1	96.0
0.25	5SE-RGB	96.7	0.956	95.8	97.3
0.5	5SE-RGB	94.6	0.930	95.8	95.8
0.75	5SE-RGB	96.2	0.951	95.6	97.0
1	5SE-RGB	94.3	0.925	93.2	95.6
2	5SE-RGB	92.2	0.898	91.1	93.6

Remote Sens. **2018**, 11, x; doi: FOR PEER REVIEW

Table S5. User Accuracy (UA) and Producer Accuracy (PA) for the full set of crop classes in a pixel- and parcel-based classification at a spatial resolution of 0.5 m and the 5SE-RGB setting.

Crop class	Pixel-based		Parcel-based	
	UA (%)	PA (%)	UA (%)	PA (%)
Rapeseed	90.7	91.8	100.0	100.0
Maize	75.4	65.9	90.8	76.4
Sugar Beet	77.2	91.0	78.2	100.0
Winter Wheat	86.2	86.9	94.1	100.0
Spelt	32.2	43.8	65.1	75.8
Winter Barley	78.3	76.8	100.0	100.0
Grassland	34.3	23.5	24.2	6.7
Grass Hay	10.8	28.0	7.4	47.8
Clover	45.2	48.7	45.6	76.1
Bare Soil	62.5	72.7	85.6	90.7
Average (AA/AR)	59.3	62.9	69.1	77.3

Table S6. User Accuracy (UA) and Producer Accuracy (PA) for the merged set of crop classes in a pixel- and parcel-based classification at a spatial resolution of 0.5 m and the 5SE-RGB setting.

Crop class	Pixel-based		Parcel-based	
	UA (%)	PA (%)	UA (%)	PA (%)
Rapeseed	88.5	93.3	100.0	100.0
Maize	90.1	87.9	96.9	96.6
Sugar Beet	73.1	91.1	85.2	100.0
Cereal	89.1	87.2	96.8	100.0
Grassland	87.4	77.8	100.0	82.5
Average (AA/AR)	85.7	87.5	95.8	95.8

Chapter

3

Optimal Timing Assessment for Crop Separation Using Multispectral Unmanned Aerial Vehicle (UAV) Data and Textural Features

This chapter is based on the peer-reviewed article:
***Böhler, J. E.**, Schaepman, M. E., Kneubühler, M. (2019) Optimal Timing Assessment for Crop Separation Using Multispectral Unmanned Aerial Vehicle (UAV) Data and Textural Features. Remote Sensing 11(15), 1780; DOI: 10.3390/rs11151780*

J.E.B. designed the research and analyzed the data with scientific advice of M.K. and M.E.S., J.E.B. wrote the manuscript and all co-authors thoroughly reviewed and edited the manuscript.

remote sensing

MDPI

Article

Optimal Timing Assessment for Crop Separation Using Multispectral Unmanned Aerial Vehicle (UAV) Data and Textural Features

Jonas E. Böhler *, Michael E. Schaepman and Mathias Kneubühler

Department of Geography, Remote Sensing Laboratories (RSL), University of Zürich, Winterthurerstrasse 190, 8057 Zürich, Switzerland

* Correspondence: jonas.boehler@geo.uzh.ch; Tel.: +41-446-355-249

Received: 17 May 2019; Accepted: 27 July 2019; Published: 30 July 2019

Abstract: The separation of crop types is essential for many agricultural applications, particularly when within-season information is required. Generally, remote sensing may provide timely information with varying accuracy over the growing season, but in small structured agricultural areas, a very high spatial resolution may be needed that exceeds current satellite capabilities. This paper presents an experiment using spectral and textural features of NIR-red-green-blue (NIR-RGB) bands data sets acquired with an unmanned aerial vehicle (UAV). The study area is located in the Swiss Plateau, which has highly fragmented and small structured agricultural fields. The observations took place between May 5 and September 29, 2015 over 11 days. The analyses are based on a random forest (RF) approach, predicting crop separation metrics of all analyzed crops. Three temporal windows of observations based on accumulated growing degree days (AGDD) were identified: an early temporal window (515–1232 AGDD, 5 May–17 June 2015) with an average accuracy (AA) of 70–75%; a mid-season window (1362–2016 AGDD, 25 June–22 July 2015) with an AA of around 80%; and a late window (2626–3238 AGDD, 21 August–29 September 2015) with an AA of <65%. Therefore, crop separation is most promising in the mid-season window, and an additional NIR band increases the accuracy significantly. However, discrimination of winter crops is most effective in the early window, adding further observational requirements to the first window.

Keywords: crop type separation; temporal window; small structured agricultural area; uncalibrated consumer-grade camera; unmanned aerial vehicle (UAV); very high resolution (VHR); random forest (RF) classifier; spectral and textural features

1. Introduction

Crop type separation is a crucial requirement for the planning [1], short-term monitoring [2], management [3], high-throughput phenotyping [4–6], and climate change modeling [7] of agricultural areas. Many of these tasks need up-to-date information, in particular before the end of the growing season. These tasks require spatially explicit land cover maps. Nevertheless, this kind of information is usually reported by farmers only after the season and mostly at administrative units [8]. Even when the reporting for subsidies takes place in a geographic information system, as is the case in Switzerland, the data are only entered after the season or even in the following year [9]. Therefore, a more up-to-date assessment of crop status needs a different data collection source.

Remote sensing has proven its potential to deliver such information even before the end of season [10]. Land cover crop maps are often based on satellite data because these platforms provide data sets multiple times per month and are suitable for both single-date or multitemporal classification tasks [11,12]. Moreover, several studies have demonstrated the ability to carry out early stage crop

mapping [1,2,13,14]. However, due to fixed orbits and thus fixed observation dates, clouds can limit the amount of usable data. Furthermore, freely available data from Landsat or Sentinel satellites have coarse spatial resolution and therefore capture a high amount of mixed pixel information, especially in small structured farmlands. Hence, data sets of higher spatial resolution are necessary to acquire spectrally pure pixels that are needed in algorithm training [10,15,16]. To date, data sets gained with spaceborne sensors at an appropriate spatial resolution are still expensive and rare.

Unmanned aerial vehicles (UAVs) deliver spatially very high resolution (VHR) data sets and a 3D point-cloud with a spatial resolution of only a few centimeters [17]. UAV data creates new opportunities in agriculture [18–20], e.g., assessment of plant health status [21], water stress [22], management techniques [23], erosion of soils [24], and detection of individual plants [25], among many others. The advantages of VHR data sets compared to common satellite data sets have also been analyzed, e.g., for vegetation indices (VI) [26,27]. Further, UAVs have the ability to acquire data in a very flexible manner, e.g., by considering changing weather conditions, and they are cheap to operate compared to other carrier systems [17]. However, less sophisticated sensors are usually mounted on UAVs, containing broader spectral bands that are difficult to spectrally and radiometrically calibrate [28]. Consumer-grade cameras provide red, green and blue (RGB) wavelength bands, but they can be modified in a way to be able to acquire a near-infrared (NIR) band as well [29]. Therefore, a NIR-RGB mosaic can be built using combined data from these two camera types.

In Switzerland, farmland is often structured in small plots [30], and therefore VHR data sets are required to accurately discriminate different crops. To acquire VHR data sets for multiple dates, consumer-grade cameras with RGB and NIR-GB bands were mounted on a UAV. Uncalibrated data sets were used in this study to investigate the potential of a straightforward, user-friendly, and low-cost data acquisition and processing methodology for crop separation over a growing season. Due to the sensors' limited spectral properties, the incorporation of additional information content through textural features is a promising option to improve the accuracy of crop separation [31,32].

Using approaches, in which all available remotely sensed data sets are jointly processed for crop classification purposes, the accuracy of crop separation has been found to increase [1,11,12,14]. In very fragmented agricultural systems, with very small fields, inhomogeneous cropping cycles and stringent crop rotation schemes, such as on the Swiss Plateau, sawing and harvesting dates of crops are subject to large temporal variations and arbitrarily changing patterns of bare vs. vegetated land cover. These properties are resulting in a decrease of the overall accuracy of crop separation by more than 20% (data not shown) on the Swiss Plateau when using a stacked approach.

Since crops show a changing spectral response due to the evolution of their phenological stage over the growing season, we hypothesize that crops can be separated with varying accuracy at different observation dates over the season. Hence, the aims of this study are to (i) determine an optimal temporal window during the growing season to separate all present crop types from each other, including textural features of an uncalibrated NIR-RGB data set, (ii) evaluate the potential of an additional NIR band compared to a standard RGB configuration, and (iii) assess the potential to discriminate a single crop type from all others on different observation dates.

2. Materials and Methods

2.1. Study Area

The study area is located on the Swiss Plateau (47.312°N, 8.733°E, Figure 1) and is subject to a warm temperate humid climate [33]. Crop and grasslands mainly dominate the area. The crop types include winter and summer crops. Winter crops are cereals (winter barley, spelt, and winter wheat), rapeseed, and grassland (permanent and temporary, including clover), whereas the summer crops taken into account in this study are maize and sugar beet. For maize, rapeseed, sugar beet, and winter wheat (which represents the cereal crop type), the phenological stage of a single reference field was

Remote Sens. **2019**, *11*, 1780

recorded according to the Biologische Bundesanstalt, Bundessortenamt und Chemische Industrie (BBCH) scale for all 11 observation dates between 5 May 5 and 29 September 2015 (Table 1) [34].

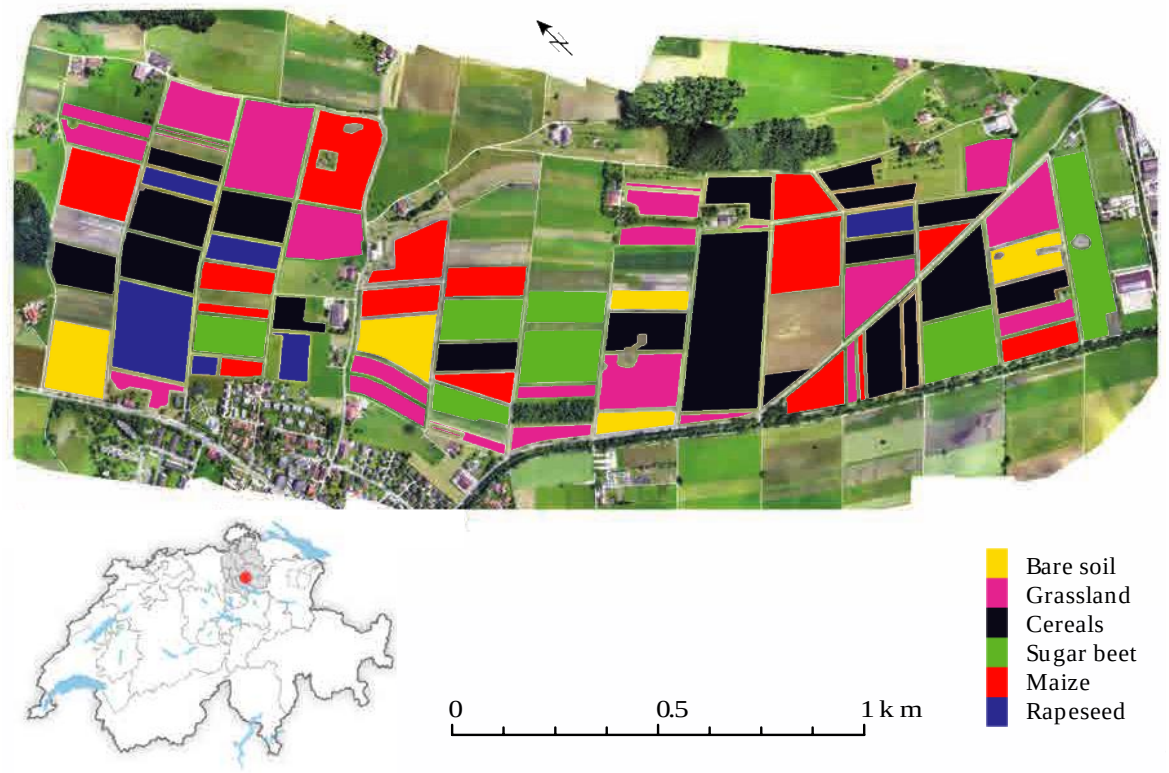

Figure 1. Mosaic of the study area near Mönchaltorf in the canton of Zurich (red dot and grey shaded area in the overview map of Switzerland, bottom left), acquired over 1362 accumulated growing degree days (AGDD, i.e., 25 June 2015) with a consumer-grade RGB camera mounted on a UAV, superimposed by the ground reference data from the same date.

Table 1. Observation dates, corresponding accumulated growing degree days (AGDD) and phenological stage (represented as BBCH) of a single reference field per crop type. Cereals are represented by phenological stage of winter wheat.

Observation Date	AGDD	Phenological Stage (BBCH)			
		Rapeseed	Maize	Sugar Beet	Cereals
5 May 2015	515	65	-	15	29
12 May 2015	635	67	14	17	29
28 May 2015	848	71	16	19	55
4 June 2015	989	79	17	19	69
17 June 2015	1232	80	17	31	73
25 June 2016	1362	80	33	39	75
3 July 2015	1556	87	38	39	77
10 July 2015	1723	89	60	39	87
22 July 2015	2016	-	65	39	-
21 August 2015	2626	-	73	39	-
29 September 2015	3238	-	-	39	-

The total number of fields for a specific crop varied between observation dates; some grassland fields were transformed first into bare soil fields before being sown as summer crop fields (i.e., sugar beet or maize). Other fields were harvested on a certain date and changed therefore to bare soil, or were sown with grass again. Fields with crop residuals were still treated as the previously harvested crop (e.g., cereals after harvesting and before they were cleared as bare soil in preparation for the planting

of a next crop). Consequently, there were no bare soil fields present on May 5, July 3, and July 10. Nevertheless, the total number of fields remained the same over the entire study period.

The agricultural area is structured into small fields ranging from 0.03 to 7.4 ha with an average size of 1.3 ha. The length of a single field varies between 140 m and 200 m and the width between 23 m and 180 m. The total area and number of fields for each class is given in Table 2 for 25 June 2015.

Table 2. Crop types and their size characteristics. The total area and number of fields are given for the extent on 25 June 2015 (1362 AGDD) where now bare soil fields were present.

Crop Type	Total Area [ha]	Number of Fields	Spacing	
			Within-Row [cm]	Row [cm]
Rapeseed	7.6	6	10	30
Maize	26.9	20	14–16	75
Sugar beet	14.1	7	16	50
Cereals	29.5	19	5	14–15
Grassland	24.1	25	-	-

2.2. Data

The image data sets were acquired with an eBee-UAV (Sensefly, Cheseaux-Lausanne, Switzerland) under sunny conditions and two consumer-grade cameras (Canon IXUS 125HS) that record NIR-GB and RGB bands. Image acquisition was performed with the software eMotion2 (Sensefly, Cheseaux-Lausanne, Switzerland), in which the flight altitude was set to 150 m above ground with a lateral overlap of 60% and a longitudinal overlap of 75%, resulting in a spatial resolution of 5 cm (nominal cruise speed 11–25 m/s). Subsequently, an ortho-photomosaic was generated for each observation date with Pix4Dmapper Pro (version 4.2.27, Pix4D S.A., Prilly, Switzerland), combining the NIR band of the one camera and the RGB bands of the other. The data set collected on June 25 was georeferenced on the basis of five ground control points (GCP) measured with a differential GPS device (dGPS), and the other data sets were subsequently georeferenced to this data set. Finally, these data sets were resampled to a spatial resolution of 0.5 m, a spatial resolution most suitable for discrimination of the present crops [32].

2.3. Methodology

In order to decouple the observation date from the phenological stage of the different investigated crops, a growing degree days (GDD) metric was used. GDD was calculated based on temperature data of the closest weather station (Zurich Fluntern, <20 km, Source: Swiss Federal Office of Meteorology and Climatology) with a base temperature T_B of 5.5 °C, the minimal growing temperature for the majority of the crops in the study area [35].

GDD was calculated for an individual day (d) based on the method of [35]

$$GDD_d = \begin{cases} T_{Md} - T_B, \; if \; T_B \leq T_M \\ 0, \; else \end{cases} \quad (1)$$

with T_{Md} being the mean temperature at day d. For each observation date the accumulated GDD (AGDD) was calculated as

$$AGDD = \sum_{d=1}^{n} \mathrm{GDD}_d \quad (2)$$

with n being the number of days between March 1 and the particular observation date (Table 1).

To incorporate contextual information, two types of features were generated for all spectral bands, i.e., first-order statistics (mean, standard deviation, range, and entropy), and mathematical morphology (dilatation/erosion, opening/closing, opening/closing top hat, opening/closing by reconstruction,

and opening/closing by reconstruction top hat). To extract rotation invariant features, a disc-shaped structuring element (SE) was applied with diameters of 3 and 5 pixels [36].

For each observation date, two band settings were built, one with all four bands (NIR-RGB) and one with the RGB bands only, each with the spatial features of the two SE sizes. The data set was subdivided class-wise into six splits and all 15 possible permutations for the selection of two splits for testing were built. Of the remaining four splits per class, two were used for training and two for validation in the classification model building. For the subsequent crop separation, a random forest (RF) algorithm was used [37] since it has been successfully applied in previous studies [38].

In order to determine the best parameters for the RF model, i.e., the number of trees, the results of models with 20 grid points for the number of trees distributed logarithmically between 10 and 1000 were evaluated. Finally, the number of trees was chosen in a way that the loss of accuracy was less than 0.1% compared to the maximum accuracy of the curve fitted to the grid points [32]. The minimal leaf size in the TreeBagger function was set to three, and for the other parameters the default settings from the MATLAB implementation were chosen [39]. The final model was applied to the test data split. A detailed description of the method can be found in [32].

The assessments of the accuracy metrics are based on the average accuracy (AA) and the user accuracy (UA) in order to focus on the needs of potential users. The values are retrieved from the confusion matrix of the classification results of the test data splits and averaged over all 15 folds. In addition, the results for overall accuracy (OA), Kappa coefficient, producer accuracy (PA), and average reliability (AR) are presented in the Appendix A (Table A1).

The entire workflow from feature calculation to crop separation and accuracy assessment for the data set of a single observation date was applied to all 11 data sets. In order to evaluate the differences in crop discrimination accuracy between the different observation dates and settings, the accuracy measurements of the single data sets were tested for significance ($p < 0.05$) against each other using the Wilcoxon signed rank test. A temporal window during the growing season to separate all crop types from each other was defined on subjective visual impression of the AA at the available observation dates (cf. Figure 2).

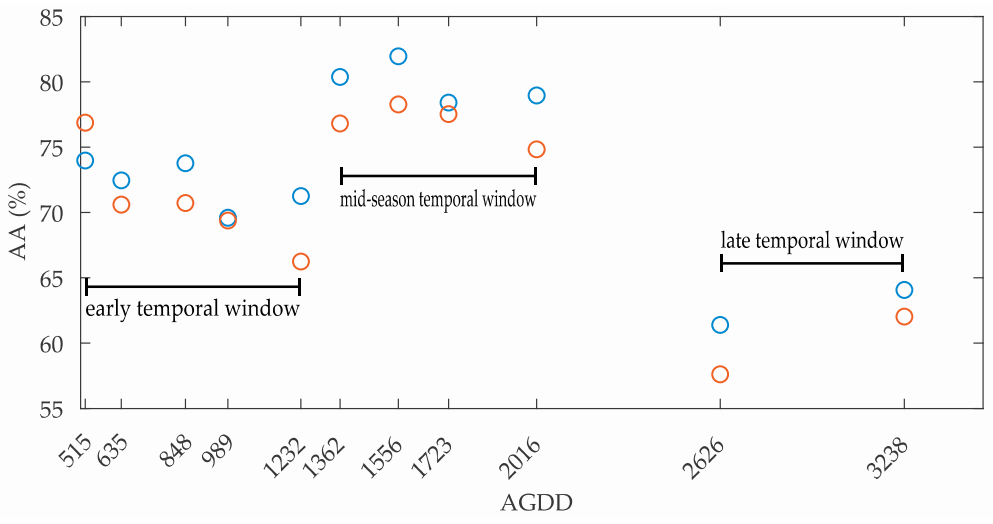

Figure 2. Average accuracy (AA) for all observation dates, represented as accumulated growing degree days (AGDD), for the NIR-RGB setting in blue and the RGB setting in red. The three temporal windows are indicated.

3. Results

The accuracy results (i.e., AA and UA) can be found in Table 3 for the two band settings (i.e., NIR-RGB and RGB, including spatial features of the two SE sizes). The OA, Kappa, and AR metrics are reported in Table A1 in the Appendix A, as well as the p-values of the significance tests (Wilcoxon

signed rank test) between the observation dates for each of the two band settings (Tables A2 and A3), and between the NIR-RGB and RGB settings (Table A4).

Table 3. Average accuracy (AA) and user accuracy (UA) for all settings and observation dates.

Setting	Observation Date (AGDD)	AA (%)	UA (%)					
			Rapeseed	Maize	Sugar Beet	Cereal	Grassland	Bare Soil
NIR-RGB	515	74.0	91.8	39.4	86.7	87.5	56.5	-
NIR-RGB	635	72.5	95.5	54.3	54.4	84.2	89.0	51.1
NIR-RGB	848	73.8	86.1	39.4	72.5	89.7	86.9	64.7
NIR-RGB	989	69.6	75.6	52.0	63.5	87.2	82.6	51.6
NIR-RGB	1232	71.3	77.1	67.0	59.8	78.4	89.9	49.5
NIR-RGB	1362	80.4	87.2	75.0	71.3	85.7	86.0	69.9
NIR-RGB	1556	82.0	69.9	91.0	68.8	86.5	89.7	-
NIR-RGB	1723	78.4	50.3	93.3	62.7	89.3	90.5	-
NIR-RGB	2016	79.0	37.4	93.6	76.0	94.9	94.3	68.7
NIR-RGB	2626	61.4	18.4	94.9	65.6	51.3	91.3	33.9
NIR-RGB	3238	64.1	52.2	91.9	72.3	7.4	98.1	42.4
RGB	515	76.9	97.9	43.0	88.1	88.1	60.0	-
RGB	635	70.6	95.6	49.0	49.3	82.2	85.9	53.2
RGB	848	70.7	80.5	38.0	71.1	87.4	82.4	60.7
RGB	989	69.4	74.1	51.6	60.8	87.0	80.7	56.7
RGB	1232	66.3	68.2	64.9	50.5	77.7	83.3	46.7
RGB	1362	76.8	79.0	69.1	72.8	82.8	80.9	67.1
RGB	1556	78.3	69.2	89.6	62.3	85.4	80.1	-
RGB	1723	77.5	50.6	91.4	60.9	89.6	89.0	-
RGB	2016	74.8	30.0	91.8	71.3	90.9	91.9	64.5
RGB	2626	57.6	11.0	93.8	60.3	51.6	91.9	29.6
RGB	3238	62.0	52.2	90.1	65.1	7.3	97.9	43.7

3.1. Temporal Windows during the Growing Season

Based on the AA metric, three temporal windows during the growing season were identified, i.e., an early temporal window from 515 to 1232 AGDD, a mid-season temporal window from 1362 to 2016 AGDD, and a late temporal window from 2626 to 3238 AGDD (Figure 2). The mid-season window shows the highest crop separation potential with an average AA value of 79.9% over the four observation dates for the NIR-RGB setting and an average AA value of 76.9% for the RGB setting. At 1556 AGDD, the maximum AA values of 82.0% and 78.3% are reached for the NIR-RGB setting and for the RGB setting, respectively (Table 3).

The five observations in the early temporal window until 1232 AGDD contain slightly lower AA values. The average AA values in this time frame are 7.7% lower for the NIR-RGB setting compared to the mid-season temporal window and, correspondingly, 14.2% lower for the RGB setting. The lowest AA values are found in the late temporal window at 62.7% and 59.8% for the NIR-RGB and RGB settings, respectively.

For the NIR-RGB setting, the AA values within a given temporal window are fairly stable but vary significantly between the three temporal windows (Table A2). In contrast, the AA values for the RGB setting are significantly less stable within both the early and late temporal windows. The AA value for the observation at 515 AGDD is not significantly different from the AA values of the mid-season, and the AA value for 1232 AGDD is not significantly different from the AA value at 3238 AGDD (Table A3).

In the early temporal window, the accuracy of the crop discrimination slightly decreases over time by 4.4% for the NIR-RGB setting (Table 3). The highest performance is achieved at 515 AGDD with an AA of 74.0%. The lowest performance is achieved at 989 AGDD with an AA of 69.6%. In case of the RGB setting, the AA values decrease by over 10% between the highest AA of 76.9% at 515 AGDD and the lowest AA of 66.3% at 1232 AGDD.

Regarding the NIR-RGB setting within the early temporal window, only the AA value at 848 AGDD is significantly different from the one at 1232 AGDD (Table A2). For the RGB setting, the AA value for

the observation at 515 AGDD is significantly higher than all other AA values in the early temporal window, whereas the AA value of the observation at 1232 AGDD is significantly lower than the AA values at 515, 635, and 848 AGDD (Table A3).

In the mid-season temporal window, the highest AA values are achieved at 1556 AGDD with 82.0% in case of the NIR-RGB setting and 78.3% in case of the RGB setting (Table 3). The lowest AA values are at 1723 AGDD with 78.4% in case of the NIR-RGB setting and at 2016 AGDD with 74.8% in case of the RGB setting. There are no significant differences between the AA values, except for the highest AA at 1556 AGDD that is significantly higher than the AA values at 1723 and 2016 AGDD for the NIR-RGB setting (Table A2). For the RGB setting, the AA value at 2016 AGDD is significantly lower than the AA values at 1556 and 1723 AGDD (Table A3). All other AA values in this temporal window are not significantly different from each other.

In the late temporal window, the AA values for both band settings are lower than the AA values in the other temporal windows (Table 3), and there is no significant difference between the AA value at 2626 and 3238 AGDD in the case of the NIR-RGB setting (Table A2). As for the RGB setting, the AA value at 3238 AGDD is significantly higher (by as much as 4.4%) than the AA value at 2626 AGDD (Table A3).

3.2. Band Settings

Considering the two investigated band settings, only minor differences in the temporal evolution of the respective AA values are found over the growing season. In the early temporal window, a minimum AA value of 69.9% is reached at 989 AGDD for the NIR-RGB setting, and a minimum AA value of 66.3% at 1232 AGDD in case of the RGB setting. For both settings, the AA values increase significantly between 1232 and 1362 AGDD when they reach the mid-season temporal window. They then fall to low values of 2626 AGDD. Overall, the additional NIR band leads to significantly better results for crop separation in terms of AA values for all observation dates at a significance level of $p < 0.05$, except for the observations at 515 and 989 AGDD (Table A4).

3.3. Discrimination of Individual Crop Types

The temporal assessment of the ability to separate a single crop from the others is very similar for both band settings (Figure 3). Rapeseed can be distinguished best in early season with a UA of over 90% until 635 AGDD. Afterwards, the UA remains above 70% until 1556 AGDD, when it decreases to a minimum of less than 20% at 2626 AGDD. On the contrary, maize can easily be discriminated after 1556 AGDD, with the UA increasing from under 75% to over 90%.

Remote Sens. **2019**, *11*, 1780

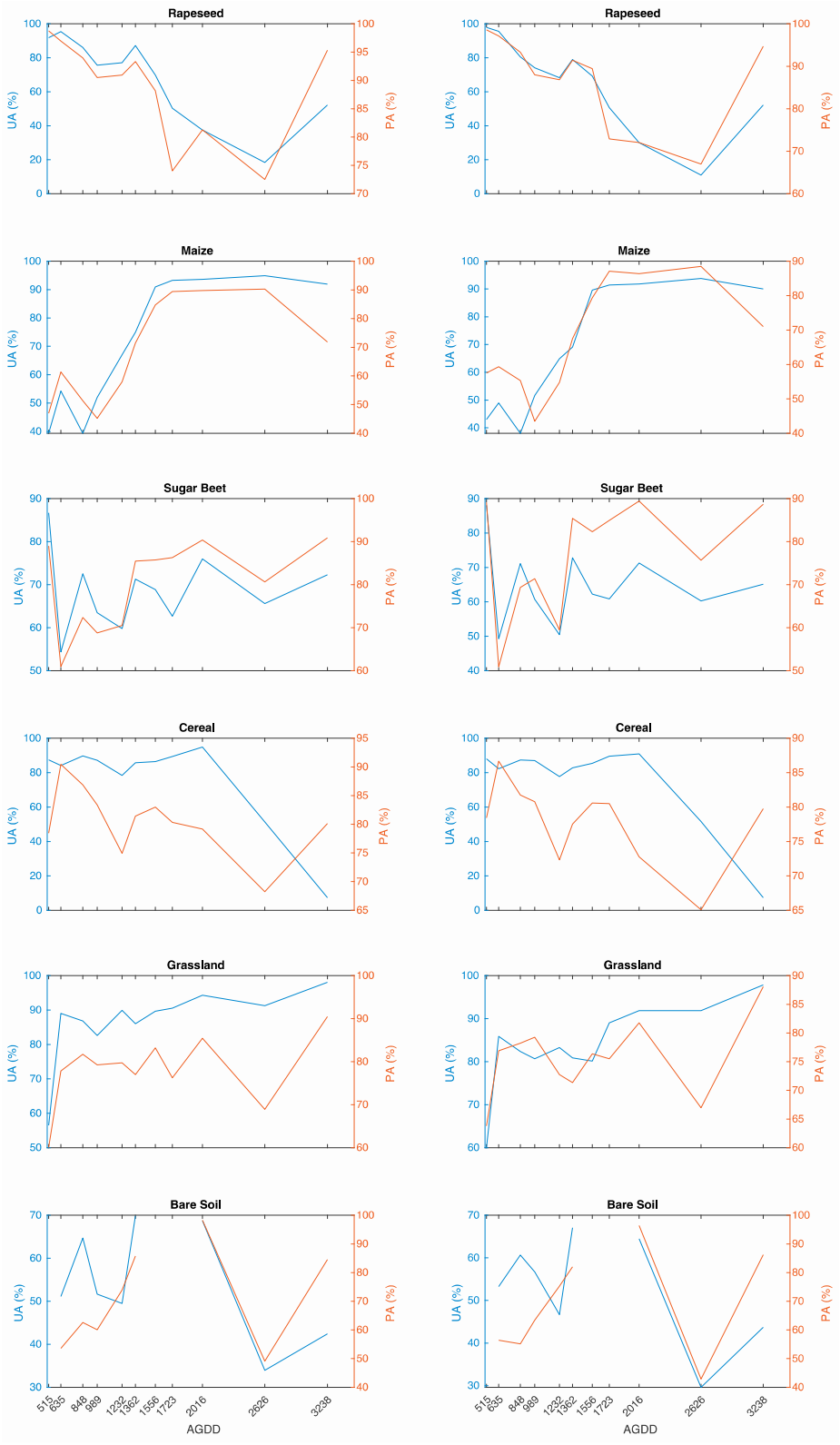

Figure 3. User accuracy (UA) and producer accuracy (PA) of the single crop types for all observation dates, represented as accumulated growing degree days (AGDD) for the NIR-RGB setting (**left**) and the RGB setting (**right**). Different scales for UA and PA apply for the two settings and individual crops.

The discrimination of sugar beet is most effective at 515 AGDD with a UA of more than 85%. At 635 AGDD, its discrimination is most difficult with a UA of less than 55%. From 848 AGDD onwards,

the UA lies between 60% and 76% except for in the case of the RGB setting, when the UA is 50.5% at 1232 AGDD.

Cereals can be distinguished with a UA between 78% and 90% from the beginning of the analyzed AGDD until 1723 AGDD. At 2016 AGDD, the UA is highest with 94.9% for the NIR-RGB setting and 91% for the RGB setting. At 2626 AGDD, the UA is around 51%, and for the last observation date it drops to 7%.

The UA of grassland is under 60% at 515 AGDD, but increases to a range of 80% to 94% from 635 AGDD onwards. On the final observation date, the UA is highest at 98%.

Bare soil can best be discriminated at 1362 and 2016 AGDD with UA values between 65% and 70%. Earlier, the UA is around 55%; it is only higher at 848 AGDD, reaching 65% for the NIR-RGB setting and 61% for the RGB setting. The UA is under 50% for the last two observation dates.

4. Discussion

4.1. Temporal Windows During the Growing Season

The phenological stage of crops is essential to discriminate them from each other in remote sensing data analysis. When considering all of the crops in the study area, the accuracy of crop separation is highest in the mid-season temporal window between 1362 and 2016 AGDD but accuracy reaches a maximum at 1556 AGDD. This is in line with other studies that report best accuracies for crop separation with data sets acquired in July [2,40,41]. At this time of the growing season, the winter crops are in a senescence stage and the summer crops in their most productive stage.

In the early temporal window, at the beginning of the growing season, maize and sugar beet are gradually sown in. Since their seedlings are difficult to distinguish [40] and can thus be mixed up with pixels from bare soil fields, the AA values are lower than in the subsequent mid-season temporal window. The slight decrease in AA values in the early temporal window is not of statistical significance.

Apart from a few exceptions, crop separation accuracies within a temporal window are not significantly different from the other observations in the same temporal window. This holds true for the two tested band settings and their textural features of the UAV data sets. Consequently, any observation of crops within a given temporal window will yield a similar, not significantly different AA.

4.2. Band Settings

An additional NIR band leads to significantly higher crop separation accuracies for most of the observation dates, as reported in several other studies [42–44]. Only at 515 AGDD does the AA value of the RGB setting become higher than in the case of the NIR-RGB setting. Since this difference is not significant, crop separation accuracy with an additional NIR band is generally higher, or at least equal to an RGB setting.

In land use/land cover classifications that are based on textural features, the applied SE sizes play a crucial role [32]. Differing spectral signatures resulting from the interplay of plant material and soil background largely define textural information in agricultural fields. Consequently, when the crop canopy is closed, the spectral, rather than the textural, properties gain in importance [45] and therefore, an additional NIR band can lead to an improvement in crop separation [43].

4.3. Discrimination of Individual Crop Types

With regard to the separation of individual crop species, their own respective phenological stages are crucial. Rapeseed, for example, produces yellow flowers up to 635 AGDD and can therefore be distinguished from all other crops with high precision, as it is the only investigated crop with this specific color. The discrimination of cereals in general, being the other winter crops in the study area, is best straight after harvesting at 2016 AGDD when the signal is dominated by the crop residuals and bare soil, and summer crops (i.e., sugar beet and maize) are in their most productive stage.

The differences between individual summer crops get more pronounced with phenological development; therefore, the UA values of maize and sugar beet increase with generally increasing AGDDs. As reported by [46], the UA of maize increases by over 50% between the first discrimination, when maize fields are freshly sown in at 515 AGDD, and before harvesting at 2626 AGDD, when all other fields are either bare soil or covered by green grassland or sugar beet.

Sugar beet is the first sown summer crop in the study area and can be accurately separated at 515 AGDD, as the spectral signal is dominated by bare soil and therefore is distinguishable from the other present crops (i.e., winter crops or grassland). At the following observation date (i.e., 635 AGDD), differentiation between maize, sugar beet and bare soil fields becomes more difficult, since the spectral signal of all three classes at this phenological stage is dominated by the signal of bare soil and indistinguishable seedlings [40].

Overall, the UA value of grassland is highest after 3238 AGDD, since late in the season it is the only crop well distinguishable from bare soil, maize (appearing brown in its final phenological stages), and sugar beet. In addition, grassland covers most of the area in late season so, consequently, the OA is also high (Table A1). Nevertheless, the AA metric, which gives equal weight to the UA values of all present crop types, is low because the other crops can no longer be distinguished accurately from each other.

Finally, bare soil can most accurately be separated from crops when their plant materials cover a large part of the area and therefore dominate the measured signal. It is particularly difficult to distinguish fields under preparation (e.g., plowed) from fields containing small seedlings. The discrimination of cereals shortly after harvesting is successful since the textural appearance of crop residuals and bare soil is different. Therefore, discrimination of bare soil is most successful at 1362 and 2016 AGGD.

4.4. Limitations and Outlook

Crop types present in an agricultural area influence the resulting separation accuracy. The more diverse they are in terms of morphology and physiology, the more accurately they can be discriminated. Consequently, it is more challenging to separate between different winter crops or between different summer crops than to differentiate winter crops from summer crops. In particular, further separation of crops that have been combined into one class in this study (e.g., cereals like winter wheat, spelt and winter barley) remains to be investigated. Moreover, the optimal temporal windows analyzed here may vary depending on the specific crop types present in an agricultural area, and the behavior between the windows must be further examined.

As shown in a range of other studies, multitemporal data sets improve the accuracies of crop classification tasks [41,47]. Therefore, it would be interesting to investigate the potential of combining data from different acquisition dates to find the most promising temporal combinations for crop separation. Due to the fact that observations with optical sensors are subject to limitations (e.g., cloudy conditions), combined analysis of data acquired in the early and mid-season temporal windows could be promising.

5. Conclusions

This paper presents a methodology to separate agricultural crops based on data sets acquired with uncalibrated consumer-grade cameras mounted on a UAV over the course of 11 observation dates between 5 May 2015 (515 AGDD) and 29 September 2015 (3238 AGDD). The obtained four bands data sets, consisting of a NIR, red, green, and blue band, were extended with textural features to differentiate cereals, grassland, maize, rapeseed and sugar beet, and, if present, bare soil, based on an RF approach.

Three temporal windows across the growing season were identified where the accuracies of crop separation between the observation dates were not significantly different. The first temporal window ranged from 515 AGDD (May 5) to 1232 AGDD (June 17), with an AA for separation between 70% and 75%. A mid-season temporal window between 1362 AGDD (June 25) and 2016 AGDD (July 22)

proved to be the most optimal for crop separation with AA values around 80%. Observations after 2626 AGDD (August 21) fell into the third group with an AA of under 65%.

An additional NIR band leads to significantly higher separation results compared to a pure RGB setting, thanks to an extended capability to spectrally discriminate the plant materials of the various crops. The accuracy of the separation of single crops varies over the course of the observed period. Winter crops can be discriminated from summer crops more accurately in the early season, whereas the accuracy of single summer crop separation from other summer crops is highest during their most productive phenological stage in the mid-season temporal window.

Overall, this paper concludes that crop separation based on uncalibrated NIR-RGB data sets in a highly fragmented and small structured agricultural area like the Swiss Plateau is most accurate between 1362 AGDD and 2016 AGDD over the investigated period.

Author Contributions: J.E.B. designed the research and analyzed the data with scientific advice of M.K. and M.E.S., J.E.B. wrote the manuscript and all co-authors thoroughly reviewed and edited the manuscript.

Funding: This research received no external funding.

Acknowledgments: The contribution of M.E.S. is supported by the University of Zurich Research Priority Program on 'Global Change and Biodiversity' (URPP GCB). The meteorological data were provided by MeteoSwiss, the Federal Office for Meteorology and Climatology. We thank staff from RSL and GRS (Wageningen University) supporting fieldwork and providing background information. Reinhard Furrer from the Department of Mathematics at UZH is thanked for guidance with statistical analyses.

Conflicts of Interest: The authors declare no conflict of interest.

Appendix A

Table A1. Overall accuracy (OA), Kappa coefficient, average accuracy (AA), and average reliability (AR) for both settings and all observation dates.

Setting	Observation Date (AGDD)	OA	Kappa	AA	AR
NIR-RGB	515	77.3	0.691	74.0	74.6
NIR-RGB	635	78.1	0.708	72.5	73.5
NIR-RGB	848	77.9	0.719	73.8	74.8
NIR-RGB	989	73.0	0.662	69.6	71.1
NIR-RGB	1232	73.0	0.663	71.3	74.7
NIR-RGB	1362	80.2	0.752	80.4	82.4
NIR-RGB	1556	84.2	0.795	82.0	84.9
NIR-RGB	1723	82.2	0.770	78.4	81.2
NIR-RGB	2016	85.8	0.819	79.0	87.3
NIR-RGB	2626	75.1	0.671	61.4	71.6
NIR-RGB	3238	85.8	0.766	64.1	85.5
RGB	515	78.8	0.713	76.9	77.5
RGB	635	75.7	0.676	70.6	71.2
RGB	848	74.3	0.674	70.7	72.1
RGB	989	72.5	0.656	69.4	71.0
RGB	1232	68.4	0.607	66.3	70.3
RGB	1362	76.5	0.707	76.8	79.2
RGB	1556	80.0	0.741	78.3	81.6
RGB	1723	81.1	0.756	77.5	80.1
RGB	2016	81.7	0.767	74.8	83.1
RGB	2626	72.4	0.637	57.6	67.7
RGB	3238	83.9	0.738	62.0	84.8

Table A2. *p*-values of significance test ($p < 0.05$) for all observation dates of the NIR-RGB setting. Not significant differences are marked in bold. The green color depicts the three temporal windows (i.e., early, medium and late) over the growing season.

AGDD	515	635	848	989	1232	1362	1556	1723	2016	2626	3238
515		**0.107**	**0.934**	**0.169**	**0.107**	0.005	0.001	0.018	0.030	0.000	0.002
635	**0.107**		**0.489**	**0.421**	**0.421**	0.000	0.000	0.001	0.002	0.000	0.002
848	**0.934**	**0.489**		**0.073**	0.041	0.000	0.000	0.005	0.000	0.000	0.000
989	**0.169**	**0.421**	**0.073**		**0.489**	0.000	0.000	0.001	0.000	0.000	0.035
1232	**0.107**	**0.421**	0.041	**0.489**		0.000	0.000	0.000	0.000	0.000	0.001
1362	0.005	0.000	0.000	0.000	0.000		**0.095**	**0.121**	**0.151**	0.000	0.000
1556	0.001	0.000	0.000	0.000	0.000	**0.095**		0.001	0.002	0.000	0.000
1723	0.018	0.001	0.005	0.001	0.000	**0.121**	0.001		**0.639**	0.000	0.000
2016	0.030	0.002	0.000	0.000	0.000	**0.151**	0.002	**0.639**		0.000	0.000
2626	0.000	0.000	0.000	0.000	0.000	0.000	0.000	0.000	0.000		**0.151**
3238	0.002	0.002	0.000	0.035	0.001	0.000	0.000	0.000	0.000	**0.151**	

Table A3. *p*-values of significance test ($p < 0.05$) for all observation dates of the RGB setting. Not significant differences are marked in bold. The green color depicts the three temporal windows (i.e., early, medium and late) over the growing season.

AGDD	515	635	848	989	1232	1362	1556	1723	2016	2626	3238
515		0.003	0.003	0.001	0.001	**0.934**	**0.359**	**0.762**	**0.330**	0.000	0.000
635	0.003		**0.934**	**0.847**	0.048	0.004	0.000	0.000	0.035	0.000	0.002
848	0.003	**0.934**		**0.359**	0.004	0.001	0.000	0.000	0.002	0.000	0.000
989	0.001	**0.847**	**0.359**		**0.151**	0.003	0.000	0.000	0.008	0.000	0.001
1232	0.001	0.048	0.004	**0.151**		0.000	0.000	0.000	0.000	0.000	**0.083**
1362	**0.934**	0.004	0.001	0.003	0.000		**0.389**	**1.000**	**0.229**	0.000	0.000
1556	**0.359**	0.000	0.000	0.000	0.000	**0.389**		**0.454**	0.000	0.000	0.000
1723	**0.762**	0.000	0.000	0.000	0.000	**1.000**	**0.454**		0.035	0.000	0.000
2016	**0.330**	0.035	0.002	0.008	0.000	**0.229**	0.000	0.035		0.000	0.000
2626	0.000	0.000	0.000	0.000	0.000	0.000	0.000	0.000	0.000		0.008
3238	0.000	0.002	0.000	0.001	**0.083**	0.000	0.000	0.000	0.000	0.008	

Table A4. *p*-values of the significance test ($p < 0.05$) for the difference between the NIR-RGB and RGB setting for overall accuracy (OA), Kappa, average accuracy (AA), and average reliability (AR). Not significant differences are marked in bold.

AGDD	OA	kappa	AA	AR
515	**0.229**	**0.208**	**0.135**	**0.083**
635	0.012	0.012	0.010	0.008
848	0.001	0.001	0.001	0.003
989	**0.599**	**0.599**	**0.599**	**0.599**
1232	0.000	0.000	0.000	0.000
1362	0.001	0.001	0.001	0.001
1556	0.000	0.000	0.000	0.000
1723	0.001	0.001	0.003	0.000
2016	0.000	0.000	0.000	0.000
2626	0.035	**0.064**	0.005	0.007
3238	0.000	0.000	0.000	0.012

References

1. Azar, R.; Villa, P.; Stroppiana, D.; Crema, A.; Boschetti, M.; Brivio, P.A. Assessing in-season crop classification performance using satellite data: A test case in Northern Italy. *Eur. J. Remote Sens.* **2016**, *49*, 361–380. [CrossRef]
2. Ozdarici-Ok, A.; Ok, A.; Schindler, K. Mapping of Agricultural Crops from Single High-Resolution Multispectral Images–Data-Driven Smoothing vs. Parcel-Based Smoothing. *Remote Sens.* **2015**, *7*, 5611–5638. [CrossRef]
3. Inglada, J.; Arias, M.; Tardy, B.; Morin, D.; Valero, S.; Hagolle, O.; Dedieu, G.; Sepulcre, G.; Bontemps, S.; Defourny, P. Benchmarking of algorithms for crop type land-cover maps using Sentinel-2 image time series. *2015 IEEE Int. Geosci. Remote Sens. Symp.* **2015**, 3993–3996. [CrossRef]
4. Holman, F.H.; Riche, A.B.; Michalski, A.; Castle, M.; Wooster, M.J.; Hawkesford, M.J. High Throughput Field Phenotyping of Wheat Plant Height and Growth Rate in Field Plot Trials Using UAV Based Remote Sensing. *Remote Sens.* **2016**, *8*. [CrossRef]
5. Shi, Y.; Thomasson, J.A.; Murray, S.C.; Pugh, N.A.; Rooney, W.L.; Shafian, S.; Rajan, N.; Rouze, G.; Morgan, C.L.S.; Neely, H.L.; et al. Unmanned Aerial Vehicles for High-Throughput Phenotyping and Agronomic Research. *PLoS ONE* **2016**, *11*, e0159781. [CrossRef]
6. Tattaris, M.; Reynolds, M.P.; Chapman, S.C. A Direct Comparison of Remote Sensing Approaches for High-Throughput Phenotyping in Plant Breeding. *Front. Plant Sci.* **2016**, *7*, 1131. [CrossRef]
7. Fuhrer, J.; Tendall, D.; Klein, T.; Lehmann, N.; Holzkämper, A. Water Demand in Swiss Agriculture Sustainable Adaptive Options for Land and Water Management to Mitigate Impacts of Climate Change. *Art-Schriftenreihe* **2013**, *19*, 56.
8. Waldhoff, G.; Lussem, U.; Bareth, G. Multi-Data Approach for remote sensing-based regional crop rotation mapping: A case study for the Rur catchment, Germany. *Int. J. Appl. Earth Obs. Geoinf.* **2017**, *61*, 55–69. [CrossRef]
9. Bundesrat, D.S. Verordnung über die Direktzahlungen an die Landwirtschaft. 2017, Volume 2013, pp. 1–152. Available online: https://www.admin.ch/opc/de/classified-compilation/20130216/index.html (accessed on 14 August 2018).
10. Atzberger, C. Advances in Remote Sensing of Agriculture: Context Description, Existing Operational Monitoring Systems and Major Information Needs. *Remote Sens.* **2013**, *5*, 949–981. [CrossRef]
11. Zhong, L.; Hu, L.; Zhou, H. Deep learning based multi-temporal crop classification. *Remote Sens. Environ.* **2019**, *221*, 430–443. [CrossRef]
12. Ouzemou, J.E.; El Harti, A.; Lhissou, R.; El Moujahid, A.; Bouch, N.; El Ouazzani, R.; Bachaoui, E.M.; El Ghmari, A. Crop type mapping from pansharpened Landsat 8 NDVI data: A case of a highly fragmented and intensive agricultural system. *Remote Sens. Appl. Soc. Environ.* **2018**, *11*, 94–103. [CrossRef]
13. Löw, F.; Duveiller, G. Defining the spatial resolution requirements for crop identification using optical remote sensing. *Remote Sens.* **2014**, *6*, 9034–9063. [CrossRef]
14. Conrad, C.; Dech, S.; Dubovyk, O.; Fritsch, S.; Klein, D.; Löw, F.; Schorcht, G.; Zeidler, J. Derivation of temporal windows for accurate crop discrimination in heterogeneous croplands of Uzbekistan using multitemporal RapidEye images. *Comput. Electron. Agric.* **2014**, *103*, 63–74. [CrossRef]
15. Vuolo, F.; Neugebauer, N.; Bolognesi, S.; Atzberger, C.; D'Urso, G. Estimation of Leaf Area Index Using DEIMOS-1 Data: Application and Transferability of a Semi-Empirical Relationship between two Agricultural Areas. *Remote Sens.* **2013**, *5*, 1274–1291. [CrossRef]
16. Whitcraft, A.K.; Becker-Reshef, I.; Killough, B.D.; Justice, C.O. Meeting earth observation requirements for global agricultural monitoring: An evaluation of the revisit capabilities of current and planned moderate resolution optical earth observing missions. *Remote Sens.* **2015**, *7*, 1482–1503. [CrossRef]
17. Pajares, G. Overview and Current Status of Remote Sensing Applications Based on Unmanned Aerial Vehicles (UAVs). *Photogramm. Eng. Remote Sens.* **2015**, *81*, 281–330. [CrossRef]
18. Maes, W.H.; Steppe, K. Perspectives for Remote Sensing with Unmanned Aerial Vehicles in Precision Agriculture. *Trends Plant Sci.* **2019**, *24*, 152–164. [CrossRef] [PubMed]
19. Manfreda, S.; Matthew, F.; Mccabe, M.; Pauline, E.; Miller, P.; Lucas, R.; Pajuelo, V.M.; Mallinis, G.; Dor, E.B.; Helman, D.; et al. On the Use of Unmanned Aerial Systems for Environmental Monitoring. *Remote Sens.* **2018**, *10*, 641. [CrossRef]

20. Adão, T.; Hruška, J.; Pádua, L.; Bessa, J.; Peres, E.; Morais, R.; Sousa, J.J. Hyperspectral imaging: A review on UAV-based sensors, data processing and applications for agriculture and forestry. *Remote Sens.* **2017**, *9*, 1110. [CrossRef]
21. Yao, H.; Qin, R.; Chen, X. Unmanned Aerial Vehicle for Remote Sensing Applications—A Review. *Remote Sens.* **2019**, *11*, 1443. [CrossRef]
22. Zarco-Tejada, P.J.; González-Dugo, V.; Berni, J.A.J. Fluorescence, temperature and narrow-band indices acquired from a UAV platform for water stress detection using a micro-hyperspectral imager and a thermal camera. *Remote Sens. Environ.* **2012**, *117*, 322–337. [CrossRef]
23. Ashapure, A.; Jung, J.; Yeom, J.; Chang, A.; Maeda, M.; Maeda, A.; Landivar, J. A novel framework to detect conventional tillage and no-tillage cropping system effect on cotton growth and development using multi-temporal UAS data. *ISPRS J. Photogramm. Remote Sens.* **2019**, *152*, 49–64. [CrossRef]
24. Glendell, M.; McShane, G.; Farrow, L.; James, M.R.; Quinton, J.; Anderson, K.; Evans, M.; Benaud, P.; Rawlins, B.; Morgan, D.; et al. Testing the utility of structure-from-motion photogrammetry reconstructions using small unmanned aerial vehicles and ground photography to estimate the extent of upland soil erosion. *Earth Surf. Process. Landforms* **2017**, *42*, 1860–1871. [CrossRef]
25. Primicerio, J.; Caruso, G.; Comba, L.; Crisci, A.; Gay, P.; Guidoni, S.; Genesio, L.; Aimonino, D.R.; Vaccari, F.P.; Ricauda Aimonino, D.; et al. Individual plant definition and missing plant characterization in vineyards from high-resolution UAV imagery. *Eur. J. Remote Sens.* **2017**, *50*, 179–186. [CrossRef]
26. Khaliq, A.; Comba, L.; Biglia, A.; Ricauda Aimonino, D.; Chiaberge, M.; Gay, P.; Aimonino, D.R.; Chiaberge, M.; Gay, P. Comparison of Satellite and UAV-Based Multispectral Imagery for Vineyard Variability Assessment. *Remote Sens.* **2019**, *11*, 436. [CrossRef]
27. Deng, L.; Mao, Z.; Li, X.; Hu, Z.; Duan, F.; Yan, Y. UAV-based multispectral remote sensing for precision agriculture: A comparison between different cameras. *ISPRS J. Photogramm. Remote Sens.* **2018**, *146*, 124–136. [CrossRef]
28. Aasen, H.; Honkavaara, E.; Lucieer, A.; Zarco-Tejada, P. Quantitative Remote Sensing at Ultra-High Resolution with UAV Spectroscopy: A Review of Sensor Technology, Measurement Procedures, and Data Correction Workflows. *Remote Sens.* **2018**, *10*, 1091. [CrossRef]
29. Zhang, J.; Yang, C.; Song, H.; Hoffmann, W.C.; Zhang, D.; Zhang, G. Evaluation of an Airborne Remote Sensing Platform Consisting of Two Consumer-Grade Cameras for Crop Identification. *Remote Sens.* **2016**, *8*, 257. [CrossRef]
30. Long, T.B.; Blok, V.; Coninx, I. Barriers to the adoption and diffusion of technological innovations for climate-smart agriculture in Europe: Evidence from the Netherlands, France, Switzerland and Italy. *J. Clean. Prod.* **2016**, *112*, 9–21. [CrossRef]
31. Laliberte, A.S.; Rango, A. Texture and Scale in Object-Based Analysis of Subdecimeter Resolution Unmanned Aerial Vehicle (UAV) Imagery. *IEEE Trans. Geosci. Remote Sens.* **2009**, *47*, 761–770. [CrossRef]
32. Böhler, J.; Schaepman, M.; Kneubühler, M. Crop Classification in a Heterogeneous Arable Landscape Using Uncalibrated UAV Data. *Remote Sens.* **2018**, *10*. [CrossRef]
33. MeteoSwiss Climate Normals Zürich Fluntern Climate Normals Zürich Fluntern. Available online: http://www.meteoswiss.admin.ch/product/output/climate-data/climate-diagrams-normal-values-station-processing/SMA/climsheet_SMA_np8110_e.pdf (accessed on 19 March 2018).
34. Meier, U.; Bleiholder, H.; Buhr, L.; Feller, C.; Hack, H.; Heß, M.; Lancashire, P.D.; Schnock, U.; Stauß, R.; van den Boom, T.; et al. The BBCH system to coding the phenological growth stages of plants-history and publications-Das BBCH-System zur Codierung der phänologischen Entwicklungsstadien von Pflanzen-Geschichte und Veröffentlichungen. *J. Für Kult.* **2009**, *61*, 41–52. [CrossRef]
35. Spinoni, J.; Vogt, J.; Barbosa, P. European degree-day climatologies and trends for the period 1951-2011. *Int. J. Climatol.* **2015**, *35*, 25–36. [CrossRef]
36. Marcos, D.; Volpi, M.; Kellenberger, B.; Tuia, D. Land cover mapping at very high resolution with rotation equivariant CNNs: Towards small yet accurate models. *ISPRS J. Photogramm. Remote Sens.* **2018**, *145*, 96–107. [CrossRef]
37. Breiman, L. Random Forests. *Mach. Learn.* **2001**, *45*, 5–32. [CrossRef]
38. Fernández-Delgado, M.; Cernadas, E.; Barro, S.; Amorim, D. Do we Need Hundreds of Classifiers to Solve Real World Classification Problems. *J. Mach. Learn. Res.* **2014**, *15*, 3133–3181.

39. MathWorks R2018a TreeBagger Class. Available online: https://ch.mathworks.com/help/releases/R2018a/stats/treebagger-class.html (accessed on 16 July 2019).
40. Van Tricht, K.; Gobin, A.; Gilliams, S.; Piccard, I. Synergistic use of radar Sentinel-1 and optical Sentinel-2 imagery for crop mapping: A case study for Belgium. *Remote Sens.* **2018**, *10*, 642. [CrossRef]
41. Vuolo, F.; Neuwirth, M.; Immitzer, M.; Atzberger, C.; Ng, W.T. How much does multi-temporal Sentinel-2 data improve crop type classification. *Int. J. Appl. Earth Obs. Geoinf.* **2018**, *72*, 122–130. [CrossRef]
42. Whitehead, K.; Hugenholtz, C.H.; Myshak, S.; Brown, O.; LeClair, A.; Tamminga, A.; Barchyn, T.E.; Moorman, B.; Eaton, B. Remote sensing of the environment with small unmanned aircraft systems (UASs), part 1: A review of progress and challenges. *J. Unmanned Veh. Syst.* **2014**, *2*, 86–102. [CrossRef]
43. Zhang, H.; Li, Q.; Liu, J.; Shang, J.; Du, X.; McNairn, H.; Champagne, C.; Dong, T.; Liu, M. Image Classification Using RapidEye Data: Integration of Spectral and Textual Features in a Random Forest Classifier. *IEEE J. Sel. Top. Appl. Earth Obs. Remote Sens.* **2017**, *10*, 5334–5349. [CrossRef]
44. Helmholz, P.; Rottensteiner, F.; Heipke, C. Semi-automatic verification of cropland and grassland using very high resolution mono-temporal satellite images. *ISPRS J. Photogramm. Remote Sens.* **2014**, *97*, 204–218. [CrossRef]
45. Norman, J.; Welles, J. Radiative transfer in an array of canopies. *Agron. J.* **1983**, *75*, 481–488. [CrossRef]
46. Demarez, V.; Helen, F.; Marais-Sicre, C.; Baup, F. In-Season Mapping of Irrigated Crops Using Landsat 8 and Sentinel-1 Time Series. *Remote Sens.* **2019**, *11*, 118. [CrossRef]
47. Cai, Y.; Guan, K.; Peng, J.; Wang, S.; Seifert, C.; Wardlow, B.; Li, Z. A high-performance and in-season classification system of field-level crop types using time-series Landsat data and a machine learning approach. *Remote Sens. Environ.* **2018**, *210*, 35–47. [CrossRef]

Chapter

4

Crop Separability from Individual and Combined Airborne Imaging Spectroscopy and UAV Multispectral Data

This chapter is based on the peer-reviewed article:
***Böhler, J. E.**, Schaepman, M. E., Kneubühler, M. (2020) Crop Separability from Individual and Combined Airborne Imaging Spectroscopy and UAV Multispectral Data. Remote Sensing 12(8), 1256; DOI: 10.3390/rs12081256*

J.E.B. designed the research and analyzed the data with scientific advice of M.K. and M.E.S., J.E.B. wrote the manuscript and all co-authors thoroughly reviewed and edited the manuscript.

remote sensing

MDPI

Article

Crop Separability from Individual and Combined Airborne Imaging Spectroscopy and UAV Multispectral Data

Jonas E. Böhler *, Michael E. Schaepman and Mathias Kneubühler

Department of Geography, Remote Sensing Laboratories (RSL), University of Zürich, Winterthurerstrasse 190, 8057 Zürich, Switzerland; michael.schaepman@geo.uzh.ch (M.E.S.); mathias.kneubuehler@geo.uzh.ch (M.K.)
* Correspondence: jonas.boehler@geo.uzh.ch; Tel.: +41-446-355-249

Received: 14 March 2020; Accepted: 13 April 2020; Published: 16 April 2020

Abstract: Crop species separation is essential for a wide range of agricultural applications—in particular, when seasonal information is needed. In general, remote sensing can provide such information with high accuracy, but in small structured agricultural areas, very high spatial resolution data (VHR) are required. We present a study involving spectral and textural features derived from near-infrared (NIR) Red Green Blue (NIR-RGB) band datasets, acquired using an unmanned aerial vehicle (UAV), and an imaging spectroscopy (IS) dataset acquired by the Airborne Prism EXperiment (APEX). Both the single usage and combination of these datasets were analyzed using a random forest-based method for crop separability. In addition, different band reduction methods based on feature factor loading were analyzed. The most accurate crop separation results were achieved using both the IS dataset and the two combined datasets with an average accuracy (AA) of >92%. In addition, we conclude that, in the case of a reduced number of IS features (i.e., wavelengths), the accuracy can be compensated by using additional NIR-RGB texture features (AA > 90%).

Keywords: crop separability; imaging spectroscopy; multispectral drone data; random forest; band reduction

1. Introduction

The accurate quantification of crop species in agricultural areas is crucial for various tasks such as decision-making and monitoring [1–3]. Many of these tasks require up-to-date information on current crop presences. However, official data are often only available at the end of or after the season, and when this is the case, they are usually aggregated by administrative units [4,5]. Remote sensing has therefore proved to be a viable alternative to human observations in the field [6,7].

Many studies of this kind are, however, conducted with satellite data [8,9], but the spatial resolution of the majority of these data is too low to provide accurate results at the field level in highly fragmented agricultural areas with small field plots [6,10,11]. Although satellite data with high spatial resolutions exist, they are often too expensive. Therefore, lower flying platforms are an option capable of collecting data at very high spatial resolutions. Using remote sensing, such studies for crop separation have been conducted with unmanned aerial vehicles (UAVs) [12–14] or airborne imaging spectrometers (IS) [15,16].

An UAV typically carries lightweight sensors, which often only contain a few spectral bands [17,18]. In addition, precise spectral calibration requires additional effort, which is subject to appropriate expertise [19]. Many UAVs carry a consumer-grade RGB camera to record data. These cameras may be modified to enable an additional near-infrared (NIR) channel to be acquired. NIR-RGB datasets with spatially very high resolutions (VHRs) can be generated from such platforms. However, additional

Remote Sens. **2020**, *12*, 1256

texture features are required to at least partially compensate for the lack of spectral information. Alternatively, imaging sensors with several bands are available, but they are costly [18].

Although IS sensors to be deployed on UAVs exist, more sophisticated sensors with very high signal-to-noise ratios are mainly operated from airborne platforms [19]. IS datasets are used in a range of applications in agriculture, i.e., biophysical properties [20,21], soil mapping [22], and, in particular, for crop separation [15,23]. Yet, the combined usage of IS and VHR datasets has so far been applied mainly in land cover studies in urban areas [24].

This study aims at evaluating the improvement of crop separation accuracy in very fragmented agricultural landscapes by combining VHR drone data and airborne imaging spectroscopy data. More specifically, the added value of the concurrent exploitation of spectral/textural features of VHR multispectral drone data and spectrally highly resolved imaging spectroscopy data is investigated and compared to single-usage scenarios of the two data sources.

Besides, this study assesses (i) the influence of feature reduction, as well as (ii) the effect of a model to fit the number of trees in the random forest (RF) model on the accuracy of crop separation.

2. Materials and Methods

2.1. Study Area

The study area is located in the Swiss Plateau next to Mönchaltorf (47.312 °N, 8.733 °E), and it is structured into numerous small plots (Figure 1). The fields have an average size of 1.3 ha (between 0.03 ha and 7.4 ha). Their lengths vary between 140 m and 200 m for a single field, and their widths between 23 m and 180 m. Cereals (winter barley, spelt, and winter wheat); rapeseed; grassland (permanent and temporary, including clover); maize; and sugar beet were included in the crop separation study. The field observations took place on 24 and 25 June 2015, corresponding to 1342 accumulated growing degree days (AGDD) and 1362 AGDD, respectively. Based on the scale of the Biologische Bundesanstalt, Bundessortenamt und Chemische Industrie (BBCH) [25], the phenological stage of a single reference field for maize (BBCH 33), rapeseed (BBCH 80), sugar beets (BBCH 39), and winter wheat (BBCH 75, representing cereal) were recorded at the time of observation.

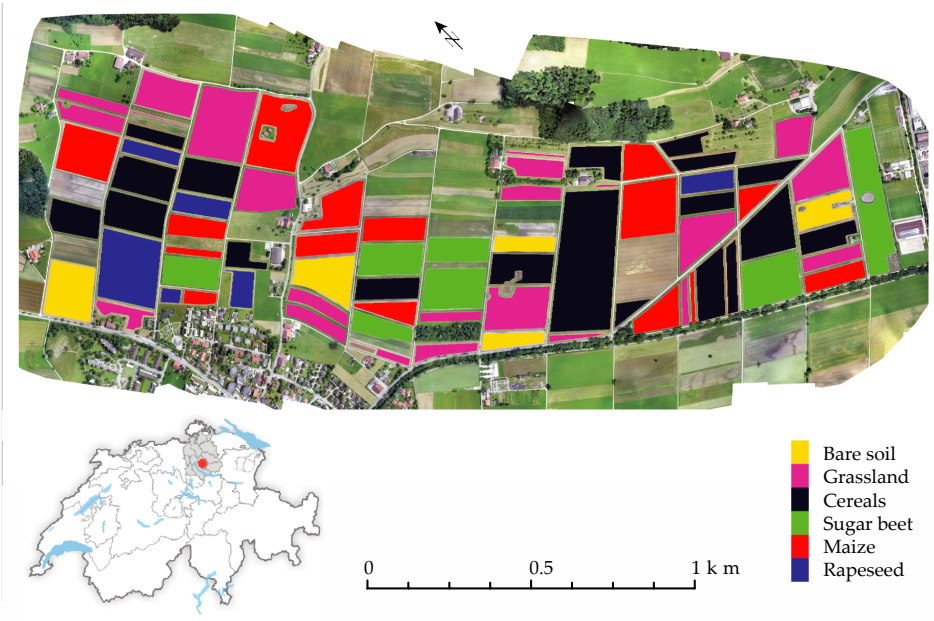

Figure 1. Mosaic of the study area (near Mönchaltorf, Switzerland; see overview map, **bottom left**) acquired on 25 June 2015 with an unmanned aerial vehicle (UAV)-mounted consumer-grade red green blue (RGB) camera. The crop classification as inventoried on the same date is superimposed (see legend, **bottom right**).

2.2. Data

The eBee dataset was based on uncalibrated VHR data acquired on 25 June 2015 with two consumer-grade cameras, i.e., an RGB and an NIR-GB, carried by an eBee-UAV (Sensefly, Cheseaux-Lausanne, Switzerland). The flight parameters were chosen in a way that the lateral overlap was 60%, and the longitudinal overlap 75%. The spatial resolution was 5 cm at a flight altitude of 150 m above the ground. Subsequently, an orthophotomosaic was built using a Pix4Dmapper Pro (version 4.2.27, Pix4D S.A., Prilly, Switzerland), and the NIR band was stacked to the RGB mosaic. This dataset was georeferenced to five ground control points (GCP), which were recorded with a differential GPS device (dGPS). Finally, the VHR dataset was resampled to a spatial resolution of 0.5 m, as this resolution proved to be the most promising spatial resolution for the investigated crops in our study area [26].

The APEX dataset was acquired the day before (24 June 2015) with the Airborne Prism EXperiment (APEX) sensor, an airborne imaging spectrometer (IS). A detailed description of the sensor properties and preprocessing chain can be found in [27,28]. The dataset was atmospherically corrected and orthorectified using a parametric geocoding approach [29]. The surface reflectance data cube contained 284 spectral bands in the range of 399–2431 nm at a spatial resolution of 2 m. Bands subject to atmospheric water vapor (i.e., the spectral ranges of 691–737 nm, 753–771 nm, 790–839 nm, 900–1008 nm, 1097–1174 nm, 1300–1513 nm, and 1753–2.050 nm) were interpolated during preprocessing and, subsequently, omitted, resulting in a dataset of 173 bands. The APEX dataset was co-registered to the eBee dataset of 25 June.

2.3. Methods

The chosen methodology of this study consists of seven steps (Figure 2). First, the input features for the random forest (RF) classifier were created on the basis of the two data sources. In the second step, the features were arranged in three settings (single and combined settings). In the third step, the dataset of each setting was split for training, validation, and testing. In the fourth step, the training split was used to calculate the feature importance and perform feature selection. In the fifth step, training of the RF model was performed. The free parameters for the RF model in the fifth step were determined on the basis of the validation split. In the sixth step, the test split was used to test the learned model from the fifth step. Finally, the crop separation accuracy was assessed. The individual steps are described in detail in the following sections.

2.3.1. Feature Extraction

The inclusion of texture information from VHR data on top of spectral information is known to improve classification results [26,30]. Therefore, first-order statistics (mean, standard deviation, range, and entropy) and mathematical morphology (dilatation/erosion, opening/closing, opening/closing top hat, opening/closing by reconstruction, and opening/closing by reconstruction top hat) were calculated from the eBee dataset, based on a disc-shaped structuring element (SE), to remain rotationally invariant. The SE has a diameter of 3 or 5 pixels. In order to form the final stack of features with the selected APEX bands, all features of the eBee dataset were resampled to a spatial resolution of 2 m by averaging.

2.3.2. Creation of Feature Settings

In order to analyze the influence of features from the two data sources (i.e., UAV-based VHR data and airborne IS data) on crop separation accuracy, three feature settings were created. The *eBee setting* contains only the eBee features, the *APEX setting* only the APEX features, and the *eBee & APEX setting* all eBee and APEX features.

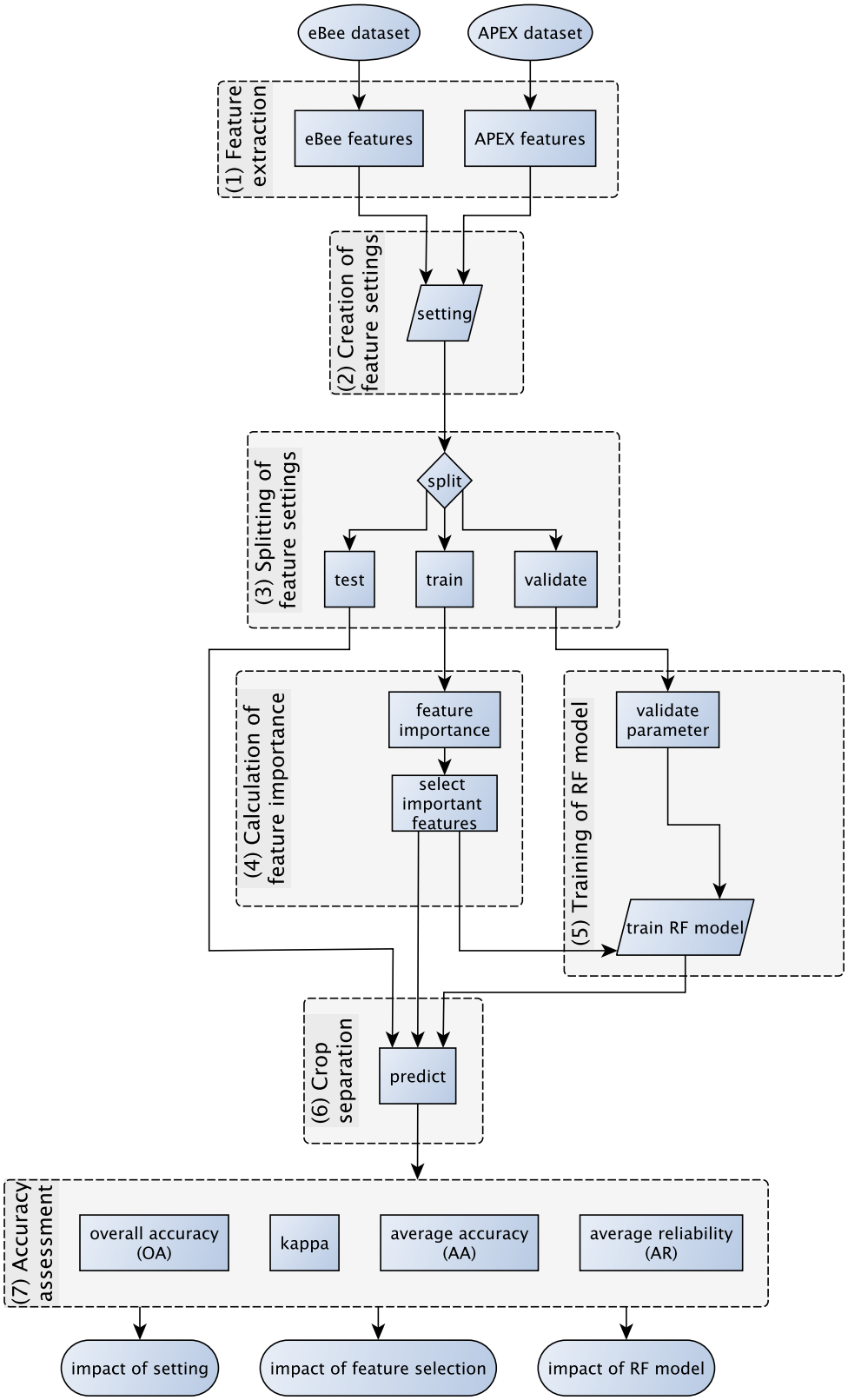

Figure 2. Data-processing scheme to assess crop separation accuracies from airborne imaging spectroscopy (IS) data, UAV-based multispectral data, and their combined usage. RF: random forest.

2.3.3. Splitting of Feature Settings

All three feature-setting datasets were divided class-wise into six splits. Two splits were selected for the RF feature selection and model training and two for validating the parameters in the RF model. In order to reduce the computational load, 1000 pixels were randomly selected for each crop class in the training and validation splits. The remaining two splits were retained for testing the learned model, resulting in a total of 15 permutations (so-called folds) [31].

2.3.4. Calculation of Feature Importance

In order to reduce the number of features in the RF model, the features were ordered into an ordered feature stack based on the sum of the factor loading of each crop class. Then, all features with higher correlation than a given correlation threshold between the first feature in the ordered feature stack and the remaining investigated features were excluded. This procedure was repeated with each remaining feature of the ordered feature stack until all features that correlate up to the threshold were excluded from the feature stack. Eleven evenly distributed threshold values between 0% and 100% were evaluated.

2.3.5. Training of RF Model

Two RF models were tested in our study. In the simple one, called *500-trees*, 500 trees were used to train the model with all data from the training and validation split that were selected from the feature stack based on the respective correlation threshold. In the second model, called *fitted-trees*, the appropriate number of trees was determined by building models with 20 logarithmically distributed grid points between 10 and 1000 trees. The trained models predicted the crop classes from the validation split. This procedure was repeated five times to obtain stable results. The resulting overall accuracy (OA) values were fitted by a curve, and the number of trees was determined, such that the loss in accuracy was less than 0.1% compared to the maximum accuracy of the fitted curve [26]. However, a minimum of 100 trees was set. In both models, the minimal leaf size was set to 3 to avoid overfitting. Default values were kept for the other parameters of the TreeBagger function in MATLAB (2018a).

2.3.6. Crop Separation

To test the previously trained model, the test data split was predicted for each of the 15 folds.

2.3.7. Accuracy Assessment

Based on the confusion matrix of the predicted test split, the average accuracy (AA) was calculated as the average AA over all folds. This allowed verifying the accuracy of crop separation of the different settings against each other for significant differences ($p < 0.05$). For this purpose, the Wilcoxon signed rank test was used. The results for the overall accuracy (OA), Kappa coefficient, and average reliability (AR) are contained in the Supplementary Materials (Tables S1–S3).

3. Results

The AA of crop separation depends on (i) the correlation threshold between the investigated features in the ordered feature stack, (ii) the RF model, and (iii) the feature setting. The results section is divided into three parts. First, the accuracy for crop separation is shown in relation to the correlation threshold. In the second part, the effects of the two evaluated RF models are highlighted, and in the third part, the differences between the three tested feature settings are presented. The exact p-values of the significance tests can be found in Tables S4–S9.

3.1. Feature Selection

All in all, crop separation in datasets with the *eBee setting* are less accurate than from settings also containing APEX data (Figure 3). The accuracy with the *eBee setting* ranges from an AA value of

Remote Sens. **2020**, *12*, 1256

80.8% for a correlation threshold between the investigated features of 90% to 43.5% for a correlation threshold of 0% in the *fitted-trees model* (Table 1). The individual AA values in this setting usually differ significantly (Table S4). Only the accuracies with a correlation threshold of 80% and 100% show no significant difference to each other, and the AA with a correlation threshold of 60% shows no significant difference to the ones with a correlation threshold of 30% or 40% (Table S4). With a correlation threshold of 90%, the amount of features can be reduced by more than 50% to an average of 56.3 features across all folds (Table 2), compared to a maximum of 116 features (correlation threshold of 100%). In addition, the reduced number of features leads to a significantly higher degree of crop separation. The complete list of selected features can be found in the Supplementary Materials (Table S10).

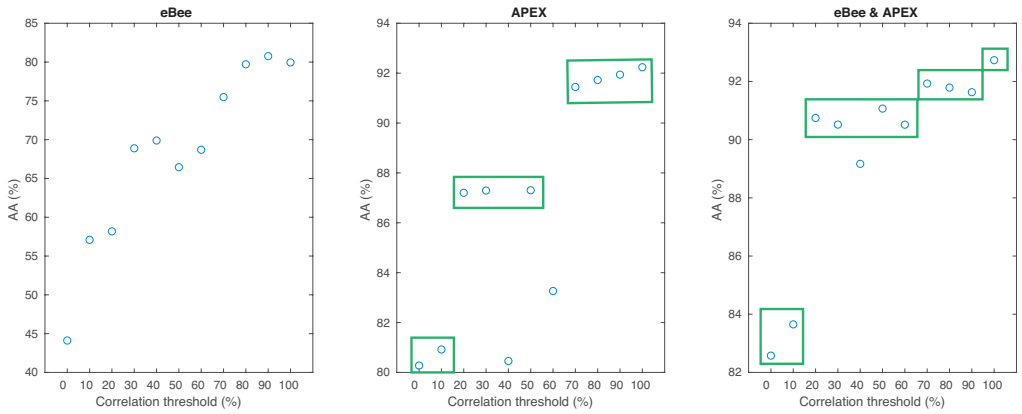

Figure 3. Average accuracy (AA) for the eBee, Airborne Prism EXperiment (APEX) and *eBee & APEX settings* for all evaluated correlation thresholds between the investigated features classified with the *fitted-trees model*. Clusters of similar values are marked in green.

Table 1. Average accuracy (AA) for all investigated settings, random forest (RF) models, and correlation thresholds between the investigated features. APEX: Airborne Prism Experiment.

Setting	Model	Correlation Threshold (%)										
		0	10	20	30	40	50	60	70	80	90	100
eBee	500-trees	44.1	57.1	58.2	68.9	69.9	66.4	68.7	75.5	79.6	80.9	79.9
eBee	fitted-trees	44.1	57.1	58.2	68.9	69.9	66.5	68.7	75.5	79.7	80.8	80.0
APEX	500-trees	80.3	81.0	87.2	87.3	80.4	87.3	83.3	91.5	91.8	91.9	92.2
APEX	fitted-trees	80.3	80.9	87.2	87.3	80.5	87.3	83.3	91.4	91.7	91.9	92.2
eBee & APEX	500-trees	82.6	83.6	90.8	90.6	89.3	91.2	90.6	92.0	91.8	91.8	92.8
eBee & APEX	fitted-trees	82.6	83.7	90.7	90.5	89.2	91.1	90.5	91.9	91.8	91.6	92.7

Table 2. Number of features for all investigated settings and correlation thresholds between the investigated features.

Setting	Correlation Threshold (%)										
	0	10	20	30	40	50	60	70	80	90	100
eBee	4.6	6.5	7.7	9.4	12.7	16.2	19.0	24.5	30.1	56.3	116
APEX	3.0	3.1	3.6	3.6	3.1	3.7	4.4	7.1	7.5	9.5	173
eBee & APEX	4.1	7.5	9.9	12.0	16.5	19.5	23.9	31.3	38.1	65.9	289

Concerning the *APEX setting*, AA values for different correlation thresholds between investigated features may be clustered into three distinct groups of AA, i.e., 0%–10%, 20%–50%, and 70%–100%, on the basis of significant differences between these groups and visual structures (Figure 3). Exceptions are the correlation thresholds of 40% and 60%, which do not fit into the pattern of a decreasing accuracy with a decreasing correlation threshold. The cluster of low AA values with correlation thresholds of 0%–10% differs significantly from the other two clusters. The middle cluster with correlation thresholds

of 20%–50% shows AA values about 4% lower than the high cluster with correlation thresholds of 70%–100%. However, the AA values in the middle cluster do not differ significantly from the AA values at a correlation threshold of 70% and 80% (Table S5). The AA values in the high cluster all lie between 91.4% and 92.2% (Table 1). Nevertheless, some of them differ significantly from each other, i.e., the AA values for a correlation threshold of 70% and 80%, 80% and 90%, and 90% and 100% differ significantly in each case from the other two values in the high cluster (Table S5). Finally, the AA for a correlation threshold of 40% fits into the first cluster from 0% to 10%, and the AA for the 60% threshold only exhibits insignificant differences with the AA values with a correlation threshold of 20% (Table S5).

The total amount of APEX features of 173 will be reduced to 9.5 on average, with a correlation threshold between investigated features of 90% (Table 2). The amount of features is not always an integer, as the number of features selected for different training splits may vary in different folds. With a correlation threshold of 0%, the average number of APEX features is reduced to three (although the AA remains 80.3% (Table 1)). Selected features in the case of APEX are wavelength bands (Table 3).

Table 3. Selected APEX features (i.e., wavelengths) for different correlation thresholds between the investigated features in the *APEX setting*. The numbers in the table correspond to the frequency at which a given feature was selected in a fold per the correlation threshold.

Wavelength (nm)	Correlation Threshold (%)									
	0	**10**	**20**	**30**	**40**	**50**	**60**	**70**	**80**	**90**
399						1		15		15
413							9		15	
427										15
490								1		2
509										2
553	15	15	15	15	15			15	15	
581										15
594									5	
681		15	15	15		15	15	15		
684			9			15		15	15	15
688				9		1	15	15	15	
785										1
1051	15				15	15	15		2	
1261							1			15
1521								1		
1549									1	
1567										1
1666	15	15	15	15	15	9	2	15	15	15
2057					1		9		15	15
2356										15
2388									15	
2419								15		15
2432										2

In the combined setting, i.e., eBee & APEX, four clusters of AA values could be defined based on a combined visual and statistical assessment (Figure 3). The first, with correlation thresholds between 0% and 10%, contains AA values that are significantly lower than the others (Table S6). The AA values in the second cluster with correlation thresholds of 20%–60% are between 90.5% and 91.1% (Table 1) and do not differ significantly from each other. In the third cluster, with correlation thresholds of 70%–90%, the AA values are between 91.6% and 91.9% (Table 1) and, again, do not differ significantly from each other. The highest AA value in this cluster is 91.9 % with a correlation threshold of 70%. The fourth cluster contains only the highest AA value (92.7%) with a correlation threshold of 100%, which also differs significantly from the other AA values. Again, the AA value for a correlation threshold of 40%

is significantly lower than the others in the second cluster of 20%–60% but significantly higher than in the first cluster of 0%–10%. Furthermore, there are no significant differences between the AA values for a correlation threshold of 20% and 80%, 20% and 90%, and 50% and 90%.

The number of features for a correlation threshold of 70% is reduced to 31.3 on average (Table 1). Compared to a total of 289 features (173 APEX features and 116 eBee features), this relates to a reduction by more than 90%. The number of APEX features will be reduced by up to three features (with a correlation threshold of 10%), with only one APEX feature being selected in that case (Table 2 and Table S12). Only with correlation thresholds of 60% and 90% will additional APEX features be chosen in comparison to the *APEX setting* (Table 2 and Table S12). In the case of correlation thresholds of 60%, this amounts to 1.3 features and, at 90%, to 7.8 features (Table 2 and Table S12). The complete list of selected features in the *eBee & APEX setting* can be found in the Supplementary Materials (Tables S11 and S12).

3.2. RF Model

The estimated number of trees with the *fitted-trees model* is about 500 trees for the *APEX setting* and the *eBee & APEX setting* and 770 for the *eBee setting* (Table 4). The difference in the number of trees is large between the 15 folds in all three settings, and for all correlation thresholds between the investigated features, and ranges from 100 trees (the set minimum) to about 900 trees (Figure S1).

Table 4. Number of trees in the *fitted-trees model* for all investigated settings and correlation thresholds between the investigated features.

Setting	Correlation Threshold (%)										
	0	**10**	**20**	**30**	**40**	**50**	**60**	**70**	**80**	**90**	**100**
eBee	776	893	749	886	824	754	794	791	732	490	785
APEX	350	436	413	630	406	467	403	414	414	559	440
eBee & APEX	578	334	502	654	545	466	625	494	529	500	567

There is no significant difference in the *eBee setting* between the mean AA values of the *500-trees model* and the *fitted-trees model* (Table S7). In general, the *fitted-trees model* leads to equal or higher AA values, except for a correlation threshold of 90%, where the AA value for the *500-trees model* is 0.14% higher.

There are no significant differences between the two RF models in the case of the *APEX setting*, either (Table S7). With correlation thresholds of 40% and 90%, the AA values are 0.04% and 0.05% higher for the *fitted-trees model*, respectively. For the *eBee & APEX setting*, significantly different AA values are observed for the correlation thresholds of 30%, 40%, and 90%, with AA differences amounting to 0.10%, 0.13%, and 0.14%, respectively (Table 1). Nevertheless, the differences in the AA values between the two RF models are less than 0.15%.

3.3. Sensor Data Combination

Since the AA values differ only slightly between the two RF models, only the results for the *fitted-trees model* are compared here. AA values of the *APEX setting* are significantly higher than the ones of the *eBee setting* for all corresponding correlation thresholds between the investigated features (Table S8). AA values of the *APEX setting* with low correlation thresholds, i.e., 0%, 10%, and 40%, are not significantly different from AA values of the *eBee setting* with high correlation thresholds, i.e., 80%–100%.

The AA values of the *eBee & APEX setting* are always significantly higher than those of the *eBee setting*. Compared to the *APEX setting*, AA values of the *eBee & APEX setting* are significantly higher, with corresponding correlation thresholds of 0% and 60% between the investigated features (Table S9).

4. Discussion

4.1. Feature Selection

Overall, we observe a decrease in AA values with decreasing correlation thresholds between the investigated features (Figure 3). Nevertheless, depending on the datasets, reduction of the amount of features, as investigated in our study, is a reasonable approach, even with the RF algorithm known to be resistant to the curse of dimensionality (Hughes' phenomenon) [32] and, therefore, able to handle large feature sets, as there is no significant decrease in AA values with decreased amounts of features.

In particular, reducing the number of features for the *eBee setting* leads to the most accurate crop separation, with a correlation threshold of 90% (AA significantly different from AA with a correlation threshold of 100%, Table 1). In a previous study, we examined in detail the effects of differing spatial resolutions of an eBee dataset. We concluded that a spatial resolution of 0.5 m leads to the highest accuracy in crop separation [26]. It was further found that average accuracies remained the same whether texture features were used that were calculated directly from the data with a spatial resolution of 0.5 m or aggregated to a 2-m resolution (see Section 2.3.1). In the case of the *APEX setting*, in contrast, crop separation does not improve with lower correlation thresholds (i.e., fewer features). However, the accuracy does not significantly decrease with a correlation threshold of 90% compared to 100%. Hence, the number of APEX features can be reduced by over 95%, i.e., corresponding to a reduction from 173 to 9.5 features (Table 2).

Elaborating on the physical background of the selected features in an RF model, the relevant APEX features (Table 3) are situated in spectral ranges which are sensitive to (i) pigments (413 nm, 553 nm, and 594 nm); (ii) biophysical traits (684 nm, 688 nm, and 1051 nm); (iii) plant water (2057 nm); or (iv) lignin; cellulose; or senescent material (1549 nm, 1666 nm, and 2388 nm) [20,21]. It is worth noting that selected features are considered important for low correlation thresholds (e.g., 0%–40% for a feature at 553 nm in Table 3), while they are not important for higher correlation thresholds (e.g., 50%–60%). Table 3 indicates that APEX features at a wavelength of 681 nm are important for separating the present crops. Therefore, a significant decrease of the AA value with a correlation threshold of 40% compared to 30% can be observed. At a correlation threshold of 60%, the excluded feature at a wavelength of 1666 nm leads most likely to a drop in the AA value compared to AA values with higher or lower correlation thresholds.

Three main categories of eBee features in our study are based on first-order statistics, morphology, or spectral bands (Table S10). Remarkably, all original spectral bands are excluded in the feature selection for all correlation thresholds from 0% to 90%. Among the top 20 features (most used over all correlation thresholds), morphological features are much more common than first-order statistical features. Spectral bands used to calculate textural features were most frequently the NIR, followed by the green and red bands. The blue band occurs to be the least relevant band (selected only once). Both structuring element (SE) sizes occur almost equally frequently.

4.2. RF Model

The proposed *fitted-trees model* to estimate the appropriate number of trees in the RF classifier leads only to small differences in the AA compared to the *500-trees model*. The average number of trees is close to 500 trees, or even considerably higher, in the case of the *eBee setting*. However, the accurate determination of the number of trees in a preliminary estimation with the *500-trees model* requires additional effort (user input), whereas the *fitted-trees model* can automatically determine the number of trees for the RF model.

4.3. Comparison of Sensor Data Settings

Crop separation based on the *eBee setting* results in the lowest observed AA values for the present crops. The methodology in its current state only includes the original bands and texture features, i.e., the eBee features. However, implementing additional information on field boundaries would

most likely increase the AA values by about 10% [26]. This result would be consistent with another multispectral study that achieves an OA of 91.5% (AA 90.7%) for a separation of 10 different classes based on an object-based RF approach [33].

Separation of crops based on the *APEX setting* results in significantly better AA values compared to the *eBee setting* (Table 1). Only the low cluster of AA values for the *APEX setting* with correlation thresholds of 0%–10% leads to similar AA values as the *eBee setting* with correlation thresholds of 80%–100%. Therefore, it is possible to obtain similar crop separation results on the basis of a multispectral dataset obtained with consumer-grade cameras, compared to an IS dataset being drastically reduced to a few bands.

A recent study based on Hyperion data, which used up to 30 best-performing bands to classify maize, cotton, rice, soybeans, and winter wheat in different images, achieved an OA of over 90% for distinguishing two individual crops using a support-vector machine (SVM) based approach [15]. However, for three or more crops, the OA fell below 89%. Therefore, our approach presented here with the *APEX setting* may yield a more precise separation of crops. Reasons for these differences may include differences in the investigated crops, as well as differing sensor characteristics. Besides a different number of bands and center wavelengths, the Hyperion sensor has two independent optical paths for the visible and near-infrared (VNIR) and short-wavelength infrared (SWIR) spectral ranges and a spatial resolution of 30 m, compared to a single optical path and a resolution of 2 m in the case of the APEX spectrometer.

The most accurate separation of crops can be achieved with the combined *eBee & APEX setting* (Table 1). However, using all available features, there is no significant difference to the *APEX setting* (with a correlation threshold of 100%), even if the AA value for the combined *eBee & APEX setting* is slightly higher. Nevertheless, the *eBee & APEX setting* with a reduced number of features leads to more accurate results than in the case of the *APEX setting*. In particular, crop separation with a correlation threshold of 20% yields better results in the combined setting (AA of 90.7%), with only 9.9 features being required (average over all folds), which is equivalent to the *APEX setting* with a correlation threshold of 60% (AA of 83.3%). The number of features obtained by imaging spectroscopy (APEX features) may be reduced to 1.7 on average (correlation threshold of 30%, Table S12), with an AA value still remaining over 90% (AA of 90.5%). Therefore, eBee texture features based on NIR-RGB bands can effectively compensate for a reduced number of APEX spectral features (narrow bands). This is particularly important in the case of multispectral camera systems that only allow the selection of a few, narrow preconfigured bands in addition to an RGB image. In addition, the operation of UAVs is usually more cost-effective than using an aircraft [34,35]. Similarly, data acquisition is more flexible in terms of weather conditions and flight planning [17,36], while fidelity and accuracy are usually superior from less-frequent airborne data acquisition.

5. Conclusions

This study presents a methodology for separating crops in a highly fragmented landscape with small structured plots, as in the Swiss Plateau, based on two different datasets. On the one hand, a multispectral VHR dataset with red (R), green (G), blue (B) and near-infrared (NIR) bands and texture features thereof, obtained with consumer-grade cameras, was investigated. On the other hand, an airborne imaging spectroscopy (IS) dataset of 2-m spatial resolution and 173 spectral bands between 399 nm to 2431 nm was used.

The highest AA values of over 92% could be achieved with the IS features (the *APEX setting*) and the combination of IS and VHR features (the *eBee & APEX setting*). Overall, we conclude that the reduction of features based on factor loading (decreasing correlation thresholds) results in significantly lower accuracies. Especially for the IS dataset (the *APEX setting*), the AA values will drop to almost 80%. For the combined dataset (the *eBee & APEX setting*), the accuracy with less features is also significantly lower but remains above 90%. With the VHR dataset (the *eBee setting*), the crops can be separated with

a maximum accuracy of around 80%. The proposed automatic selection of RF parameters is as good as the preliminary estimation.

In summary, this paper concludes that the accuracy of crop separation based on IS data exceeds the accuracy based on an NIR-RGB dataset and its texture features. Nevertheless, if the number of used IS features is reduced, additional NIR-RGB texture features (the morphological features of the NIR G and R bands are most important) can compensate a decrease in crop separation accuracy.

Supplementary Materials: The following are available online at http://www.mdpi.com/2072-4292/12/8/1256/s1, Figure S1. Boxplot of the number of trees in the *fitted-trees model* for the *eBee setting* (left), *APEX setting* (middle), and *eBee & APEX setting* (right), Table S1. Overall accuracies (OA) for all settings, models, and correlation thresholds, Table S2. Kappa coefficient for all settings, models, and correlation thresholds, Table S3. Average reliability (AR) for all settings, models, and correlation thresholds, Table S4. The p-values of the significance test ($p < 0.05$) for the *eBee setting* with all correlation thresholds, Table S5. The p-values of the significance test ($p < 0.05$) for the *APEX setting* with all correlation thresholds, Table S6. The *p*-values of the significance test ($p < 0.05$) for the *eBee & APEX setting* with all correlation thresholds, Table S7. The *p*-values of the significance test ($p < 0.05$) for the differences between the *500-trees model* and the *fitted-trees model* for each setting with all correlation thresholds, Table S8. The p-values of the significance test ($p < 0.05$) for the comparison of the *eBee setting* versus the *APEX setting* with all correlation thresholds, Table S9. The p-values of the significance test ($p < 0.05$) for the comparison of the *eBee & APEX setting* versus the *APEX setting* with all correlation thresholds, Table S10. Selected eBee features for the different correlation thresholds in the *eBee setting*. We report the frequency how many folds a feature was selected for each correlation threshold. A feature is defined by its size of the structuring element (SE), feature type, and spectral band of the eBee sensor, Table S11. Selected eBee features for different correlation thresholds in the *eBee & APEX setting*. The numbers in the table give the frequency in how many folds of a feature were selected per correlation threshold. A feature is defined through the size of the structuring element (SE), feature type, and band of the eBee sensor, Table S12. Selected APEX features and the mean number of features per fold for different correlation thresholds in the *eBee & APEX setting*. The numbers in the table give the frequency in how many folds of a feature were selected per correlation threshold.

Author Contributions: J.E.B. designed the research and analyzed the data with scientific advice from M.K. and M.E.S., J.E.B. wrote the manuscript. All authors have read and agreed to the published version of the manuscript.

Funding: This research received no external funding.

Acknowledgments: The contribution of M.E.S. is supported by the University of Zurich Research Priority Program on "Global Change and Biodiversity" (URPP GCB). We would like to thank the staff of R.S.L. and G.R.S. (Wageningen University) for their support in the fieldwork and for providing background information. We would like to thank Reinhard Furrer from the Department of Mathematics at UZH for his advice on statistical analyses.

Conflicts of Interest: The authors declare no conflicts of interest.

References

1. Azar, R.; Villa, P.; Stroppiana, D.; Crema, A.; Boschetti, M.; Brivio, P.A. Assessing in-season crop classification performance using satellite data: A test case in Northern Italy. *Eur. J. Remote Sens.* **2016**, *49*, 361–380. [CrossRef]
2. Ozdarici-Ok, A.; Ok, A.; Schindler, K. Mapping of Agricultural Crops from Single High-Resolution Multispectral Images–Data-Driven Smoothing vs. Parcel-Based Smoothing. *Remote Sens.* **2015**, *7*, 5611–5638. [CrossRef]
3. Inglada, J.; Arias, M.; Tardy, B.; Morin, D.; Valero, S.; Hagolle, O.; Dedieu, G.; Sepulcre, G.; Bontemps, S.; Defourny, P. Benchmarking of algorithms for crop type land-cover maps using Sentinel-2 image time series. In Proceedings of the 2015 IEEE International Geoscience and Remote Sensing Symposium, Milan, Italy, 26–31 July 2015; pp. 3993–3996. [CrossRef]
4. Waldhoff, G.; Lussem, U.; Bareth, G. Multi-Data Approach for remote sensing-based regional crop rotation mapping: A case study for the Rur catchment, Germany. *Int. J. Appl. Earth Obs. Geoinf.* **2017**, *61*, 55–69. [CrossRef]
5. Bundesrat, D.S. *Verordnung über die Direktzahlungen an die Landwirtschaft*; The Swiss Federal Council: Berne, Switzerland, 2017; Volume 2013, pp. 1–152.
6. Atzberger, C. Advances in Remote Sensing of Agriculture: Context Description, Existing Operational Monitoring Systems and Major Information Needs. *Remote Sens.* **2013**, *5*, 949–981. [CrossRef]
7. Burke, M.; Lobell, D.B. Satellite-based assessment of yield variation and its determinants in smallholder African systems. *Proc. Natl. Acad. Sci. USA* **2017**, *114*, 2189–2194. [CrossRef]

8. Zhong, L.; Hu, L.; Zhou, H. Deep learning based multi-temporal crop classification. *Remote Sens. Environ.* **2019**, *221*, 430–443. [CrossRef]
9. Ouzemou, J.-E.; El Harti, A.; Lhissou, R.; El Moujahid, A.; Bouch, N.; El Ouazzani, R.; Bachaoui, E.M.; El Ghmari, A. Crop type mapping from pansharpened Landsat 8 NDVI data: A case of a highly fragmented and intensive agricultural system. *Remote Sens. Appl. Soc. Environ.* **2018**, *11*, 94–103. [CrossRef]
10. Vuolo, F.; Neugebauer, N.; Bolognesi, S.; Atzberger, C.; D'Urso, G. Estimation of Leaf Area Index Using DEIMOS-1 Data: Application and Transferability of a Semi-Empirical Relationship between two Agricultural Areas. *Remote Sens.* **2013**, *5*, 1274–1291. [CrossRef]
11. Whitcraft, A.K.; Becker-Reshef, I.; Killough, B.D.; Justice, C.O. Meeting earth observation requirements for global agricultural monitoring: An evaluation of the revisit capabilities of current and planned moderate resolution optical earth observing missions. *Remote Sens.* **2015**, *7*, 1482–1503. [CrossRef]
12. Zhang, J.; Zhao, Y.; Abbott, A.L.; Wynne, R.H.; Hu, Z.; Zou, Y.; Tian, S. Automated mapping of typical cropland strips in the North China Plain using small Unmanned Aircraft Systems (sUAS) photogrammetry. *Remote Sens.* **2019**, *11*, 2343. [CrossRef]
13. Zhao, L.; Shi, Y.; Liu, B.; Hovis, C.; Duan, Y.; Shi, Z. Finer Classification of Crops by Fusing UAV Images and Sentinel-2A Data. *Remote Sens.* **2019**, *11*, 3012. [CrossRef]
14. Yan, Y.; Deng, D.; Liu, L.; Zhu, Z. Application of UAV-Based Multi-Angle Hyperspectral Remote Sensing in Fine Vegetation Classification. *Remote Sens.* **2019**, *11*, 2753. [CrossRef]
15. Aneece, I.; Thenkabail, P. Accuracies Achieved in Classifying Five Leading World Crop Types and their Growth Stages Using Optimal Earth Observing-1 Hyperion Hyperspectral Narrowbands on Google Earth Engine. *Remote Sens.* **2018**, *10*, 2027. [CrossRef]
16. Thenkabail, P.S.; Gumma, M.K.; Teluguntla, P.; Mohammed, I.A. Hyperspectral remote sensing of vegetation and agricultural crops. *Photogramm. Eng. Remote Sens.* **2014**, *80*, 697–709. [CrossRef]
17. Pajares, G. Overview and Current Status of Remote Sensing Applications Based on Unmanned Aerial Vehicles (UAVs). *Photogramm. Eng. Remote Sens.* **2015**, *81*, 281–330. [CrossRef]
18. Yao, H.; Qin, R.; Chen, X. Unmanned Aerial Vehicle for Remote Sensing Applications—A Review. *Remote Sens.* **2019**, *11*, 1443. [CrossRef]
19. Aasen, H.; Honkavaara, E.; Lucieer, A.; Zarco-Tejada, P. Quantitative Remote Sensing at Ultra-High Resolution with UAV Spectroscopy: A Review of Sensor Technology, Measurement Procedures, and Data Correction Workflows. *Remote Sens.* **2018**, *10*, 1091. [CrossRef]
20. Thenkabail, P.S.; Mariotto, I.; Gumma, M.K.; Middleton, E.M.; Landis, D.R.; Huemmrich, K.F. Selection of hyperspectral narrowbands (hnbs) and composition of hyperspectral twoband vegetation indices (HVIS) for biophysical characterization and discrimination of crop types using field reflectance and hyperion/EO-1 data. *IEEE J. Sel. Top. Appl. Earth Obs. Remote Sens.* **2013**, *6*, 427–439. [CrossRef]
21. Hank, T.B.; Berger, K.; Bach, H.; Clevers, J.G.P.W.; Gitelson, A.; Zarco-Tejada, P.; Mauser, W. Spaceborne Imaging Spectroscopy for Sustainable Agriculture: Contributions and Challenges. *Surv. Geophys.* **2019**, *40*, 515–551. [CrossRef]
22. Diek, S.; Chabrillat, S.; Nocita, M.; Schaepman, M.E.; de Jong, R. Minimizing soil moisture variations in multi-temporal airborne imaging spectrometer data for digital soil mapping. *Geoderma* **2019**, *337*, 607–621. [CrossRef]
23. Marshall, M.; Thenkabail, P. Advantage of hyperspectral EO-1 Hyperion over multispectral IKONOS, GeoEye-1, WorldView-2, Landsat ETM+, and MODIS vegetation indices in crop biomass estimation. *ISPRS J. Photogramm. Remote Sens.* **2015**, *108*, 205–218. [CrossRef]
24. Gamba, P.; Dell'Acqua, F. 18 Spectral Resolution in the Context of Very High Resolution Urban Remote Sensing. In *Urban Remote Sensing*; Weng, Q., Quattrochi, D., Gamba, P.E., Eds.; CRC Press: Boca Raton, FL, USA, 2018; p. 377.
25. Meier, U.; Bleiholder, H.; Buhr, L.; Feller, C.; Hack, H.; Heß, M.; Lancashire, P.D.; Schnock, U.; Stauß, R.; van den Boom, T.; et al. The BBCH system to coding the phenological growth stages of plants-history and publications-Das BBCH-System zur Codierung der phänologischen Entwicklungsstadien von Pflanzen-Geschichte und Veröffentlichungen. *J. Für Kult.* **2009**, *61*, 41–52. [CrossRef]
26. Böhler, J.; Schaepman, M.; Kneubühler, M. Crop Classification in a Heterogeneous Arable Landscape Using Uncalibrated UAV Data. *Remote Sens.* **2018**, *10*, 1282. [CrossRef]

27. Hueni, A.; Lenhard, K.; Baumgartner, A.; Schaepman, M.E. Airborne Prism Experiment Calibration Information System. *IEEE Trans. Geosci. Remote Sens.* **2013**, *51*, 5169–5180. [CrossRef]
28. Schaepman, M.E.; Jehle, M.; Hueni, A.; D'Odorico, P.; Damm, A.; Weyermann, J.J.; Schneider, F.D.; Laurent, V.; Popp, C.; Seidel, F.C.; et al. Advanced radiometry measurements and Earth science applications with the Airborne Prism Experiment (APEX). *Remote Sens. Environ.* **2015**, *158*, 207–219. [CrossRef]
29. Hueni, A.; Biesemans, J.; Meuleman, K.; Dell'Endice, F.; Schlapfer, D.; Odermatt, D.; Kneubuehler, M.; Adriaensen, S.; Kempenaers, S.; Nieke, J.; et al. Structure, Components, and Interfaces of the Airborne Prism Experiment (APEX) Processing and Archiving Facility. *Geosci. Remote Sens. IEEE Trans.* **2009**, *47*, 29–43. [CrossRef]
30. Laliberte, A.S.; Rango, A. Texture and Scale in Object-Based Analysis of Subdecimeter Resolution Unmanned Aerial Vehicle (UAV) Imagery. *IEEE Trans. Geosci. Remote Sens.* **2009**, *47*, 761–770. [CrossRef]
31. Böhler, J.E.; Schaepman, M.E.; Kneubühler, M. Optimal Timing Assessment for Crop Separation Using Multispectral Unmanned Aerial Vehicle (UAV) Data and Textural Features. *Remote Sens.* **2019**, *11*, 1780. [CrossRef]
32. Belgiu, M.; Drăgu, L. Random forest in remote sensing: A review of applications and future directions. *ISPRS J. Photogramm. Remote Sens.* **2016**, *114*, 24–31. [CrossRef]
33. Lee, R.-Y.; Chang, K.-C.; Ou, D.-Y.; Hsu, C.-H. Evaluation of crop mapping on fragmented and complex slope farmlands through random forest and object-oriented analysis using unmanned aerial vehicles. *Geocarto Int.* **2019**, 1–18. [CrossRef]
34. Colomina, I.; Molina, P. Unmanned aerial systems for photogrammetry and remote sensing: A review. *ISPRS J. Photogramm. Remote Sens.* **2014**, *92*, 79–97. [CrossRef]
35. Hugenholtz, C.H.; Moorman, B.J.; Riddell, K.; Whitehead, K. Small unmanned aircraft systems for remote sensing and Earth science research. *EOS Trans. Am. Geophys. Union* **2012**, *93*, 236. [CrossRef]
36. Whitehead, K.; Hugenholtz, C.H.; Myshak, S.; Brown, O.; LeClair, A.; Tamminga, A.; Barchyn, T.E.; Moorman, B.; Eaton, B. Remote sensing of the environment with small unmanned aircraft systems (UASs), part 2: Scientific and commercial applications 1. *J. Unmanned Veh. Syst.* **2014**, *2*, 86–102. [CrossRef]

remote sensing

MDPI

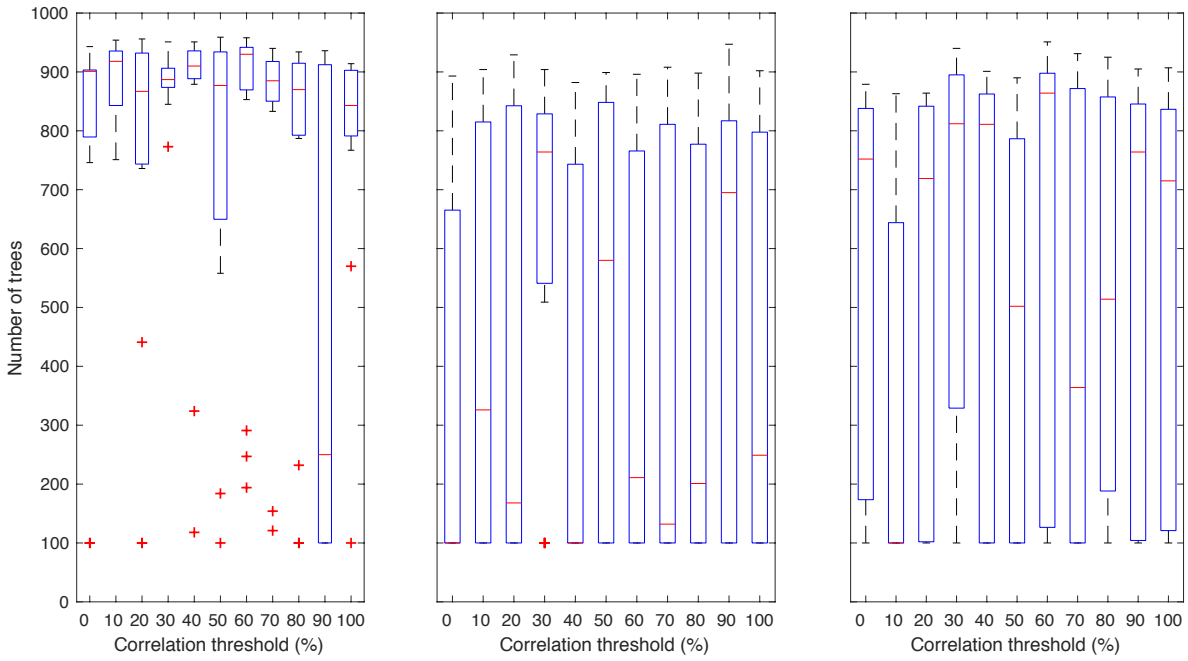

Figure S1. Boxplot of the number of trees in the *fitted-trees* model for the *eBee setting* (left), *APEX setting* (middle), and *eBee & APEX setting* (right).

Table S1. Overall accuracies (OA) for all settings, models, and correlation thresholds.

Setting	Model	Correlation threshold (%)										
		0	10	20	30	40	50	60	70	80	90	100
eBee	500-trees	44.1	59.2	60.3	70.7	71.2	66.4	69.3	74.6	78.5	79.9	78.9
eBee	fitted-trees	44.1	59.2	60.3	70.7	71.2	66.4	69.3	74.7	78.6	79.7	79.0
APEX	500-trees	78.4	79.2	86.1	86.1	78.6	86.1	81.9	90.7	91.0	91.2	91.5
APEX	fitted-trees	78.4	79.3	86.1	86.1	78.5	86.2	81.9	90.8	91.0	91.1	91.5
eBee & APEX	500-trees	81.5	82.7	89.7	89.4	88.3	90.0	89.6	91.2	90.9	91.0	91.9
eBee & APEX	fitted-trees	81.5	82.7	89.7	89.3	88.2	89.9	89.5	91.2	90.9	90.8	91.9

Table S2. Kappa coefficient for all settings, models, and correlation thresholds.

Setting	Model	Correlation threshold (%)										
		0	10	20	30	40	50	60	70	80	90	100
eBee	500-trees	30.2	47.9	49.1	62.0	62.7	56.3	60.2	66.9	71.9	73.6	72.4
eBee	fitted-trees	30.2	47.9	49.1	62.0	62.7	56.4	60.2	67.0	72.0	73.4	72.4
APEX	500-trees	71.7	73.0	81.7	81.7	71.9	81.8	76.3	87.9	88.2	88.2	88.8
APEX	fitted-trees	71.7	72.8	81.6	81.8	72.0	81.7	76.2	87.8	88.1	88.3	88.8
eBee & APEX	500-trees	75.8	77.3	86.4	86.1	84.6	86.8	86.2	88.4	88.0	88.1	89.3
eBee & APEX	fitted-trees	75.7	77.3	86.4	85.9	84.4	86.7	86.2	88.4	88.0	87.9	89.3

Table S3. Average reliability (AR) for all settings, models, and correlation thresholds.

Setting	Model	Correlation threshold (%)										
		0	**10**	**20**	**30**	**40**	**50**	**60**	**70**	**80**	**90**	**100**
eBee	500-trees	51.0	63.5	64.4	73.3	74.5	71.2	73.6	78.1	81.1	82.1	81.3
eBee	fitted-trees	51.0	63.5	64.4	73.3	74.6	71.2	73.6	78.1	81.1	81.9	81.3
APEX	500-trees	81.3	82.1	87.9	87.9	81.5	88.0	84.4	92.5	92.7	92.7	93.0
APEX	fitted-trees	81.3	82.1	87.9	87.9	81.5	87.9	84.4	92.4	92.7	92.8	93.0
eBee & APEX	500-trees	83.9	84.9	91.4	91.1	90.3	91.7	91.5	92.9	92.7	92.6	93.4
eBee & APEX	fitted-trees	83.9	84.9	91.4	91.0	90.2	91.6	91.4	92.9	92.6	92.5	93.4

Table S4. p-values of significance test ($p < 0.05$) for the *eBee setting* with all correlation thresholds.

		Correlation threshold (%)										
		0	**10**	**20**	**30**	**40**	**50**	**60**	**70**	**80**	**90**	**100**
Correlation threshold (%)	**0**	1.000										
	10	0.000	1.000									
	20	0.000	0.007	1.000								
	30	0.000	0.000	0.000	1.000							
	40	0.000	0.000	0.000	0.000	1.000						
	50	0.000	0.002	0.001	0.003	0.000	1.000					
	60	0.000	0.000	0.000	0.679	0.188	0.000	1.000				
	70	0.000	0.000	0.000	0.000	0.001	0.000	0.000	1.000			
	80	0.000	0.000	0.000	0.000	0.000	0.000	0.000	0.000	1.000		
	90	0.000	0.000	0.000	0.000	0.000	0.000	0.000	0.000	0.005	1.000	
	100	0.000	0.000	0.000	0.000	0.000	0.000	0.000	0.007	0.561	0.004	1.000

Table S5. p-values of significance test ($p < 0.05$) for the *APEX setting* with all correlation thresholds.

		Correlation threshold (%)										
		0	**10**	**20**	**30**	**40**	**50**	**60**	**70**	**80**	**90**	**100**
Correlation threshold (%)	**0**	1.000										
	10	0.489	1.000									
	20	0.004	0.001	1.000								
	30	0.003	0.001	0.151	1.000							
	40	0.524	0.330	0.003	0.004	1.000						
	50	0.007	0.005	0.330	0.847	0.007	1.000					
	60	0.003	0.001	0.055	0.048	0.002	0.048	1.000				
	70	0.000	0.000	0.073	0.135	0.000	0.135	0.000	1.000			
	80	0.000	0.000	0.055	0.095	0.000	0.107	0.000	0.208	1.000		
	90	0.000	0.000	0.018	0.030	0.000	0.035	0.000	0.022	0.064	1.000	
	100	0.000	0.000	0.005	0.008	0.000	0.008	0.000	0.003	0.022	0.454	1.000

Table S6. p-values of significance test ($p < 0.05$) for the *eBee & APEX setting* with all correlation thresholds.

		Correlation threshold (%)										
		0	**10**	**20**	**30**	**40**	**50**	**60**	**70**	**80**	**90**	**100**
Correlation threshold (%)	**0**	1.000										
	10	0.001	1.000									
	20	0.000	0.000	1.000								
	30	0.000	0.000	0.762	1.000							
	40	0.000	0.000	0.015	0.007	1.000						
	50	0.000	0.000	0.303	0.055	0.000	1.000					
	60	0.000	0.000	0.679	0.934	0.001	0.188	1.000				
	70	0.000	0.000	0.048	0.000	0.000	0.012	0.000	1.000			
	80	0.000	0.000	0.055	0.005	0.000	0.026	0.008	0.890	1.000		
	90	0.000	0.000	0.095	0.007	0.000	0.083	0.008	0.421	0.421	1.000	
	100	0.000	0.000	0.004	0.000	0.000	0.004	0.003	0.015	0.022	0.022	1.000

Table S7. p-values of significance test ($p < 0.05$) for the difference between the *500-trees model* and the *fitted-trees model* for each settings with all correlation thresholds.

	Correlation threshold (%)										
Setting	**0**	**10**	**20**	**30**	**40**	**50**	**60**	**70**	**80**	**90**	**100**
eBee	0.277	0.561	0.229	0.330	0.048	0.454	0.934	0.041	0.005	0.934	0.000
APEX	0.252	0.359	0.389	0.762	0.229	0.421	0.599	0.303	0.847	0.055	0.762
eBee & APEX	0.639	0.847	0.048	0.022	0.229	0.389	0.762	1.000	0.015	0.890	0.022

Table S8. p-values of significance test ($p < 0.05$) for the comparison of the *eBee setting* versus the *APEX setting* with all correlation thresholds.

		APEX setting										
		Correlation threshold (%)										
		0	**10**	**20**	**30**	**40**	**50**	**60**	**70**	**80**	**90**	**100**
eBee setting Correlation threshold (%)	**0**	0.000	0.000	0.000	0.000	0.000	0.000	0.000	0.000	0.000	0.000	0.000
	10	0.000	0.000	0.000	0.000	0.000	0.000	0.000	0.000	0.000	0.000	0.000
	20	0.000	0.000	0.000	0.000	0.000	0.000	0.000	0.000	0.000	0.000	0.000
	30	0.000	0.000	0.000	0.000	0.000	0.000	0.000	0.000	0.000	0.000	0.000
	40	0.000	0.000	0.000	0.000	0.000	0.000	0.000	0.000	0.000	0.000	0.000
	50	0.000	0.000	0.000	0.000	0.000	0.000	0.000	0.000	0.000	0.000	0.000
	60	0.000	0.000	0.000	0.000	0.000	0.000	0.000	0.000	0.000	0.000	0.000
	70	0.026	0.004	0.000	0.000	0.012	0.000	0.000	0.000	0.000	0.000	0.000
	80	0.421	0.151	0.000	0.000	0.330	0.000	0.000	0.000	0.000	0.000	0.000
	90	0.762	0.804	0.000	0.000	0.762	0.000	0.001	0.000	0.000	0.000	0.000
	100	0.804	0.208	0.000	0.000	0.720	0.000	0.000	0.000	0.000	0.000	0.000

Table S9. p-values of significance test ($p < 0.05$) for the comparison of the *eBee & APEX setting* versus the *APEX setting* with all correlation thresholds.

		APEX setting										
		Correlation threshold (%)										
		0	**10**	**20**	**30**	**40**	**50**	**60**	**70**	**80**	**90**	**100**
eBee & APEX setting Correlation threshold (%)	**0**	0.000	0.008	0.026	0.026	0.000	0.026	0.890	0.000	0.000	0.000	0.000
	10	0.000	0.000	0.073	0.073	0.000	0.073	0.359	0.000	0.000	0.000	0.000
	20	0.000	0.000	0.000	0.001	0.000	0.001	0.000	0.330	0.277	0.208	0.030
	30	0.000	0.000	0.005	0.012	0.000	0.012	0.000	0.208	0.169	0.035	0.018
	40	0.000	0.000	0.277	0.330	0.000	0.359	0.000	0.003	0.005	0.001	0.003
	50	0.000	0.000	0.002	0.003	0.000	0.004	0.000	0.330	0.277	0.107	0.022
	60	0.000	0.000	0.073	0.083	0.000	0.083	0.000	0.026	0.018	0.015	0.012
	70	0.000	0.000	0.001	0.001	0.000	0.001	0.000	0.135	0.252	0.524	0.934
	80	0.000	0.000	0.000	0.001	0.000	0.001	0.000	0.229	0.252	0.679	0.847
	90	0.000	0.000	0.001	0.002	0.000	0.002	0.000	0.454	0.720	1.000	0.561
	100	0.000	0.000	0.000	0.000	0.000	0.000	0.000	0.000	0.003	0.004	0.095

Remote Sens. **2019**, *11*, x FOR PEER REVIEW 5 of 9

Table S10. Selected eBee size and feature type for different correlation thresholds in the eBee setting. We report the frequency how many fold a feature was selected for each correlation threshold. A feature is defined by its size of the structuring element (SE), feature type and spectral band of the eBee sensor.

			Correlation threshold (%)									
SE size	Feature type	Band	0	10	20	30	40	50	60	70	80	90
3	dilate	R		5	2	15	15	15	15		1	15
3	dilate	Nir		15	15	2	2	15		15	15	15
5	dilate	B										15
5	dilate	G										15
5	dilate	R			5	15		2	15		15	5
3	erode	B										15
5	erode	B				1			15	15		15
5	erode	G			1		15	15	15	15	15	
5	erode	R								1	15	15
5	erode	Nir							1	15	15	15
3	open	R										15
5	open	G										15
3	close	B								1		1
3	close	G						15		15	15	15
3	close	R										1
3	close	Nir			15		15	15	15		15	15
5	close	R	2			15	15	15	15	15	15	15
3	tophat	B								15	15	15
3	tophat	G				1				15	1	15
3	tophat	R									15	15
3	tophat	Nir					15			15	15	15
5	tophat	B									1	15
5	tophat	G								15	15	15
5	tophat	R						15			15	15
5	tophat	Nir		1	15	15		15	15			
3	bothat	B								1		15
3	bothat	G					1			15	5	15
3	bothat	R									9	15
3	bothat	Nir							15		15	15
5	bothat	B									15	
5	bothat	G								15		15
5	bothat	R						15		9	15	15
5	bothat	Nir						15			2	15
5	openRec	Nir									1	15
3	tophatRec	B				2			15	15	15	15
3	tophatRec	G		15	15	15	15	15	15	15	15	
3	tophatRec	R									1	15
3	tophatRec	Nir	15			15	15	1	1	5	15	

			Correlation threshold (%)									
SE size	**Feature type**	**Band**	**0**	**10**	**20**	**30**	**40**	**50**	**60**	**70**	**80**	**90**
5	tophatRec	G			15		15	15	2	15	2	15
5	tophatRec	R			2		15	15	15	15		15
5	tophatRec	Nir					15			15		15
3	bothatRec	B	15				1		1	15	15	
3	bothatRec	G	6		15		5	15			15	15
3	bothatRec	R					15				15	15
3	bothatRec	Nir	15	15		15			15	2	1	
5	bothatRec	B									1	15
5	bothatRec	G		15			2	15	15	15		15
5	bothatRec	R									15	15
3	entropy	B								15	15	15
3	entropy	G							15			15
3	entropy	R										15
3	entropy	Nir				15			9	2		15
5	entropy	B									1	
5	entropy	G								15		15
5	entropy	R	15	2					15		2	15
5	entropy	Nir										15
3	range	B										15
3	range	G									15	
3	range	R									1	15
3	range	Nir			1			15	15	15	15	15
5	range	B									15	15
5	range	G							1		15	15
5	range	R								1		15
5	range	Nir							15			
5	mean	Nir	1	15	15	15	15		15	15	2	15

34
35

Remote Sens. **2019**, *11*, x FOR PEER REVIEW 7 of 9

Table S11. Selected eBee features for different correlation thresholds in the *eBee & APEX setting*. The numbers in the table give the frequency in how many folds a feature was selected per correlation threshold. A feature is defined trough the size of the structuring element (SE), feature type and band of the eBee sensor.

			Correlation threshold (%)									
SE size	**Feature type**	**Band**	**0**	**10**	**20**	**30**	**40**	**50**	**60**	**70**	**80**	**90**
3	dilate	B	1		15		15	1	2		15	2
5	dilate	B								15	5	15
5	dilate	G				15	15	15	15	15		15
5	dilate	R						1	9	15	2	
5	dilate	Nir				15	15	15	15	15	9	15
3	erode	B							15	15	15	15
3	erode	G									15	
3	erode	R									1	
5	erode	B						15			15	
5	erode	G								15		15
5	erode	R					1	15		15		15
5	erode	Nir						15		15	15	15
5	open	Nir										1
3	close	G										15
3	close	R								1		15
3	close	Nir									15	15
5	close	B										2
5	close	Nir										1
3	tophat	B								15	15	15
3	tophat	G							15		15	15
3	tophat	R									15	
3	tophat	Nir					15	15				15
5	tophat	B									15	15
5	tophat	G								15	2	15
5	tophat	R					15	1	15	15	15	
5	tophat	Nir								15	15	15
3	bothat	B									15	15
3	bothat	G								15		15
3	bothat	R					15		2	15	5	15
3	bothat	Nir										2
5	bothat	B								1	15	
5	bothat	G							1	15		15
5	bothat	R									15	15
5	bothat	Nir						15		15	1	15
3	closeRec	Nir										15
5	closeRec	B										15
3	tophatRec	B				1	15	15	15	2	2	15
3	tophatRec	G									15	15

			Correlation threshold (%)									
SE size	**Feature type**	**Band**	**0**	**10**	**20**	**30**	**40**	**50**	**60**	**70**	**80**	**90**
3	tophatRec	R									1	
3	tophatRec	Nir				15			15	15	1	15
5	tophatRec	B					15		15		15	15
5	tophatRec	G		15	15	2		15	15			15
5	tophatRec	R			2	15	15	15	15	15	1	15
5	tophatRec	Nir		15		15	15	15	15	15	15	15
3	bothatRec	B									15	
3	bothatRec	G		15	1	15	2		15			15
3	bothatRec	R					15			1	15	15
3	bothatRec	Nir		15	15	15	15	15		15	1	
5	bothatRec	B		15		15	2	15	15		15	
5	bothatRec	G		15	15			6	15			5
5	bothatRec	R	1				15		1	1	5	5
3	entropy	B								15	15	15
3	entropy	G										15
3	entropy	R			15	15	15	15	2	15	15	15
3	entropy	Nir	15		15			1	2	15	1	15
5	entropy	B									15	
5	entropy	G				1		15	15	15		15
5	entropy	R								9	15	15
5	entropy	Nir										15
3	range	R										15
3	range	Nir									15	15
5	range	B										15
5	range	G		1	15	15	15	15	15	15	15	
5	range	R									15	
5	range	Nir							15		15	1
3	stdv	B									1	15
3	stdv	G										15

Remote Sens. **2019**, *11*, x FOR PEER REVIEW

Table S12. Selected APEX features and mean number of features per fold for different correlation thresholds in the *eBee & APEX setting*. The numbers in the table give the frequency in how many folds a feature was selected per correlation threshold.

Wavelength	**Correlation threshold (%)**									
(nm)	**0**	**10**	**20**	**30**	**40**	**50**	**60**	**70**	**80**	**90**
399						1		15	15	15
413							9		1	15
427										15
490								1		15
509										2
553	15		2						1	15
581										15
594									5	
681		1			15	2	15			
684			9		2	15	15	15	15	15
688				9		9	15	15	15	15
785										1
1042	15		15	15			15	2	15	1
1261							1			15
1521								1	15	15
1549									1	15
1567										1
1675	15		15	2		15				15
2057					1		15	15		15
2349										15
2388									15	15
2419								15		15
2432										15
Mean number of features per fold	3.0	0.1	2.7	1.7	1.2	2.8	5.7	5.3	6.5	17.3

Chapter

5

Synthesis

In this Chapter the findings from the individual Chapters are brought together and rounded off. The first subsection presents the answers to the three research questions introduced in Chapter 1. Then the general contributions to the research area are shown. Finally, possible future research directions are suggested.

5.1 Main findings

The thesis tackles three main research questions, which are formulated in Chapter 1 and dealt with in Chapters 2 to 4:

I. At which spatial resolution and which spectral bands from uncalibrated multispectral UAV data can agricultural crops best be separated?

II. What is the optimal temporal window during the growing season to separate crop types in an uncalibrated NIR-RGB dataset including textural features?

III. What is the added value of simultaneously using the spectral/textural features of a multispectral VHR drone dataset and spectral high-resolution IS data?

In the following three subsections, the main findings of the three research questions are presented and discussed.

5.1.1 Optimized spatial and spectral sampling strategies for crop type separation

Until now, only very few separation efforts of crops based on uncalibrated RGB data have been performed and reported in literature, at best with additional channels in the NIR range or additional satellite data [1–3]. In Chapter 2 we presented a methodology for the separation of different crop types based on uncalibrated NIR-RGB data obtained with a UAV to answer the first research question (At which spatial resolution and which spectral bands from uncalibrated multispectral UAV data can agricultural crops best be separated?). This approach allows the comparison of a variety of spatial and spectral resolutions of the dataset, different SE sizes for textural features and the verification of the results for pixel- or parcel-based spatial support. On the one hand, we analyzed ten individual crop classes, and on the other hand, we pooled maize and bare soil, the three cereals types (winter wheat, spelt, and winter barley), and grassland and clover together.

Ten crop types were examined for their separability (these are maize, bare soil, sugar beet, winter wheat, spelt, winter barley, grassland, clover, grass hay and rapeseed). Maize and bare soil, the three cereals (i.e., winter wheat, spelt, winter barley), as well as grassland and clover are difficult to separate with the available dataset. The separation of the different cereal types, and grassland from clover

is a common issue. In the case of maize and bare soil, the difficulty arises from the fact that maize was present in a variety of phenological stages at the time of sampling. These ranged from fresh sowing to stem elongation, which means that the appearance of maize in remote sensing data partially corresponds to that of bare soil. When combining the crops that are difficult to separate into one group (e.g., the three cereal types), the separation becomes easier.

Across all settings, the best results can be achieved with an RGB dataset with a spatial resolution of 0.5 m and five SE with sizes up to 29 pixels in diameter. In general, RGB datasets with more and larger SE sizes outperform datasets with the additional NIR band. However, the NIR band sometimes leads to improvements in the separation of a single crop. It should be noted, however, that this does not hold true regardless of the spatial resolution. It could be shown that for finer and coarser spatial resolutions an additional NIR band leads to better results.

It is important that the SE sizes cover the whole range of both within-row and between-row spacing of all present crops. The crop type with the largest distances between the individual plants mainly drives this issue. Consequently, our tested settings with five SE sizes exceed the settings with two SE sizes in terms of accuracy, especially at high spatial resolutions. At low spatial resolutions, the differences are not as pronounced, and only two SE sizes exceed settings with five SE sizes.

If an additional data source with field boundaries is available, it can be included in the method. In such a case, the spatial aggregation of the pixels of a single field prevents the so-called salt and pepper effect (i.e., a misclassification of adjacent pixels despite large similarities) and only one crop type is finally assigned to each field. This increases the accuracy of crop separation by up to 20%.

The achieved accuracy of crop separation is consistent with other studies based on satellite or UAV datasets [4–9]. From this it can be concluded that an uncalibrated NIR-RGB dataset captured with consumer-grade cameras mounted on a UAV is sufficient to achieve state-of-the-art crop separation even in small structured agricultural areas. The disadvantage of spectrally poorly characterized bands can be overcome with an optimal spatial resolution and well chosen textural features. As more and more space- and airborne VHR images become operationally available in the near future, the methodology presented and evaluated in Chapter 2 contributes to the production of crop maps with documented accuracy in small-scale agricultural areas.

5.1.2 Optimal temporal window for crop type separation

The collection of data in due course is essential, since the appearance of crops changes considerably as their phenology progresses. Therefore, the time of acquisition is crucial in order to improve the separability of the cultures on the one hand, and to reduce the amount of data on the other. A methodology for crop separation was developed on the basis of datasets collected with uncalibrated consumer-grade

cameras mounted on a UAV during 11 observations between 5 May 2015 (515 AGDD) and 29 September 2015 (3238 AGDD) to answer the second research question (What is the optimal temporal window during the growing season to separate crop types in an uncalibrated NIR-RGB dataset including textural features?). The NIR-RGB dataset was again supplemented with textural features to distinguish cereals, grassland, maize, rapeseed and sugar beet, and, if present, bare soil.

Three temporal windows over the growing season were identified in which the accuracy of crop separation did not differ significantly between observational data. An early temporal window was identified, ranging from the first observation on 5 May 2015 (515 AGDD) to 17 June 2015 (1232 AGDD). The AA for crop separation is between 70% and 75%. The separation between maize and sugar beet was identified as the major difficulty. As they are gradually sown in during this temporal window, their seedlings are difficult to recognize and distinguish in the bare soil [10]. The mid-season temporal window is best suited to separate the analyzed crops, as has been confirmed in other studies [5,10,11]. This temporal window lasts from 25 June 2015 (1362 AGDD) to 22 July 2015 (2016 AGDD), and the AA is about 80%. Winter crops are in a senescence stage at this time of the growing season and summer crops are in their most productive stage. Observations after 21 August 2015 (2626 AGDD) fell into the late time window with an AA of less than 65%.

If the NIR band is included in the dataset, this leads to significantly higher separation results compared to a pure RGB dataset. As known from land use/land cover classifications based on textural features, the used SE quantities play a decisive role [12]. Different spectral signatures resulting from the interaction of plant material and soil background largely determine the textural information in agricultural areas. When the canopy is closed, spectral rather than textural properties become important [13], which is the reason why an additional NIR band improves crop separation [14].

With regard to the separation of the individual agricultural crops, their respective phenological stages are decisive. Rapeseed can be distinguished from all other crops with a high degree of accuracy thanks to its yellow flowers. The differentiation of cereals from the other crops in the study area is best achieved immediately after harvesting, when the plant residues and bare soil dominate the signal, and the summer crops (i.e., sugar beet and maize) are in their most productive stage. The differences between individual summer crops become more pronounced with the phenological development. Since sugar beet is the first sown summer crop in the study area and the spectral signature is dominated by the bare soil at the beginning, it can easily be separated from the winter crops. The green grassland can best be distinguished from the summer crops at the end of the season, as maize turns brown in its final stage and sugar beet has a completely different spectral signature. Bare soil, if present, can be separated most accurately from crops if their plant material covers a large part of the area and therefore dominates the measured signal. Fields in preparation (e.g., ploughed) are particularly difficult to distinguish from fields with

small seedlings. Since the texture of crop residues and bare soil appears different, cereal fields are best differentiated after harvest.

Overall, on the basis of Chapter 3, we can conclude that crop separation with uncalibrated NIR-RGB datasets is most accurate between 1362 AGDD and 2016 AGDD in a highly fragmented and small-scale agricultural area such as the Swiss Plateau.

5.1.3 Complementarity of spectral and textural information for the separation of crop species

The separation of crops was previously reported to be successful using data from IS sensors [15,16]. However, these studies were carried out in areas with large fields, which do not correspond to the conditions in small structured agricultural areas, as it is the case in the Swiss Plateau. Chapter 4 analyzed the potential of texture features from a multispectral VHR dataset acquired with uncalibrated consumer-grade cameras mounted on a UAV, together with individual bands from an IS dataset, to answer the third research question (What is the added value of simultaneously using the spectral/textural features of a multispectral VHR drone dataset and spectral high-resolution IS data?).

The best setting corresponds to the IS data alone (AA 92.2%), and in combination with the VHR dataset (AA 92.8%). Although the combined datasets lead to a slightly higher accuracy, this difference is not significant. With a pixel-based approach, the UAV data alone leads to a significantly lower accuracy in the separation of the crops (AA 80.0%). However, the IS dataset used contains many spectral bands. A substantial reduction of the spectral bands shows that the respective accuracy decreases to the level of the pure VHR dataset.

Interestingly, a combination of a few bands from the IS dataset with the VHR dataset leads to a significantly higher accuracy (AA $>$90%). This finding is important to reduce the amount of data and thus increase the performance of the production chain from data collection to crop separation. Furthermore, it could be shown that a few spectrally well-defined bands next to a consumer-grade NIR-RGB camera are sufficient to achieve the same accuracy, as with a high quality IS system.

The removal of correlated bands in the datasets also showed that the number of bands in the IS dataset can be reduced from 173 to about 10 bands without significantly affecting accuracy. However, a further reduction to less than 7 bands significantly impairs the ability to separate the crops. The analysis of the VHR dataset indicates that textural features are superior to purely spectral features and lead to a decisive increase in accuracy.

In summary, Chapter 4 concludes that the accuracy of crop separation with an IS dataset exceeds the accuracy with a NIR-RGB dataset and its textural features.

However, if the number of IS features used is reduced, additional NIR-RGB textural features (especially the morphological features of the NIR, G and R bands) may compensate for a reduction in the accuracy of the crop separation.

5.2 General contributions

The spatial, spectral and temporal resolutions of remote sensing datasets are crucial for the separation of crops. In order to achieve high accuracy, these three dimensions must be optimized to simultaneously keep factors such as computing time, data storage or costs as low as possible [17]. However, all three dimensions are closely related to each other and must be adapted to the specific data collection issue. Still, there is no uniform approach for crop separation because different datasets require different algorithms or methods that can process, for example, multi-temporal information, different spatial resolutions or additionally derived features.

5.2.1 Spatial resolution

The spatial resolution of a dataset decisively determines the measured level of detail. In crop separation, there are mainly two drivers for the appropriate spatial resolution. One is the field size and the other is the relationship between plants and background, e.g., bare soil. In general, it is crucial for the classification algorithm that the variability within a class differs from the variability between classes. For the separation of crops, this means that the difference between the within-field variability and the between-field variability is a critical issue [18].

To properly account for the between-field variability and to train a classification algorithm, enough spectrally pure pixels are needed, preferably several per field. Consequently, the optimal spatial resolution depends on the field size in the study area. The variation in field size is very large globally, ranging from less than 0.4 ha (1 acre) in rural Africa [19] to more than 30 ha per field in the Central Plain of the USA [20], for example. However, the pixel size should be as large as possible to keep the processing time in a feasible manner [17].

The components within a field determine its variability, i.e., mainly the individual plants and the soil background. In datasets with a spatial resolution that does not allow the recognition of individual plants, the differences between adjacent pixels are therefore small. The within-field variability is then driven by the different growth stages of the plants, e.g., due to differences in soil properties. In VHR datasets in which the individual plants can be identified, the plant cover additionally determines the variability within the field [12]. The row spacing and the within-row spacing of plants cause strong textural effects with bare soil. When the canopy is completely closed, the shading of the leaves and different reflection properties at different leaf

angles mainly cause such effects [13]. Determining the optimal spatial resolution therefore means to find the optimal balance between the between-field and within-field variability.

Besides the spatial resolution, the spectral resolution also plays an important role to be considered. As shown in Chapter 4, IS data with a spatial resolution of 2 m are superior to uncalibrated NIR RGB data with a spatial resolution of 0.5 m. Furthermore, it could be shown in Chapter 2 that the additionally used textural features have an influence on the optimal spatial resolution. Hence, the optimal spatial resolution also depends on the methodology. Thus, the methodology must be chosen according to the available data, respectively.

If the spatial resolution is high enough to cover a field with several pixels, it is also possible to apply object-based approaches. These usually promise a higher accuracy than pixel-based approaches [21], and can be considered the state of the art in crop mapping [5]. This also applies to uncalibrated multispectral datasets (Chapter 2). However, field-based analysis requires additional field boundaries, which either come from an additional source or can be determined directly from the data [6,22].

5.2.2 Spectral resolution

With a high spectral resolution, a lower spatial resolution can not only be compensated but also exceeded (Chapter 4). However, the collection of IS data is still rather expensive and complex and only possible for limited, regional areas, usually confined to individual strips of a few kilometers width.

In Chapter 2, it could be shown that crop separation with uncalibrated NIR-RGB data of very high spatial resolution leads to at least as good results as with conventional multispectral satellite data. This opens up a number of completely new opportunities. Since texture information is of crucial importance, textural features obtained from satellite data of different sensors can be combined regardless of their spectral characteristics. Aerial imagery that has become widely used, such as the *SWISSIMAGE* product of *swisstopo*, can also be used to separate crops.

The comparison with an IS dataset shows that the capabilities of uncalibrated NIR-RGB data for crop separation are limited (Chapter 4). The addition of some selected IS bands already lead to equally good results as in the case of a pure IS dataset. Adding individual spectral bands in the NIR range is possible for various sensor technologies, which can be used both in aircraft and UAV settings [23]. As a result, the entire process from data acquisition to the final product of crop separation can be made more efficient by carefully selecting the appropriate sensor technology and the spectral bands used.

5.2.3 Temporal resolution

The optimal timing of data collection reduces the effort for data acquisition and data processing. This becomes particularly important when timely information on crop type and growth stage is required, e.g., for early crop mapping [24]. There are, however, numerous reasons that prevent data collection at the optimal moment, such as clouds, availability of airspace, or wind, to name just a few. It is therefore important to have some flexibility in the timing of the recording. In Chapter 3 an optimal temporal window for accurate crop separation using UAV data and textural features in the middle of the phenological season could be determined.

The temporal resolution of recordings with satellites, airborne systems and UAVs varies considerably. Satellites have a fixed revisit time, which varies depending on the spatial resolution and ranges, for example, from 1-2 days (MODIS) to 16 days (Landsat). Airborne systems are more flexible, but require considerable planning and preparation time. Consequently, the phenology of crops must be taken into account when planning potential flight windows. If at all, very few revisits of the same site in the same year are usually possible. In contrast, UAVs have an almost unlimited temporal resolution. Thus, a recording can take place up to several times a day and depends mainly on the available manpower and the weather conditions.

5.2.4 General remarks

The three dimensions related to resolution, as discussed above, are strongly interconnected. Finding optimal sensor data puts up the large bottleneck in precise crop mapping [25]. Satellites have a rather high temporal resolution, but mostly a low spatial resolution and a reduced number of spectral bands. In general, they are radiometrically very precisely characterized. Airborne IS has a very low temporal resolution, but an excellent spectral and high spatial resolution. UAVs offer the best temporal resolution, and with increasing automation manpower requirements decrease. The spatial resolution is almost freely selectable and only limited by the system-dependent minimum flight altitudes and legal regulations. However, their spectral resolution is often limited, since miniaturization of size and weight considerably reduces the spectral properties. Nevertheless, studies such as the present thesis show that satisfactory results can also be achieved with simple cameras.

For operational purposes, however, the coverage rate is of central importance [26]. Using UAVs, only local coverage can be obtained. Airborne systems can cover at least regional areas, while satellites potentially cover the entire globe. It is therefore important to transfer the knowledge gained with sensors on UAVs to airborne and spaceborne platforms.

The proposed methodology for crop separation opens up a range of new possibilities. The biggest advantage is that a statistical comparison of different settings

(SE size, spectral bands, etc.) is possible with splits of a single dataset. In principle, this would always be feasible once the dataset for training and testing has been split. However, care must be taken to ensure that sufficient splits are selected for the statistical analyses and that they are spatially separated. When incorporating texture features, there must be a spatial gap between the splits to ensure that any information from adjacent pixels belongs to only one individual split. This so-called n-fold cross-validation is often used in machine learning [27,28].

For the actual classification, any suitable algorithm can be selected. In this study, the RF algorithm was used [29]. In principle, a whole range of algorithms can be considered, for example, with decision trees, SVM or Gaussian modeling [25,30–32]. However, RF often outperforms other algorithms [33], is easy to set up and does not suffer from overlearning [34] or the so-called curse of dimensionality (Hughes phenomenon) [35].

5.3 Final considerations and future directions

The present thesis closes some gaps related to spatial, spectral and temporal resolution issues when using remotely sensed datasets for agricultural purposes. It should be noted that *more is not always better*. The optimal choice of these factors reduces for instance computing time and memory requirements, and thus enables large data operations. However, there are still numerous open issues concerning accurate and effective crop separation:

- First of all, and perhaps most important to the whole research area, is a review of crop separation in the context of the spatial, spectral, and temporal resolution, which is accessible to the scientific community. Different agricultural management practices should be considered, so that not only fields of different sizes, but also cultivation practices can be considered. There will also be problems with differing combinations of crops in other areas that may be considered. Furthermore, single fields with combined mixtures of crops offer new opportunities in agriculture and are becoming increasingly important in view of climate change. The monitoring of such fields, in contrast, poses new challenges for remote sensing, since the classical approaches are based on monocultures. With regard to global analyses, small fields will play an important role, since a large part of agricultural production is still run by smallholder farming [36].

- Taking a closer look at other data sources in support of crop separation is important. It has already been shown that additional data on field boundaries can substantially improve the accuracy of crop separation [12]. Delineating these plot limits directly from remotely sensed imagery would greatly facilitate

data processing. In addition, the fusion of different data sources, e.g., stemming from Synthetic Aperture Radar (SAR) and optical satellites such as Sentinel-2 or Landsat must be further promoted. A combined approach using SAR and optical data has already produced promising results and offers new options, especially with regard to independence from cloud cover [37].

- The obvious next step consists in transferring the findings from UAV data to other spatial high-resolution remote sensing systems. On the one hand, aerial photographs with 10 cm resolution for the whole of Switzerland exist, which are suitable for such analyses. On the other hand, there are already satellites with a spatial resolution of less than 50 cm in orbit, which therefore also provide potentially suitable data. However, this would require initial clarification of some of the most imminent big data issues [38].

- Cloud computing and machine learning methods should make it possible to meet the long-standing expectations of remote sensing in agriculture [25]. Besides the already mentioned ML algorithms, deep learning algorithms such as Neural Networks (NN) and Convolutional Neural Networks (CNN) should certainly be considered and examined for aspects of spatial, spectral and temporal resolution of the input datasets. Important next steps for deep learning are, among others the recognition of particular features of the data to identify spatial and multitemporal relationships, improving interpretability to recognize physical relationships, increased quantification of uncertainties, and comparison with complex physical models [39].

5.4 References

1. Zhang, J.; Zhao, Y.; Abbott, A. L.; Wynne, R. H.; Hu, Z.; Zou, Y.; Tian, S. Automated mapping of typical cropland strips in the North China Plain using small Unmanned Aircraft Systems (sUAS) photogrammetry. *Remote Sens.* **2019**, *11*, doi:10.3390/rs11202343.
2. Zhao, L.; Shi, Y.; Liu, B.; Hovis, C.; Duan, Y.; Shi, Z. Finer Classification of Crops by Fusing UAV Images and Sentinel-2A Data. *Remote Sens.* **2019**, *11*, 3012, doi:10.3390/rs11243012.
3. Yan, Y.; Deng, D.; Liu, L.; Zhu, Z. Application of UAV-Based Multi-Angle Hyperspectral Remote Sensing in Fine Vegetation Classification. *Remote Sens.* **2019**, *11*, 2753, doi:10.3390/rs11232753.
4. Immitzer, M.; Vuolo, F.; Atzberger, C. First experience with Sentinel-2 data for crop and tree species classifications in central Europe. *Remote Sens.* **2016**, *8*, doi:10.3390/rs8030166.

5. Ozdarici-Ok, A.; Ok, A.; Schindler, K. Mapping of Agricultural Crops from Single High-Resolution Multispectral Images--Data-Driven Smoothing vs. Parcel-Based Smoothing. *Remote Sens.* **2015**, *7*, 5611–5638, doi:10.3390/rs70505611.
6. Ahmed, O. S.; Shemrock, A.; Chabot, D.; Dillon, C.; Williams, G.; Wasson, R.; Franklin, S. E. Hierarchical land cover and vegetation classification using multispectral data acquired from an unmanned aerial vehicle. *Int. J. Remote Sens.* **2017**, *38*, 2037–2052, doi:10.1080/01431161.2017.1294781.
7. Zhang, J.; Yang, C.; Song, H.; Hoffmann, W. C.; Zhang, D.; Zhang, G. Evaluation of an Airborne Remote Sensing Platform Consisting of Two Consumer-Grade Cameras for Crop Identification. *Remote Sens.* **2016**, *8*, 257, doi:10.3390/rs8030257.
8. Wu, M.; Yang, C.; Song, X.; Hoffmann, W. C.; Huang, W.; Niu, Z.; Wang, C.; Li, W. Evaluation of orthomosics and digital surface models derived from aerial imagery for crop type mapping. *Remote Sens.* **2017**, *9*, 239, doi:10.3390/rs9030239.
9. Zhang, J.; Yang, C.; Zhao, B.; Song, H.; Hoffmann, W. C.; Shi, Y.; Zhang, D.; Zhang, G. Crop classification and LAI estimation using original and resolution-reduced images from two consumer-grade cameras. *Remote Sens.* **2017**, *9*, doi:10.3390/rs9101054.
10. Van Tricht, K.; Gobin, A.; Gilliams, S.; Piccard, I. Synergistic use of radar Sentinel-1 and optical Sentinel-2 imagery for crop mapping: a case study for Belgium. *Remote Sens.* **2018**, 1–22, doi:10.20944/preprints201808.0066.v1.
11. Vuolo, F.; Neuwirth, M.; Immitzer, M.; Atzberger, C.; Ng, W.-T. How much does multi-temporal Sentinel-2 data improve crop type classification? *Int. J. Appl. Earth Obs. Geoinf.* **2018**, *72*, 122–130, doi:10.1016/j.jag.2018.06.007.
12. Böhler, J.; Schaepman, M.; Kneubühler, M. Crop Classification in a Heterogeneous Arable Landscape Using Uncalibrated UAV Data. *Remote Sens.* **2018**, *10*, doi:10.3390/rs10081282.
13. Norman, J.; Welles, J. Radiative transfer in an array of canopies. *Agron. J.* **1983**, *75*, 481–488, doi:10.2134/agronj1983.00021962007500030016x.
14. Zhang, H.; Li, Q.; Liu, J.; Shang, J.; Du, X.; McNairn, H.; Champagne, C.; Dong, T.; Liu, M. Image Classification Using RapidEye Data: Integration of Spectral and Textual Features in a Random Forest Classifier. *IEEE J. Sel. Top. Appl. Earth Obs. Remote Sens.* **2017**, *10*, 5334–5349, doi:10.1109/JSTARS.2017.2774807.
15. Aneece, I.; Thenkabail, P. Accuracies Achieved in Classifying Five Leading World Crop Types and their Growth Stages Using Optimal Earth Observing-1 Hyperion Hyperspectral Narrowbands on Google Earth Engine. *Remote Sens.* **2018**, *10*, 2027, doi:10.3390/rs10122027.
16. Thenkabail, P. S.; Gumma, M. K.; Teluguntla, P.; Mohammed, I. A. Hyperspectral remote sensing of vegetation and agricultural crops. *Photogramm. Eng. Remote Sensing* **2014**, *80*, 697–709, doi:10.1201/b11222-41.

17. Waldner, F.; Duveiller, G.; Defourny, P. Local adjustments of image spatial resolution to optimize large-area mapping in the era of big data. *Int. J. Appl. Earth Obs. Geoinf.* **2018**, *73*, 374–385, doi:10.1016/j.jag.2018.07.009.
18. Atkinson, P. M. Selecting the spatial resolution of airborne MSS imagery for small-scale agricultural mapping. *Int. J. Remote Sens.* **1997**, *18*, 1903–1917, doi:10.1080/014311697217945.
19. Burke, M.; Lobell, D. B. Satellite-based assessment of yield variation and its determinants in smallholder African systems. *Proc. Natl. Acad. Sci.* **2017**, *114*, 2189–2194, doi:10.1073/pnas.1616919114.
20. Wardlow, B. D.; Egbert, S. L.; Kastens, J. H. Analysis of time-series MODIS 250 m vegetation index data for crop classification in the U.S. Central Great Plains. *Remote Sens. Environ.* **2007**, *108*, 290–310, doi:10.1016/j.rse.2006.11.021.
21. Whitehead, K.; Hugenholtz, C. H.; Myshak, S.; Brown, O.; LeClair, A.; Tamminga, A.; Barchyn, T. E.; Moorman, B.; Eaton, B. Remote sensing of the environment with small unmanned aircraft systems (UASs), part 1: a review of progress and challenges. *J. Unmanned Veh. Syst.* **2014**, *02*, 86–102, doi:10.1139/juvs-2014-0006.
22. Debats, S. R.; Luo, D.; Estes, L. D.; Fuchs, T. J.; Caylor, K. K. A generalized computer vision approach to mapping crop fields in heterogeneous agricultural landscapes. *Remote Sens. Environ.* **2016**, *179*, 210–221, doi:10.1016/j.rse.2016.03.010.
23. Pajares, G. Overview and Current Status of Remote Sensing Applications Based on Unmanned Aerial Vehicles (UAVs). *Photogramm. Eng. Remote Sens.* **2015**, *81*, 281–330, doi:10.14358/PERS.81.4.281.
24. Skakun, S.; Franch, B.; Vermote, E.; Roger, J.-C.; Becker-Reshef, I.; Justice, C.; Kussul, N. Early season large-area winter crop mapping using MODIS NDVI data, growing degree days information and a Gaussian mixture model. *Remote Sens. Environ.* **2017**, *195*, 244–258.
25. Weiss, M.; Jacob, F.; Duveiller, G. Remote sensing for agricultural applications: A meta-review. *Remote Sens. Environ.* **2020**, *236*, 111402, doi:10.1016/j.rse.2019.111402.
26. Defourny, P.; Bontemps, S.; Bellemans, N.; Cara, C.; Dedieu, G.; Guzzonato, E.; Hagolle, O.; Inglada, J.; Nicola, L.; Rabaute, T.; Savinaud, M.; Udroiu, C.; Valero, S.; Bgu, A.; Dejoux, J.-F.; El Harti, A.; Ezzahar, J.; Kussul, N.; Labbassi, K.; Lebourgeois, V.; Miao, Z.; Newby, T.; Nyamugama, A.; Salh, N.; Shelestov, A.; Simonneaux, V.; Traore, P. S.; Traore, S. S.; Koetz, B. Near real-time agriculture monitoring at national scale at parcel resolution: Performance assessment of the Sen2-Agri automated system in various cropping systems around the world. *Remote Sens. Environ.* **2019**, *221*, 551–568, doi:10.1016/j.rse.2018.11.007.

27. Foody, G. M.; Mathur, A. A relative evaluation of multiclass image classification by support vector machines. *Geosci. Remote Sensing, IEEE Trans.* 2004, *42*, 1335–1343.
28. Belousov, A. I.; Verzakov, S. A.; von Frese, J. A flexible classification approach with optimal generalisation performance: support vector machines. *Chemom. Intell. Lab. Syst.* **2002**, *64*, 15–25, doi:https://doi.org/10.1016/S0169-7439(02)00046-1.
29. Breiman, L. Random Forests. *Mach. Learn.* **2001**, *45*, 5–32, doi:10.1023/A:1010933404324.
30. Inglada, J.; Arias, M.; Tardy, B.; Hagolle, O.; Valero, S.; Morin, D.; Dedieu, G.; Sepulcre, G.; Bontemps, S.; Defourny, P.; Koetz, B. Assessment of an operational system for crop type map production using high temporal and spatial resolution satellite optical imagery. *Remote Sens.* **2015**, *7*, 12356–12379, doi:10.3390/rs70912356.
31. Santos, C. L. M. de O.; Lamparelli, R. A. C.; Figueiredo, G. K. D. A.; Dupuy, S.; Boury, J.; Luciano, A. C. dos S.; Torres, R. da S.; Maire, G. le Classification of Crops , Pastures , and Tree Plantations along the Season with Multi-Sensor Image Time Series in a Subtropical Agricultural Region. *Remote Sens.* **2019**, *11*, 1–27, doi:10.3390/rs11030334.
32. Liakos, K. G.; Busato, P.; Moshou, D.; Pearson, S.; Bochtis, D. Machine learning in agriculture: A review. *Sensors (Switzerland)* 2018, *18*, 2674.
33. Fernndez-Delgado, M.; Cernadas, E.; Barro, S.; Amorim, D. Do we Need Hundreds of Classifiers to Solve Real World Classification Problems? *J. Mach. Learn. Res.* **2014**, *15*, 3133–3181.
34. Rodriguez-Galiano, V. F.; Ghimire, B.; Rogan, J.; Chica-Olmo, M.; Rigol-Sanchez, J. P. An assessment of the effectiveness of a random forest classifier for land-cover classification. *ISPRS J. Photogramm. Remote Sens.* **2012**, *67*, 93–104, doi:10.1016/j.isprsjprs.2011.11.002.
35. Belgiu, M.; Drgu, L. Random forest in remote sensing: A review of applications and future directions. *ISPRS J. Photogramm. Remote Sens.* **2016**, *114*, 24–31, doi:10.1016/j.isprsjprs.2016.01.011.
36. Leah, H. S.; James, S. G.; Navin, R.; Mario, H.; Paul, C. W. Subnational distribution of average farm size and smallholder contributions to global food production. *Environ. Res. Lett.* **2016**, *11*, 124010.
37. Joshi, N.; Baumann, M.; Ehammer, A.; Fensholt, R.; Grogan, K.; Hostert, P.; Jepsen, M. R.; Kuemmerle, T.; Meyfroidt, P.; Mitchard, E. T. A.; Reiche, J.; Ryan, C. M.; Waske, B. A Review of the Application of Optical and Radar Remote Sensing Data Fusion to Land Use Mapping and Monitoring. *Remote Sens.* **2016**, *8*, 70, doi:10.3390/rs8010070.
38. Gorelick, N.; Hancher, M.; Dixon, M.; Ilyushchenko, S.; Thau, D.; Moore, R. Google Earth Engine: Planetary-scale geospatial analysis for everyone. *Remote Sens. Environ.* **2017**, *202*, 18–27, doi:10.1016/j.rse.2017.06.031.

39. Reichstein, M.; Camps-Valls, G.; Stevens, B.; Jung, M.; Denzler, J.; Carvalhais, N.; Prabhat Deep learning and process understanding for data-driven Earth system science. *Nature* **2019**, *566*, 195–204, doi:10.1038/s41586-019-0912-1.

Curriculum vitae

Jonas E. Böhler

Education

2014–2020	**University of Zurich, PhD candidate at the Remote Sensing Laboratories** PhD thesis: *TODO*
2013–2014	**University of Zurich, Master of Science** Major: Geography Specialization: Remote Sensing Master Thesis: *Discrimination of Agricultural Crop Types Using a Spectral- Spatial Unmixing Approach*
2009–2013	**University of Zurich, Bachelor of Science** Major: Geography Minor: Mathematics
2003–2005	**Kantonale Maturitatsschule für Erwachsene, Zurich, Matura** Special Subject: Latin Complementary Subject: Applications of Mathematics
1999–2003	**Technische Berufsmaturitätsschule, Winterthur, vocational school-leaving certificate**
1999–2003	**Elektroniker EFZ, MSW-Winterthur, Winterthur, Apprenticeship** Special Subject: Research and Development

Teaching and supervision

2014–2018	Teaching assistant within the Department of Geography, University of Zurich for the course GEO442 Spectroscopy of the Earth System.
2015–2018	Supervision and correction of various exams within the Department of Geography, University of Zurich.
2017–2018	Teaching and organization of outreach activities within the RSL and Department of Geography, University of Zurich. Namely: Lecture in RSL Colloquium 2018, Scientifica 2017, Information Days at UZH 2017.

Graduate courses and training

- PhD Seminars I & II
- Graduate School Retreat Seminar (I & II)
- Principles and Theory in Geography
- Scientific Writing
- Project Management
- Spass an der Lehre
- Zeit- und Selbstmanagement
- How to give a presentation effectively and persuasively
- Machine Learning and Geosciences
- Scheitern und Improvisation
- Fit für die Karriere

Publications

Böhler, J.E., Schaepman, M.E. & Kneubühler, M. (2020): Crop Separability from Individual and Combined Airborne Imaging Spectroscopy and UAV Multispectral Data. *Remote Sensing 12(8), 1256; doi: 10.3390/rs12081256*

Böhler, J.E., Schaepman, M.E. & Kneubühler, M. (2019): Optimal Timing Assessment for Crop Separation Using Multispectral Unmanned Aerial Vehicle (UAV) Data and Textural Features. *Remote Sensing 11(15), 1780; doi: 10.3390/rs11151780*

Böhler, J.E., Schaepman, M.E. & Kneubühler, M. (2018): Crop Classification in a Heterogeneous Arable Landscape Using Uncalibrated UAV Data. *Remote Sensing 10(8), 1282; doi: 10.3390/rs10081282*

Conference Talks

Böhler, J.E., Schaepman, M.E. & Kneubühler, M. (2019). Best spatial scale for crop classification using uncalibrated UAV data. *11th EARSeL SIG Imaging Spectroscopy Workshop, Brno, Czech Republic*

Böhler, J.E., Kneubühler, M., Tuia, D. & Schaepman, M.E. (2015). Improved land cover assessment in agriculture with optical remote sensing data. *13th Swiss Geoscience Meeting, Basel, Switzerland*

Conference Poster

Böhler, J.E., Kneubühler, M. & Schaepman, M.E. (2019). Assessing optimal specifications for crop classification in Switzerland using uncalibrated UAV data. *1st Swiss Workshop on Machine Learning for Environmental and Geosciences (MLEG), Dübendorf, Switzerland*

Böhler, J.E., Kneubühler, M. & Schaepman, M.E. (2018). From Images to Land Cover Maps - Classification of Field Crops Based on UAV Data. *GEOSummit, Bern, Switzerland*

Acknowledgements